CHEMICAL REVIEWS

Review

pubs.acs.org/CR

Lanthanide Single-Molecule Magnets

Daniel N. Woodruff,[†] Richard E. P. Winpenny,[†,‡] and Richard A. Layfield*,[†]

[†]School of Chemistry, and [‡]The Photon Science Institute, The University of Manchester, Oxford Road, Manchester M13 9PL, United Kingdom

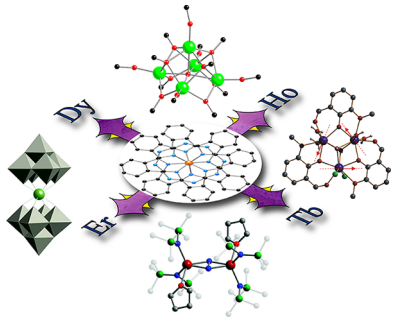

CONTENTS

1. INTRODUCTION

In the early 1990s, great excitement followed the discovery that a molecular transition metal coordination compound could, at liquid-helium temperatures, retain magnetization for long periods of time in the absence of an external magnetic field.[1] The famous dodecametallic manganese-acetate cage $[Mn_{12}O_{12}(OAc)_{16}(H_2O)_4]$ ($Mn_{12}Ac$) became the progenitor of a large family of magnetic materials known as single-molecule magnets (SMMs).[2] Notwithstanding the huge intrinsic interest in SMMs, it was also realized that they could in principle be developed for new technological applications. SMMs can be considered as molecular analogues of classical bulk ferromagnets; hence, it might be possible to develop them for applications involving the storage and processing of digital information. However, in contrast to bulk magnets currently used for this purpose, such as neodymium−iron boride magnets,[3] the molecular nature of SMMs offers unique attributes that may allow information to be stored with much higher densities, and to be processed at unprecedented speeds.[4] Completely new applications of SMMs have also been envisaged, including in the development of molecular spintronics.[5] Ultimately, however, SMM-based technology can only be realized when two major problems have been solved. First, the unique properties of SMMs are currently only accessible using liquid helium cooling; therefore, either the operating temperatures need to rise significantly, or applications so novel and important need to be discovered that temperature ceases to be an issue. Second, depositing and addressing individual molecules of SMMs on surfaces have only been explored with very few examples. One of the grand challenges in this field is still, therefore, to design and to synthesize efficient SMMs that function at temperatures likely to be of practical use, or which show physics that goes beyond what can be achieved with classical magnets.

The success (or not) of an SMM can be measured in more than one way. First, the magnetic blocking temperature, T_B, is the highest temperature at which an SMM displays hysteresis in plots of magnetization (M) versus magnetic field (H). It is important to note that the value of T_B strongly depends on the sweep rate of the magnetic field; hence, comparing the blocking temperatures of different SMMs should be done cautiously. Gatteschi, Villain, and Sessoli have proposed T_B as being the temperature at which the time (τ) taken for the magnetization to relax is 100 s:[2] it would be useful if this definition was universally adopted. Second, the coercive magnetic field, H_c, is the strength of the magnetic field needed to drive the magnetization of an SMM back to zero following saturation. Third, the effective energy barrier to reversal of the magnetization (also called the anisotropy barrier), U_{eff}, is the energy required to convert an SMM back into a simple paramagnet. By far the most popular parameter is U_{eff}, which is used in the vast

Received: January 15, 2013

   dx.doi.org/10.1021/cr400018q | Chem. Rev. XXXX, XXX, XXX−XXX

majority of SMM studies, and to observe SMM behavior at higher temperatures U_{eff} should be large. Although $M(H)$ hysteresis and measurements of coercive fields have been used to characterize some SMMs, both T_B and H_c are used less frequently than U_{eff}, due largely to the phenomenon of quantum tunneling of the magnetization that is particularly prominent in Ln-SMMs (see section 2.1). The blocking temperature is also dependent on the technique used for the measurement, and so is not an ideal parameter for judging the quality of an SMM.

To date, the largest anisotropy barrier claimed in a transition metal SMM is 67 cm^{-1}, which was obtained from studies of the cobalt(II) complex $[Co(hfpip)_2\{D2py_2(TBA)\}]_2$, where hfpip is hexafluoro-4-(4-*tert*-butylphenylimino)-2-pentanoate and $D2py_2(TBA)$ is a diazo-dipyridyl ligand.[6] Very recently, larger (104−181 cm^{-1}) barriers have been determined in various applied fields for a series of linear two-coordinate complexes of iron(II).[7] However, for the first 15 years, the SMM field was dominated by the Jahn−Teller ion high-spin manganese(III).[8] In 3d-SMMs, the reversal of the magnetization is blocked by a combination of two properties, the Ising-type magnetic anisotropy, which can be expressed as the axial zero-field splitting parameter, D, and the total spin on the molecule, S. The simple equations $U_{eff} = |D|S^2$ and $U_{eff} = |D|(S^2 - 0.25)$ then allow U_{eff} to be determined for SMMs with integer or noninteger total spin, respectively. From the outset, almost all efforts to generate SMMs with large U_{eff} values focused on synthesizing exchange-coupled cages with the largest possible spin. However, as the field matured, it became apparent that this strategy might not necessarily produce the desired outcome, as three important examples illustrate.

The original $Mn_{12}Ac$ was determined to have $U_{eff} = 51$ cm^{-1}, which arises from the product of $S = 10$ and $D = -0.51$ cm^{-1}.[1] One of the largest anisotropy barriers in a 3d-SMM (measured in zero applied magnetic field) occurs in the hexametallic manganese(III) cage $[Mn_6O_2(sao)_6(O_2CPh)_2(EtOH)_4]$ ($\{Mn_6\}$) (saoH$_2$ = 2-hydroxybenzaldehye oxime), where a combination of $S = 12$ and $D = -0.43$ cm^{-1} results in $U_{eff} = 62$ cm^{-1}.[9] However, a key result was the Mn_{19} cage $[Mn_{19}O_8(N_3)_8(HL)_{12}(MeCN)_6]^{2+}$, or $\{Mn_{19}\}$ (H_3L = 2,6-bis(hydroxymethyl)-4-methylphenol), which has a large total spin of $S = 83/2$. If the strategy of maximizing the total spin of a cage to increase U_{eff} is generally correct, then $\{Mn_{19}\}$ could reasonably be expected to be an SMM with a large anisotropy barrier: instead, $\{Mn_{19}\}$ has $U_{eff} = 4$ cm^{-1}.[10] The "problem" is that molecules of $\{Mn_{19}\}$ have high symmetry, which means that the anisotropies on the individual manganese(III) centers cancel each other out almost completely, that is, for molecules of $\{Mn_{19}\}$, $D \approx 0$, hence the very small anisotropy barrier. A further problem, which can be seen from studying Bencini and Gatteschi's text "EPR Spectroscopy of Exchange-Coupled Systems", is that ferromagnetic exchange between ions inevitably leads to a ZFS significantly smaller for an exchange-coupled cage complex than found for the corresponding single ions.[11] This correlation has been used by Waldmann and by Ruiz to examine how high the energy barriers in 3d-SMMs could go.[12] The general conclusion, highlighted by $\{Mn_{19}\}$, is that even if the total spin of an exchange-coupled 3d cage compound is very large, a lack of anisotropy will preclude SMM behavior. In an enlightening theoretical study entitled "What is not needed to make a single-molecule magnet", Neese and Pantazis state the case for anisotropy in the design of transition metal SMMs, and this article is recommended reading for those new to the field.[13]

There has been a growing realization that single-ion anisotropy is the crucial property to consider when designing SMMs with large anisotropy barriers;[14] perhaps the clue was always in the name. Since 2003, and especially in the last five years, considerable attention has therefore focused on the elements whose single-ion anisotropies are unrivalled throughout the periodic table: the lanthanides and actinides. SMMs based on coordination compounds of the f-elements, particularly those of the lanthanides, have accounted for some of the most eye-catching recent advances in molecular magnetism.[15] Possibly of even greater significance is that lanthanide SMMs (Ln-SMMs) have already shown considerable potential to be developed for surface deposition and device applications. Herein, we review the first decade of progress in studies of SMMs based solely on complexes of the lanthanides. Hybrid d−f compounds constitute an important class of SMM, but coverage of this area is beyond the scope of our Review.[16] Actinide SMMs represent a small-but-growing class of SMM,[17] but we also do not cover them in this Review.

2. DESIGNING AND CHARACTERIZING LANTHANIDE SMMS

A recent review by Rinehart and Long provides a lucid account of how f-element electronic structure can in principle be manipulated to develop new SMMs.[15a] In this section, we summarize the important features of lanthanide electronic structure that should be appreciated to interpret the properties of Ln-SMMs. Irrespective of the type of metal, the two strict prerequisites for a molecule to be an SMM are that the electronic ground state must be bistable, and that magnetic anisotropy must be present. For lanthanide ions with ground electronic terms other than $^1S_0$ and $^8S_{7/2}$, the orbital contribution to the magnetic moment is large and unquenched, and ligand field effects in lanthanide complexes can be regarded as a small-but-significant perturbation.[18] In contrast, for 3d transition metals, spin−orbit coupling is subordinate to ligand field effects, and Ln-SMMs therefore differ fundamentally from transition metal SMMs in the nature of their bistable ground state. For transition metal SMMs, the total spin S and the ensuing $[2S + 1]$ m_S substates lead to ground-state bistability.[2] In contrast, for Ln-SMMs, ground-state bistability arises from the $[2J + 1]$ m_J microstates within the spin−orbit-coupled ground term, $^{2S+1}L_J$. Simply considering the number of unpaired electrons yields little insight into the magnetic properties of lanthanide ions.

An additional property (although not a strict prerequisite) of the metal ions in Ln-SMMs is that the ground state should have a large value of m_J, which confers an appreciable magnetic moment. For the reasons discussed above, the lanthanide ions most commonly used in SMMs are terbium(III), dysprosium(III), erbium(III), and holmium(III) (Table 1). Because of the strong angular dependence of the 4f orbitals, the electronic structures of terbium(III) and dysprosium(III) ions possess

Table 1. Lanthanide(III) Ions Commonly Used in SMMs

	Tb^{3+}	Dy^{3+}	Ho^{3+}	Er^{3+}
$4f^n$	$4f^8$	$4f^9$	$4f^{10}$	$4f^{11}$
spin−orbit ground term	$^7F_6$	$^6H_{15/2}$	$^5I_8$	$^4I_{15/2}$
free-ion g-value	3/2	4/3	5/4	6/5

dx.doi.org/10.1021/cr400018q | *Chem. Rev.* XXXX, XXX, XXX−XXX

substantial anisotropy: as section 3 and Tables 2−7 show, the vast majority of Ln-SMMs contain either terbium or dysprosium, and in Ln-SMMs containing two or more lanthanide ions dysprosium is ubiquitous. Several Ln-SMMs based on erbium or holmium are known, but they are much less common. It is also noteworthy that although Dy-SMMs easily outnumber Tb-SMMs, the latter group provides some of the largest U_{eff} values. In a simple approximation, this trend can be interpreted in terms of electronic structure. Dy-SMMs have high U_{eff} values because Dy(III) ions have high magnetic anisotropy, and the energy gap between ground and first-excited m_J levels is often large. Dy-SMMs are the most numerous because dysprosium(III) is a Kramers' ion (it has an odd number of f-electrons), meaning that the ground state will always be bistable irrespective of the ligand field symmetry (see below). Some Tb-SMMs have very large U_{eff} values because Tb(III) can have greater magnetic anisotropy and larger Δm_J gaps than Dy(III); however, there are fewer Tb-SMMs because terbium(III) is a non-Kramers' ion, meaning that the ground state is only bistable when the ligand field has axial symmetry.

The approach generally adopted in the design of SMMs is to use the ligand field symmetry to enhance the single-ion anisotropy of Ln^{3+}. For example, it has been shown that the 4f electron density of terbium(III) in its ground state has a distinct oblate shape (i.e., it extends into the *xy* plane).[15a,19] Therefore, using ligands that generate an axially symmetrical complex should enhance the anisotropy simply based on an electrostatic model, and for Ln-SMMs that contain only a single lanthanide ion (section 3.1) this approach has indeed been remarkably successful. However, as a note of caution, recent studies have shown that the direction of the easy axis of magnetization may not necessarily coincide with the "obvious" molecular symmetry axis (see section 3.1.2). As the number of lanthanide ions in the SMM increases, exerting control over the symmetry of the coordination environments becomes increasingly difficult (or impossible), and our survey of the literature has identified that SMM properties generally tend to diminish as molecular structures become more elaborate.

2.1. Characterization of Ln-SMMs

The vast majority of SMMs are characterized in crystalline forms using conventional SQUID magnetometers. The standard experiment used to establish the credentials of an SMM involves measurement of the magnetic susceptibility (χ) using a very small alternating current (ac), or dynamic, magnetic field of about 1−5 Oe, across a range of temperatures (T = 1.5−50 K accounts for most SMMs). These ac measurements should be made in the absence of a direct current (dc) or static magnetic field. Using a standard magnetometer, the frequency ν of the ac field can usually be varied in the range 1−1500 Hz, and so the ensuing magnetic moment is time dependent and can be characterized by a relaxation time, τ, at a given temperature. Because individual SMM molecules have their own magnetic moment, the magnetization of the SMM will lag behind the driving ac field as it alternates across the sample, such that the actual measured magnetic susceptibility will incorporate a phase shift. This experiment gives rise to the so-called in-phase and out-of-phase susceptibilities, denoted by χ' and χ'', respectively.

One of the most reliable ways of identifying an SMM is to inspect the variation of χ' and χ'' with temperature at several different frequencies. As the temperature decreases, if the plot of χ'' gradually increases to reach a maximum and then decreases at even lower temperatures, then this indicates that reversal of the spin has been blocked. Furthermore, as the ac frequency is changed, so too is the position of the maximum in the $\chi''(T)$ plot. Similarly, plots of $\chi''(\nu)$ at different temperatures are also widely used to establish SMM behavior. The absence of maxima in the $\chi''(T)$ plots, or the lack of frequency-dependent χ'', in zero field creates ambiguity over true SMM behavior. The $\chi''(\nu)$ isotherms also provide the most reliable means of determining the energy barrier to magnetization reversal, or the anisotropy barrier, U_{eff}. Each $\chi''(\nu)$ curve allows one to establish an average relaxation time, τ, at a given temperature,[20] and the relationship of τ with temperature is given by the well-known equation:

$$\tau = \tau_0 \exp(U_{eff}/k_B T) \quad (1)$$

Equation 1 is an Arrhenius-type relationship, and so it can be used to determine the anisotropy barrier from the slope of ln τ versus T^{-1} where the graph is both linear and ln τ is temperature dependent. When these conditions are met, the magnetization in the SMM is said to relax via a thermally assisted mechanism. The physics can be described by an Orbach process, in which there are two energetically low-lying, degenerate states of the lanthanide ion, and an excited state that lies above the ground state by U_{eff}. If the lanthanide ion in the low-lying state with $m_J = +J$ absorbs a phonon with a frequency equivalent to U_{eff}, it can reach the excited state and then relax to the other low-lying state with $m_J = -J$. This temperature-dependent process establishes a thermal equilibrium between the two components of the degenerate ground state, resulting in relaxation of the magnetization.[18b] Alternative relaxation mechanisms are the direct process and the Raman process, in which phonons can cause a "spin flip" within the ground doublet.

For many Ln-SMMs, the Arrhenius plots are only linear with a positive gradient across a limited temperature range, and very often at lower temperatures the plot will feature a series of consecutive data points for which ln τ is independent of the temperature. Using terbium as the example again, instances when the gradient in an Arrhenius plot is zero provide strong evidence for the magnetization relaxing directly from $m_J = +6$ to $m_J = -6$, via quantum tunneling of the magnetization (QTM). Regions of the Arrhenius plot that fall between the two extremes produce curvature in ln τ versus T^{-1}, which implies that the thermal and the QTM mechanisms can occur concurrently.

The qualitative picture painted above belies the truly complex nature of the relaxation of the magnetization in Ln-SMMs. As the following sections describe, it is not uncommon for more than one thermally activated mechanism to occur in the same SMM, and it is also possible that the magnetization relaxes almost entirely via QTM. Identifying the occurrence of multiple relaxation processes is relatively straightforward to do by modeling the ac susceptibility data (including the Cole−Cole plot of χ' vs χ''). Understanding precisely why such phenomena occur in the way that they do is much more challenging. Indeed, this is one of the most exciting aspects of working in the field: methods for synthesizing and characterizing Ln-SMMs are well developed; however, our theoretical understanding of their fascinating properties is still evolving.

3. SURVEY OF LANTHANIDE SMMS

Interpretation of magnetic susceptibility data would be difficult without prior characterization of the crystal and molecular

dx.doi.org/10.1021/cr400018q | *Chem. Rev.* XXXX, XXX, XXX−XXX

Table 2. Monometallic Lanthanide SMMs[a]

Ln-SMM	U_{eff}/cm^{-1} (H_{dc}/Oe)	hysteresis (K)	ref
$[Bu_4N][Tb_{0.2}Y_{0.8}Pc_2]$ (**1a**)	230		21
$[Bu_4N][Dy_{0.2}Y_{0.8}Pc_2]$ (**2a**)	28		21
$[Bu_4N][Tb_{0.02}Y_{0.98}Pc_2]$ (**1b**)	260	1.7	32
$[Bu_4N][Dy_{0.02}Y_{0.98}Pc_2]$ (**2b**)	31	1.7	32
$[Bu_4N][TbPc_2]$ (**1**)	584[b]		34
$[TbPc_2]/[Bu_4N][Br]$ 1:143 (**1c**)	641[b]		34
$[Bu_4N][Ho_{0.02}Y_{0.98}Pc_2]$ (**3b**)		0.04−0.50[c]	33
$[H][Dy\{Pc(CN)_8\}_2]$ (**7**)			35
$[H][Dy_{0.1}Y_{0.9}\{Pc(CN)_8\}_2]$ (**7a**)	5.1	1.8, 1.6[d]	35
$[Bu_4N][Tb\{Pc(phth^1)\}_2]$ (**8a**)	445	2	36
$[Bu_4N][Tb\{Pc(phth^2)\}_2]$ (**8b**)	428	2	36
$[Bu_4N][Tb\{Pc(phth^3)\}_2]$ (**8c**)	463	2	36
$[TbPc_2]$ (**9**)	410		38
$[Tb\{Pc(ODd)_8\}_2]$ (**10**)			38
$[Tb\{Pc(OEt)_8\}_2][SbCl_6]$ (**12**)	550		39
$[Bu_4N][Tb\{Pc(OEt)_8\}_2]$ (**13**)	509		39
$[Dy\{Pc(OEt)_8\}_2][SbCl_6]$ (**15**)	55	1.8	40
$[Bu_4N][Dy\{Pc(OEt)_8\}_2]$ (**16**)	27	1.8	40
$[Tb\{Pc(IPD)_4\}_2]^-$ (**17**)		1.5[d]	41
$[Tb\{Pc(IPD)_4\}_2]$ (**18**)		1.5[d]	41
$[Tb\{Pc(IPD)_4\}_2]^+$ (**19**)		1.5[d]	41
$[Tb\{Pc(S\text{-}DOP)_8\}_2]$, crystalline ($\mathbf{20}_{cr}$)	480		42
$[Tb\{Pc(S\text{-}DOP)_8\}_2]$, disordered ($\mathbf{20}_{dis}$)	422		42
$[Dy(Pc)(TClPP)]$ (**21**)	16		43
$Dy\{Pc(OPn)_4\}(TClPP)]$ (**22**)	30 (2000)		43
$[DyH\{Pc(OPn)_4\}(TClPP)]$ (**23**)	40 (2000)		43
$Na[Dy(DOTA)(H_2O)]\cdot 4H_2O$ (**24**)	42 (900)		44, 45
$[(sal)Dy(NO_3)(\mu\text{-}L^1)ZnBr]$ (**25**)	231		46
$[(\eta^5\text{-}Cp^*)Dy_{0.05}Y_{0.95}(\eta^8\text{-}COT)]$ (**27a**)	18		47b
$[(\eta^5\text{-}Cp^*)Ho_{0.05}Y_{0.95}(\eta^8\text{-}COT)]$ (**28a**)	23, 17		47b
$[(\eta^5\text{-}Cp^*)Er(\eta^8\text{-}COT)]$ (**29**)	224, 137		47a
$[(\eta^5\text{-}Cp^*)Er_{0.05}Y_{0.95}(\eta^8\text{-}COT)]$ (**29a**)		5	47a
$[Dy(\eta^8\text{-}COT'')(\mu\text{:}\eta^8\text{:}\eta^2\text{-}COT'')Li(dme)(thf)]$ (**31**)	12.5		49
$Na_9[Er(W_5O_{18})_2]$ (**35**)	38		50
$[Dy_4\{As_5W_{40}O_{144}(H_2O)(glycine)\}]^{21-}$ (**36**)	2.7		51
$[Dy(tmtaa)_2K(DME)_2]$ (**37**)			52
$[Dy_{0.05}Y_{0.95}(tmtaa)_2K(DME)_2]$ (**37a**)	20 (100)		52
$[K(DME)(18\text{-crown-6}][Y_{0.95}Dy_{0.05}(tmtaa)_2]$ (**38a**)	24 (100)		52
$[Dy_aY_b(H_2BPzMe_2)_3]$ a = 1, b = 65 (**39a**)	16		53
$[Dy_aY_b(H_2BPzMe_2)_3]$ a = 1, b = 130 (**39b**)	16		53
$[Dy_{0.195}Y_{0.805}(L^2H_3)_2]^+$ (**40a**)	42 (200)		54
$[Dy(hmb)(NO_3)_2(dmf)]$ (**41**)	24 (1800)		55
$[Dy(acac)_3(H_2O)_2]$ (**42**)	47		56
$[Dy(acac)_3(1,10\text{-phen})]$ (**43**)	44.4		57
$[Dy(TTA)_3(2,2\text{-bipy})]$ (**44**)	40		58
$[Dy(TTA)_3(1,10\text{-phen})]$ (**45**)	59		58
$[Dy_{0.05}Y_{0.95}(TTA)_3(2,2\text{-bipy})]$ (**44a**)	67	1.9	58
$[Dy_{0.05}Y_{0.95}(TTA)_3(1,10\text{-phen})]$ (**45a**)	75	1.9	58
$[Dy(TTA)_3(4,5\text{-PBP})]$ (**46**)	28.5 (2000)		59
$[Dy(FTA)_3(BBO)]$ (**47**)	37.8		60
$[Dy(Ph_2acac)_3(R\text{-}L^3)]$ (**48**)	33		61
$[Dy(NTA)_3(S,S\text{-}Ph_2en)]$ (**49a**)	21.1 (2000)		62
$[Dy_2(hfac)_6(H_2O)_2(L^4)]$ (**50**)	11		63
$[Dy(9Accm)_2(NO_3)(dmf)_2]$ (**52**)	16 (1000)		64
$[Tb(hfac)_3(NIT\text{-}2py)]$ (**53**)	11.9		66
$[Tb(hfac)_3(NIT\text{-}PhOEt)_2]$ (**57**)	20.4		69
$[Dy(tfa)_3(NIT\text{-}2py)]$ (**58**)	14.8		70
$[Tb(tfa)(NIT\text{-}BzImH)]$ (**59**)	9.7		71
$[Dy(tfa)(NIT\text{-}BzImH)]$ (**60**)	3.2		71
$[Tb(NIT\text{-}pic)_3]$ (**61**)	15.8	3.0	72
$[Cs\{Dy(Ph_2acac)_4\}]_n$ (**63**)		0.5	74

dx.doi.org/10.1021/cr400018q | *Chem. Rev.* XXXX, XXX, XXX−XXX

Table 2. continued

Ln-SMM	U_{eff}/cm^{-1} (H_{dc}/Oe)	hysteresis (K)	ref
$[Yb(H_3L^5)_2]Cl_3$ (**64**)	3.5 (400)		75

[a] U_{eff} values are extracted from measurements in zero applied dc field, unless followed by a number in parentheses to indicate the strength of the applied field. Hysteresis measurements correspond to polycrystalline samples, except where indicated. Lattice solvent molecules are not listed. [b] Solid-state ^{1}H NMR spectroscopy. [c] Single-crystal micro-SQUID. [d] Magnetic circular dichroism spectroscopy.

structure of an SMM. We therefore divide Ln-SMMs into sections defined by the number of lanthanide ions present in the molecular structure. For SMMs containing either one or two lanthanide ions, it is convenient to subdivide the sections based on the ligand type, and in particular by the μ-bridging ligand for dimetallic Ln-SMMs. For trimetallic and higher-nuclearity SMMs, the lanthanide ions are often bridged by more than one type of ligand; however, the occurrence of certain geometrically regular structural motifs provides a convenient means of subdividing the SMMs. Our aim in adopting this approach is to enable comparisons of isostructural SMMs that contain either different lanthanide ions or different ligands. However, we point out that because of the strong influence of single-ion effects on lanthanide magnetic properties, insight into one SMM can be derived from considerations of other examples with a different number of metal ions. Furthermore, there is appreciable experimental and theoretical evidence that intermolecular magnetic dipole−dipole interactions between Ln(III) ions influence SMM properties, which suggests that even considering only individual molecules could be an oversimplification. Boundaries between different "types" of Ln-SMM are artificial and are used in this Review only for convenience.

3.1. Monometallic Ln-SMMs

One of the most striking developments that accompanied the advent of Ln-SMMs is the fact that slow relaxation of the magnetization can be observed in complexes that contain only a single lanthanide ion. The structural simplicity of monometallic Ln-SMMs contrasts sharply with the elaborate architectures of many polymetallic 3d metal cage complexes. As discussed in section 1, a complication with 3d-SMMs is the need to align the easy axes of magnetization of multiple metal centers to generate large overall magnetic anisotropy. Monometallic Ln-SMMs therefore afforded the first opportunities to develop systems in which the key properties of anisotropy and ligand field symmetry could be expressed without such complications.

Table 2 lists the monometallic Ln-SMMs published up to the end of 2012, along with any relevant parameters used to characterize their SMM properties. The structures of selected ligands are displayed throughout this Review.

3.1.1. Monometallic Ln-SMMs with Phthalocyanine Ligands. The lanthanide SMM era began with Ishikawa's seminal 2003 communication entitled "Lanthanide double-decker complexes functioning as magnets at the single-molecular level", in which SMM behavior was described in the phthalocyanine complexes $[Bu_4N][LnPc_2]$, with Ln = Tb (**1**) and Dy (**2**).[21] Ln-SMMs containing ligands derived from phthalocyanine (Pc) are among the most important SMMs ever reported.[22] The most common molecular structural motif is the double-decker, or sandwich, structure containing $[Pc'_2Ln]^{\pm/0}$ units, usually with a D_{4d}-symmetric, square-antiprismatic lanthanide coordination geometry. Pc′ can be the parent phthalocyaninate ligand or a substituted analogue (Figure 1), and the complex can be a cation, an anion, or uncharged by virtue of the redox noninnocence of Pc ligands (see section

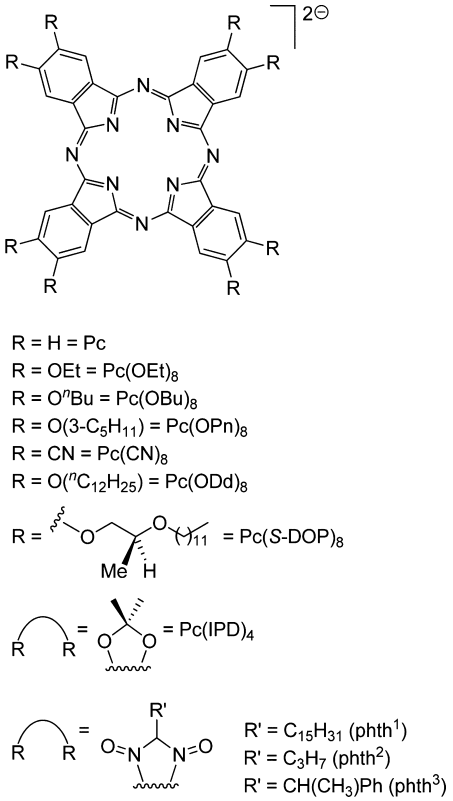

Figure 1. 2,3,9,10,16,17,23,24-Substituted phthalocyanine ligands used in Ln-SMMs.

3.1.1.1). Lanthanide-phthalocyanine SMMs have become the $Mn_{12}Ac$ of the Ln-SMM field: surveying the literature reveals that they are the most "introduced" Ln-SMMs; they are the most widely studied Ln-SMMs, and consequently the best understood; and, significantly, they are seemingly the SMMs (of any metal) with the most potential to be developed for surface deposition, and hence for device applications. Indeed, the properties of $[TbPc_2]$ SMMs on a range of surface types such as graphene,[23] highly ordered pyrolitic graphite,[24] carbon nanotubes,[25] copper(111),[26] and gold(111)[27] have been studied using a range of techniques, and have been the subject of recent reviews.[28] Remarkable physical phenomena have resulted from this work, including the use of $[TbPc_2]$ as a molecule-based transistor used to measure a single nuclear spin,[29] and the potential development of new molecular spintronic devices by using $[TbPc_2]$ and single-walled carbon nanotubes as a "supramolecular spin valve".[30]

Another feature of $[Pc'_2Ln]$ SMMs that echoes the development of the $Mn_{12}Ac$ SMMs is that derivatization of Pc ligands can be undertaken relatively easily. Octa-substituted Pc ligands, with substituents in the 2,3,9,10,16,17,23,24-positions, are particularly popular, and they can be accessed using conventional organic chemistry. However, care must be exercised during the purification steps to avoid contamination of the desired $[Pc'_2Ln]^{\pm/0}$ complex with concomitantly formed

dx.doi.org/10.1021/cr400018q | Chem. Rev. XXXX, XXX, XXX−XXX

isostructural complexes carrying different charges. The drawback of the often challenging purification steps is that overall yields of $[Pc'_2Ln]^{\pm/0}$ can be very low. However, in contrast to the limited changes in magnetic properties obtained through chemical modification of $Mn_{12}Ac$ SMMs, the resulting impact of ligand functionalization on the SMM behavior of $[Pc'_2Ln]$ compounds can be significant (see below).

The salts $[Bu_4N][LnPc_2]$, in which the $[Pc]^{2-}$ ligands are unsubstituted, are known with Ln = Tb (**1**), Dy (**2**), Ho (**3**), Er (**4**), Tm (**5**), and Yb (**6**). Compounds **1**–**6** are isostructural, and **1** and **2** are the prototypical phthalocyanine Ln-SMMs (Figure 2).

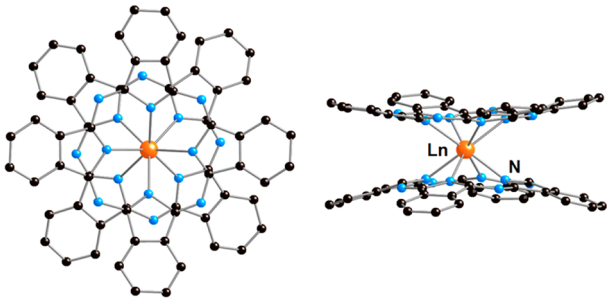

Figure 2. Molecular structure of $[Pc_2Ln]^-$. Hydrogen atoms are omitted.

Both **1** and **2** feature one Ln^{3+} cation sandwiched between two mutually staggered dianionic $[Pc]^{2-}$ ligands, with four nitrogen atoms from each ligand coordinating to the metal. The lanthanides in **1** and **2** therefore occupy eight-coordinate, D_{4d}-symmetric environments because of the mutually staggered conformation of the Pc ligands.[21]

In a small ac magnetic field of 3.5 G oscillating at 10, 100, and 997 Hz, the in-phase and the out-of-phase magnetic susceptibility of polycrystalline **1** (Figure 3) and **2** are temperature dependent. The measurements on both **1** and **2** were conducted on pure samples, and also on samples doped into the isostructural diamagnetic host $[Bu_4N][YPc_2]$, with an Ln:Y ratio of 1:4, effectively corresponding to $[Bu_4N][Ln_{0.2}Y_{0.8}Pc_2]$ (Ln = Tb **1a**; Dy **2a**). Diamagnetic host lattices can slow the dynamics of the magnetization, and yttrium is typically selected for this purpose in studies of Ln-SMMs because the ionic radius of Y^{3+} is very similar to that of the mid-late lanthanides, and is almost identical to that of Ho^{3+} for a given coordination number. The impact of studying the dilute samples **1a** and **2a** was to shift the maxima in the susceptibility curves to higher temperatures, which corresponds to a removal of the dipolar interactions between Ln^{3+} ions in nearest-neighbor $[LnPc_2]^-$ complexes, and to a slowing of the rate at which the magnetization reversal occurs. Hence, it was possible to conclude that the slow relaxation of magnetization in $[TbPc_2]^-$ and $[DyPc_2]^-$ is a molecular property. Applying the Arrhenius analysis to **1a** and **2a** produced anisotropy barriers of U_{eff} = 230 and 28 cm^{-1}, respectively. Raising the dilution levels to $[Bu_4N][Ln_{0.02}Y_{0.98}Pc_2]$ (Ln = Tb **1b**; Dy **2b**) resulted in increases in the anisotropy barriers to U_{eff} = 260 and 31 cm^{-1} in **1b** and **2b**, respectively, and also allowed hysteresis to be observed at 1.7 K in the field dependence of the magnetization.

The anisotropy barriers determined for **1a** and **1b** were noteworthy for three reasons. First, the magnitudes of U_{eff} for **1a**/**b** were (and still are) considerably greater than anything that has been recorded for a 3d-SMM. Second, it became

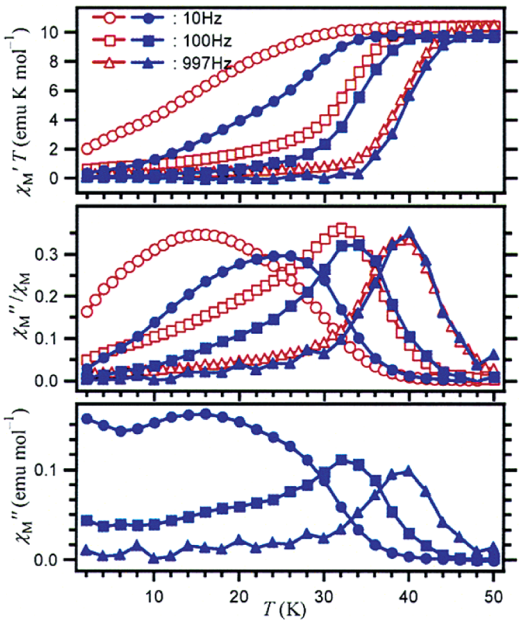

Figure 3. $\chi'T$ versus T (top), χ''/χ_M versus T (middle), and χ'' versus T for a powdered sample of **1** (open points), and for **1** diluted in diamagnetic $[Bu_4N][Pc_2Y]$ (filled points). Data collected in a 3.5 Oe ac magnetic field oscillating at the indicated frequencies. Image taken from ref 21.

apparent that the matrix in which the lanthanide complex is enclosed can influence the dynamics of the magnetization (see below). Third, a very insightful observation was that the U_{eff} value for **1a** is of a magnitude similar to that of the energetic separation between the ground and first excited m_J sublevels of the Tb(III) ion. Detailed studies using ligand-field parameters and ac susceptibility data allowed the relaxation of the magnetization at higher temperatures to be assigned to an Orbach mechanism, proceeding from the ground sublevel with $|m_J| = 6$ via the first excited m_J sublevel with $|m_J| = 5$.[31] At lower temperatures, the relaxation of the magnetization can be accounted for by tunneling directly from the ground state, or a Raman process.

Single crystals of **1b** were subsequently analyzed using a micro-SQUID device at milli-Kelvin temperatures, in which the magnetic field was aligned parallel to the easy-axis of magnetization.[32] The resulting plot of magnetization versus field showed "irregularly arranged staircase" hysteresis loops, which gave a clear indication of quantum tunneling of the magnetization (Figure 4). The appearance of the stepped

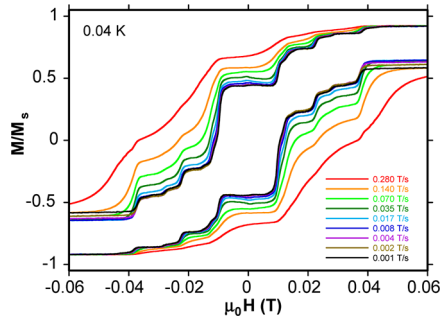

Figure 4. Hysteresis for a single crystal of **1b**, measured at T = 40 mK and several scan rates (from ref 32).

dx.doi.org/10.1021/cr400018q | *Chem. Rev.* XXXX, XXX, XXX–XXX

hysteresis loops was explained by considering that quantum tunneling can occur as a result of entanglement between the ground doublet of Tb(III) with $m_J = \pm 6$ and the nuclear spin of terbium, the latter conveniently being limited to a single, naturally occurring isotope, that is, ^{159}Tb with $I = 3/2$. Combining each of $m_J = +6$ and $m_J = -6$ with $m_I = \pm 3/2$ and $\pm 1/2$ was found to produce intersections or so-called "avoided crossings" at 13 different magnetic fields, each of which elegantly corresponded to a step in the hysteresis loop determined by the micro-SQUID experiment.

The same analysis was also applied to **2b**; however, the hysteresis is more complicated due to dysprosium occurring naturally as seven isotopes, five of which have $I = 0$, but ^{161}Dy (18.91%) and ^{163}Dy (24.90%) both have $I = 5/2$. A dilute sample of the holmium analogue **3b**, that is, $[Bu_4N][Ho_{0.02}Y_{0.98}Pc_2]$, was also studied by the micro-SQUID technique, and the magnetization versus field hysteresis revealed extensive QTM.[33] As with **1b** and **2b**, the QTM in very dilute **3b** could be assigned to entanglement of the nuclear (^{165}Ho, $I = 7/2$, 100%) and the electronic spin of holmium. A more general conclusion from the observations on **1**−**3** is that the relaxation of magnetization in monometallic Ln-SMMs, arising from entanglement of nuclear and electronic spin, is a mechanism fundamentally different from those thought to occur in transition metal SMMs.

A solid-state ^{1}H NMR spectroscopy study of undiluted **1**, and of **1** diluted into $[Bu_4N][Br]$, further illustrated the effects that the matrix surrounding a phthalocyanine Ln-SMM can have on the crystal-field splitting, and hence the dynamic magnetism.[34] Remarkably, the anisotropy barrier for undiluted **1** was estimated to be $U_{eff} = 584$ cm^{-1}, and the barriers for **1** diluted at levels of 1:9 (**1c**) and 1:143 (**1d**) were found to be $U_{eff} = 641$ cm^{-1}.

The cyano-substituted dysprosium sandwich complex $[H][Dy\{Pc(CN)_8\}_2]$ (**7**) was synthesized to develop an alternative way of arranging phthalocyanine SMMs on surfaces, and also to explore the effects of electron-withdrawing substituents on the magnetic properties.[35] The UV/vis spectrum of **7** indicated that the cyano groups increase the extent of the ligand π-system. Although magnetization studies of pure **7** did not produce hysteresis loops, a dilution study on $[H][Dy_{0.1}Y_{0.9}\{Pc(CN)_8\}_2]$ (**7a**) showed narrow hysteresis but with no coercive field, most likely due to hyperfine interactions with the dysprosium nuclei, as discussed above for **2b**. At 1.6 K, hysteresis in magnetic circular dichroism (MCD) measurements on a dilute solution of **7a** was observed, and revealed a coercive field of $H_c = 0.2$ T. The anisotropy barrier in **7a** in zero field was measured at only $U_{eff} = 5.1$ cm^{-1}, with the value increasing to 40 cm^{-1} in an applied field of 3000 Oe.

Modification of the phthalocyanine ligand periphery to incorporate electron-withdrawing phthalimide substituents introduces a means of increasing the stability of SMMs of the type $[LnPc_2]^-$ with respect to oxidation (see below).[36] Thus, the terbium-containing sandwich complexes $[Bu_4N][Tb\{Pc(phth^1)\}_2]$ (**8a**), $[Bu_4N][Tb\{Pc(phth^2)\}_2]$ (**8b**), and $[Bu_4N][Tb\{Pc(phth^3)\}_2]$ (**8c**) (Figure 1) are stabilized with respect to oxidation by 0.7 V relative to **1**, and ac susceptibility studies produced large anisotropy barriers of $U_{eff} = 445$ ($\tau_0 = 6.35 \times 10^{-11}$ s), 428 ($\tau_0 = 1.34 \times 10^{-10}$ s), and 463 cm^{-1} ($\tau_0 = 2.22 \times 10^{-11}$ s), respectively.

3.1.1.1. New SMMs from Oxidation of [LnPc$_2$]$^-$. The highest occupied molecular orbital (HOMO) of $[LnPc_2]^-$ complexes are π-type antibonding orbitals located on the $[Pc]^{2-}$ ligands, and the HOMO is susceptible to one- and two-electron oxidation to give $[LnPc_2]$ and $[LnPc_2]^+$, respectively.[37] The significance of the oxidations is that changes in the molecular structure of the sandwich unit can occur, which should impact on the ligand field experienced by the lanthanide trications, and which should, in turn, result in greater energetic separation of the ground m_J sublevel from the excited states. A density functional theory (DFT) study of the two-electron oxidation of $[YPc_2]^-$ to give $[YPc_2]^+$ did indeed predict a significant contraction of the sandwich structure, consistent with the removal of antibonding electrons: the two N_4 planes containing the nitrogen atoms directly bonded to yttrium were calculated to be 0.08 Å closer together, and the Y−N distances were predicted to shorten by 0.03 Å (Scheme 1).

Scheme 1. Contraction of the Square-Antiprismatic Coordination Environment upon Two-Electron Oxidation of $[LnPc_2]^-$ To Give $[LnPc_2]^+$[a]

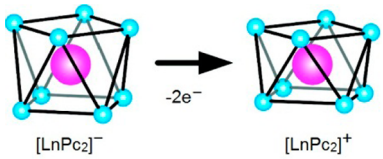

[a]Adapted from ref 37.

In the neutral terbium(III) complex $[TbPc_2]$ (**9**), one of the ligands is formally present as the $S = 1/2$ radical $[Pc]^-$ and the other as $[Pc]^{2-}$; however, the unpaired π electron can be delocalized across both ligands. The plot of $\chi''(T)$ for **9** showed a strong frequency dependence, with a peak maximum even being observed at a temperature of ca. 50 K. The resulting Arrhenius analysis produced a remarkable $U_{eff} = 410$ cm^{-1}, which is considerably higher than any analogous value extracted for **1** from ac susceptibility data (Table 1).[38] As with the anionic complexes $[LnPc_2]^-$, the molecular origin of the SMM behavior in **9** was also established, but in this instance by studying the long-chain-substituted complex $[Tb\{Pc(ODd)_8\}_2]$ (**10**) as a frozen solution in eicosane.

The ethoxy-substituted complex $[Tb\{Pc(OEt)_8\}_2]$ (**11**) undergoes one-electron oxidation or one-electron reduction to give $[Tb\{Pc(OEt)_8\}_2][SbCl_6]$ (**12**) or $[Bu_4N][Tb\{Pc(OEt)_8\}_2]$ (**13**), respectively (Scheme 2).[39]

Scheme 2

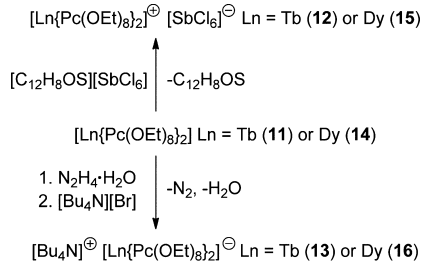

Compounds **12** and **13** are SMMs with similar features in their ac susceptibility data, and a two-phonon Orbach mechanism between $m_J = +6$ and $m_J = -6$ describes the relaxation in both. For the $[Tb\{Pc(OEt)_8\}_2]^-$ anion in **13**, a maximum in $\chi''(T)$ was observed at 52 K, using an ac frequency of $\nu = 997$ Hz, and the analogous peak for the [Tb{Pc-

dx.doi.org/10.1021/cr400018q | Chem. Rev. XXXX, XXX, XXX−XXX

$(OEt)_8\}_2]^+$ in **12** occurred at 40 K. The anisotropy barrier in **12** was found to be U_{eff} = 550 cm^{-1}, whereas a lower barrier of 510 cm^{-1} was determined for **13**. The difference in the anisotropy barriers in **12** and **13** was assigned to a contraction of the $\{TbN_8\}$ coordination environment that accompanies formal oxidation of $[Tb\{Pc(OEt)_8\}_2]^-$ to $[Tb\{Pc(OEt)_8\}_2]^+$ (Scheme 2). The geometric contraction enhances the ligand-field potential, which is thought to increase the energy separation between ground and first-excited m_J levels, and so reduce the rate at which the magnetization reaches thermal equilibrium. The same series of redox experiments was conducted on the dysprosium analogue $[Dy\{Pc(OEt)_8\}_2]$ (**14**), giving $[Dy\{Pc(OEt)_8\}_2][SbCl_6]$ (**15**) or $[Bu_4N][Tb\{Pc(OEt)_8\}_2]$ (**16**).[40] In the case of **15**, the maximum in the $\chi''(T)$ curve at ν = 1000 Hz occurred at about 25 K, which is an increase of 15 K relative to **16**. Furthermore, **15** has U_{eff} = 55 cm^{-1}, which is double the value of 27 cm^{-1} measured for **16**, that is, a much bigger increase than that observed in the case of **12** and **13**. Also significant is that, although both **15** and **16** show hysteresis in the $M(H)$ plots, only the cation-containing **15** has remanent magnetization, which is thought to be the result of significantly longer relaxation times arising from the compression of the coordination environment.

MCD spectroscopy was used to study hysteresis in the electrochemically generated SMMs $[Tb\{Pc(IPD)_4\}_2]^n$, where n = −1 (**17**), n = 0 (**18**), or n = +1 (**19**) (IPD = isopropylidenedioxy).[41] The spectra were recorded as glasses in CH_2Cl_2/$[Bu_4N][BF_4]$ to minimize any intermolecular interactions, and the variation in the intensity of the MCD bands observed around 701, 660, and 624 nm for **17**, **18**, and **19**, respectively, was studied across a magnetic field range of H = ±2 T. Butterfly shaped hysteresis was observed in each case, with sharps drops in MCD intensity in fields of less than 0.09 T for **17** and **19**. Complexes **17** and **19** differ in the magnitude of their coercive fields, which was H_c = 0.023 T for **17** and 0.072 T for **19**, and the wider hysteresis loops observed for **19** suggest that the ground m_J state is separated from the first excited to a greater extent than in **17**. These observations probably reflect a relatively contracted coordination environment in **19**, as per Scheme 1. In contrast, the MCD hysteresis loops for neutral **18** remain wide at low magnetic fields, and show a larger H_c of 0.16 T. The observations on **18** are particularly significant because, under the conditions of the MCD experiment, it is apparent that the neutral complex is better suited to SMM applications than its cationic analogue, that is, the opposite conclusion of that reached for related bis(phthalocyanine) complexes studied by solid-state ac susceptibility measurements.

The neutral complex $[Tb\{Pc(S\text{-}DOP)_8\}_2]$ (**20**), where *S*-DOP = (*S*)-2-(dodecyloxy)propan-1-oxy (Figure 1), possesses the unique combination of being a liquid crystalline material at room temperature and an SMM at cryogenic temperatures.[42] Complex **20** is polymorphic and can adopt a disordered form ($\mathbf{20}_{dis}$), a partially ordered form ($\mathbf{20}_{po}$), or a crystalline form ($\mathbf{20}_{cr}$). Because the magnetic properties of phthalocyanine SMMs are sensitive to their environment, interconverting the different phases of **20** potentially provides a means of modifying SMM behavior in a controlled way. This was achieved by quenching **20** from 333 to 150 K to obtain $\mathbf{20}_{dis}$, and $\mathbf{20}_{cr}$ was obtained by warming $\mathbf{20}_{dis}$ and then cooling the sample slowly. The plots of $\chi''(\nu)$ at 25 K for $\mathbf{20}_{cr}$ and $\mathbf{20}_{dis}$ have the common feature of two peaks, corresponding to a slow relaxation process centered on ν = 0.3 Hz and a fast relaxation process at ν = 40 Hz. However, the ratio of fast:slow relaxation for $\mathbf{20}_{cr}$ is 27:73, but for $\mathbf{20}_{dis}$ it is 59:41, indicating that the slow relaxation process characterizes the crystalline form. The mesophase $\mathbf{20}_{po}$ was obtained by equilibrating a sample of $\mathbf{20}_{cr}$ at room temperature for several weeks, and then quenching to 150 K. The magnetic measurements on $\mathbf{20}_{po}$ revealed that the slowly relaxing species only contributes 32% of the sample, and the process was found to be reversible. An Arrhenius analysis revealed a linear temperature dependence above 30 K, allowing U_{eff} = 480 cm^{-1} and 422 cm^{-1} to be extracted for $\mathbf{20}_{cr}$ and $\mathbf{20}_{dis}$, respectively.

The series of phthalocyaninate-porphyrinate dysprosium complexes $[Dy(Pc)(TClPP)]$ (**21**), $[Dy\{Pc(OPn)_4\}(TClPP)]$ (**22**), and "neutral protonated" $[DyH\{Pc(OPn)_4\}(TClPP)]$ (**23**), where $Pc(OPn)_4$ = 1,8,15,22-tetrakis(3-pentyloxy)-phthalocyaninate and TClPP = *meso*-tetrakis-(4-chlorophenyl)-porphyrinate, all feature eight-coordinate dysprosiums, and they provide an interesting illustration of how lower ligand field symmetry can impact on dynamic magnetic properties.[43] Whereas **21** is an SMM with U_{eff} = 16 cm^{-1}, complexes **22** and **23** do not show any maxima in their $\chi''(T)$ plots in zero field, although applying H_{dc} = 2000 Oe produced U_{eff} = 30 and 40 cm^{-1} for **22** and **23**, respectively. These observations have been interpreted in terms of deviations in the twist angle ϕ, defined as the dihedral angle formed between the two N_4 planes of the ligands (Figure 5), from the ideal angle in D_{4d} symmetry of 45°. In **21**, ϕ = 43.6°; however, in **22** and **23**, which are isostructural with each other, ϕ = 38.0°.

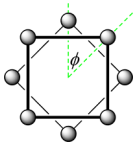

Figure 5. Twist angle ϕ in square-prism-derived $\{LnX_8\}$ complexes.

Another intriguing observation on **22** and **23** was that greater disorder in the lattice chloroform molecules found in the crystal structure of **23** was proposed to play an influential role in reducing the QTM rate in zero field.

3.1.2. Non-phthalocyanine Monometallic Ln-SMMs. Not only has the use of Pc-type ligands resulted directly in some of the most impressive SMMs, these studies have also inspired new lanthanide coordination chemistry and the reinvestigation of well-known lanthanide compounds, with the aim of developing new SMMs in rational and well-defined ways. Here, the aim is to apply the symmetry-based design principles that have arisen from the extensive investigations of Pc-SMMs. Not only have large U_{eff} values been achieved through this approach, Ln-SMMs with alternative ligands environments have also furnished considerable new fundamental insight into the magnetic properties and electronic structure of the lanthanides. A selection of ligands used in the development of monometallic SMMs is shown in Figures 6, 7, 13, and 15.

A recent study by Sessoli and co-workers provided valuable insight into the relationship between the symmetry of the coordination environment and the presumed orientation of the easy axis of magnetization.[44,45] The dysprosium ion in $Na[Dy(DOTA)(H_2O)]\cdot 4H_2O$ (**24**) is in a capped square prismatic coordination environment, with the capping aquo ligand occupying a site that coincides with the molecular C_4 axis

dx.doi.org/10.1021/cr400018q | *Chem. Rev.* XXXX, XXX, XXX−XXX

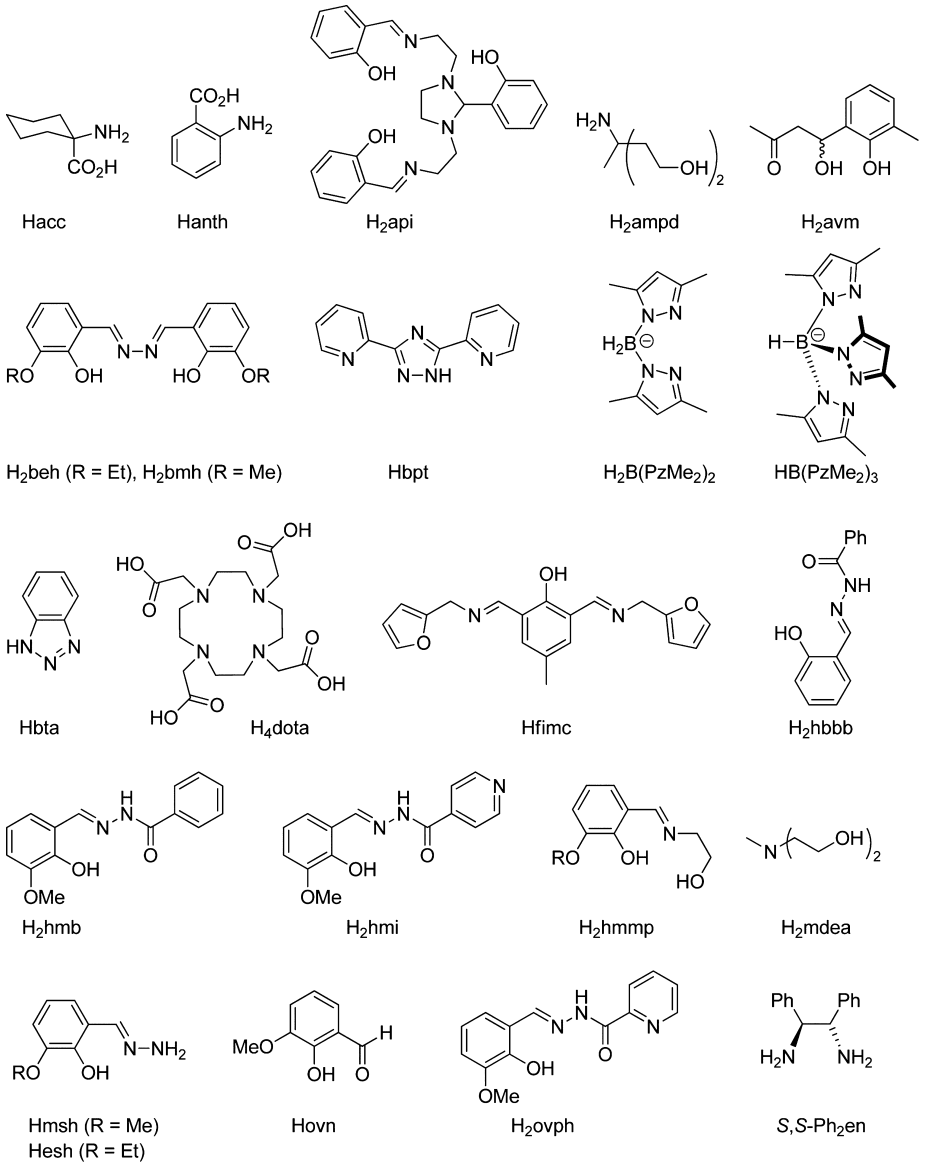

Figure 6. Structures of selected pro-ligands, listed in alphabetical order (a–p).

of the $[Dy(DOTA)(H_2O)]^-$ complex (Figure 8). Although the magnetization relaxation times determined for polycrystalline samples of **24** show very little temperature dependence in zero applied field, in H_{dc} = 900 Oe an anisotropy barrier of U_{eff} = 42 cm^{-1} was determined.[44] In the three-dimensional plot of $\chi''(\nu)$ with varying magnetic field for **24**, at relatively low fields a single relaxation process dominates the landscape at higher frequencies. As the field strength is increased, the emergence of a second relaxation process at much lower frequencies gradually supplants the first process, but even more remarkable is that the relaxation time, τ, associated with the field-induced relaxation process at 1000 Oe was found to be 6 orders of magnitude greater than that in zero field. A magnetic dilution experiment on **24**, using a Dy:Y ratio of 18:82, revealed that the relaxation time is reduced, indicating that dipolar interactions between molecules of **24** are important.

Complex **24** was also analyzed by single-crystal magnetic susceptibility measurements, luminescence spectroscopy, and ab initio calculations.[45] The single-crystal susceptibility experiments revealed that the easy axis of magnetization is almost perpendicular to the molecular C_4 axis, and the ab initio calculations identified that the same axis has an orientation very similar to that determined by experiment. These results are surprising and suggest that the electronic structure of **24** does not possess axial symmetry. The emission spectrum of **24** at room temperature features a series of bands corresponding to transitions of the type $^4F_{9/2} \rightarrow {}^6H_J$ with J = 11/2, 13/2, and 15/2. Simulation of the emissions to the ground $^6H_{15/2}$ state allowed the energy gap between the two lines of highest energy to be determined as 53 ± 8 cm^{-1}, which is similar to the U_{eff} value of 42 cm^{-1} found in **24**. This observation strongly suggests that population of the first excited m_J level leads to reversal of the magnetization, and provided the first example of lanthanide luminescence and magnetization reversal in an SMM being closely correlated.

Taking into account not only ligand field symmetry but also the likely ligand field potential created by different types of donor atoms proved to be an effective strategy for developing the Ln-SMM $[(sal)Dy(NO_3)(\mu\text{-}L^1)ZnBr]$ (**25**), where (sal)H is salicylaldehyde and L^1 is the Schiff-base/phenoxide ligand depicted in the structure of **25**.[46] Complex **25** contains dysprosium in a $\{DyO_9\}$ environment, and the ac susceptibility

dx.doi.org/10.1021/cr400018q | Chem. Rev. XXXX, XXX, XXX–XXX

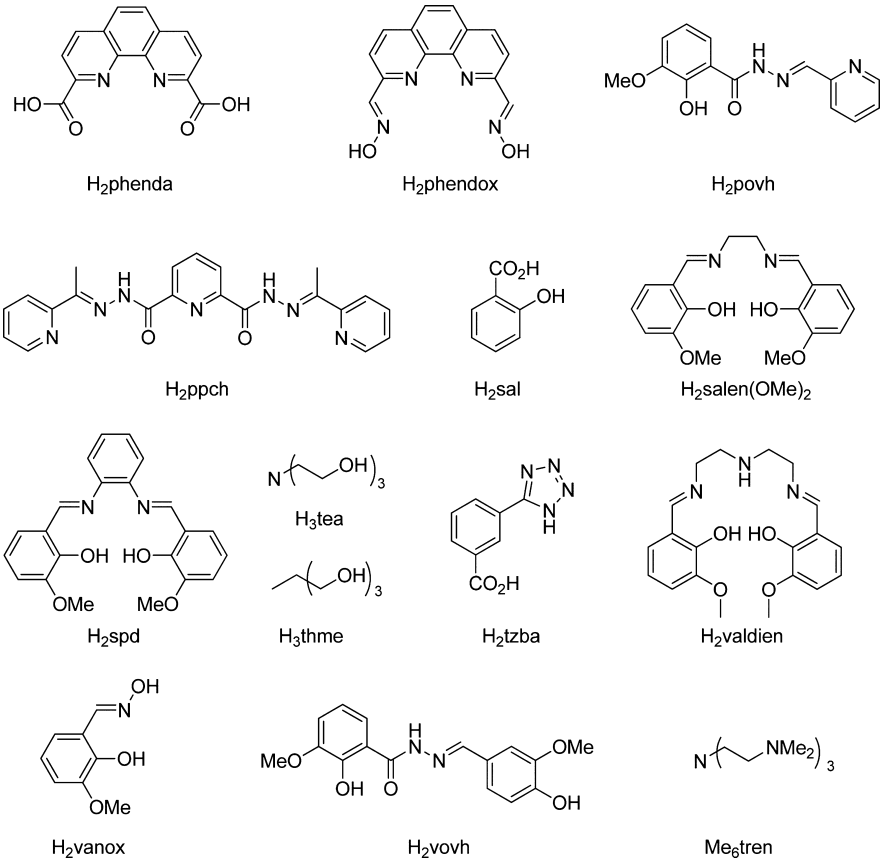

Figure 7. Structures of selected pro-ligands, listed in alphabetical order (p–t).

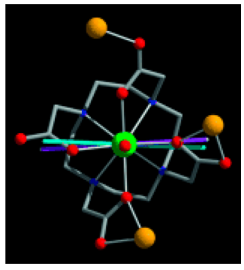

Figure 8. Molecular structure of **24**, viewed along the molecular pseudo-C_4 axis. Green = Dy, blue = N, red = O, orange = Na. The purple rod represents the easy axis determined by experiment, and the turquoise rod represents the calculated axis. Image from ref 45.

studies revealed an impressive anisotropy barrier of U_{eff} = 231 cm^{-1} with $\tau_0 = 1.1 \times 10^{-9}$ s, in zero applied field.

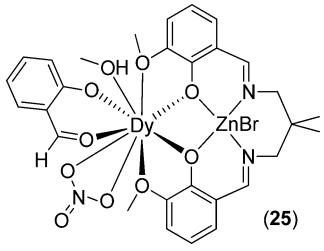

In designing **25**, an important consideration was the magnitude of the formal negative charge on the various types of *O*-donor atoms, which were determined as Mulliken charges through a density functional theory (DFT) study. The DFT study found that the negative charge on the phenoxo oxygens should have a much greater magnitude than those found on the methanol, methoxy, and nitrate ligands in **25**. The three phenoxo donor atoms are regarded as occupying axial positions, which enhances the oblate nature of the electron density of dysprosium(III) in its electronic ground state, and produces a relatively large anisotropy barrier.

The series of single-ion organometallic complexes [(η^5-Cp*)Ln(η^8-COT)], with Ln = Tb (**26**), Dy (**27**), Ho (**28**), Er (**29**), or Tm (**30**), feature lanthanide(III) ions complexed by softer carbon atoms with relatively low charge density.[47] The synthesis and structure of **26**–**30** had been previously reported by Schumann et al. and by Evans et al.[48] The crystal structures of **26**–**30** reveal the presence of two conformations of each complex, staggered and eclipsed, each of which is defined by different positions of atoms within the planar $[C_8H_8]^{2-}$ rings. A slight bending of each structure at the lanthanide results in **26**–**30** having C_s point symmetry, with the mirror plane coinciding with the centroids of the two ligands and the lanthanide ion (Figure 9). Complexes **27**–**29** are SMMs in zero dc field; however, the dysprosium and holmium versions only show maxima in the $\chi''(T)$ plots in an yttrium matrix, that is, [(η^5-Cp*)$Ln_{0.05}Y_{0.95}$(η^8-COT)] with Ln = Dy (**27a**) or Ho (**28a**). The anistropy barrier for **27a** was measured as U_{eff} = 18 cm^{-1}, and the two relaxation processes in **28a** have U_{eff} = 23 and 17 cm^{-1}, respectively. The most pronounced SMM properties were observed in **29**, which shows maxima in the $\chi''(T)$ plots at frequencies in the range ν = 1–997 Hz, with the maximum for the highest frequency occurring at about 22 K. The two thermally activated relaxation processes in **29** have U_{eff} = 224 and 137 cm^{-1}, and corresponding pre-exponential factors of $\tau_0 = 8.17 \times 10^{-11}$ s and $\tau_0 = 3.13 \times 10^{-9}$ s, respectively. It was also possible to observe $M(H)$ hysteresis below 5 K in [(η^5-

dx.doi.org/10.1021/cr400018q | *Chem. Rev.* XXXX, XXX, XXX–XXX

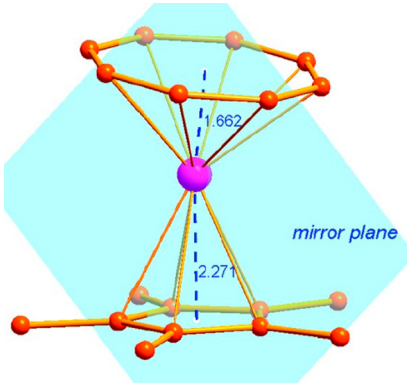

Figure 9. Molecular structure of **30** (from ref 47a).

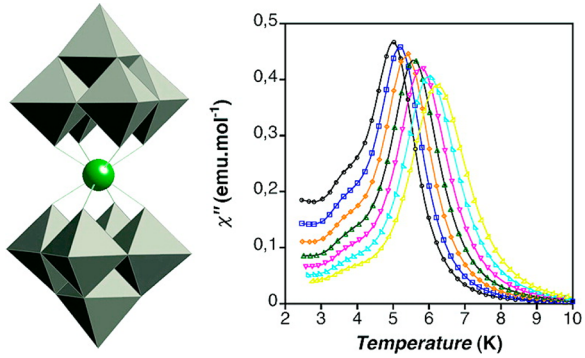

Figure 10. Structure of **35** and the out-of-phase susceptibility as a function of temperature, at several frequencies (ref 50a).

Cp*)$Er_{0.05}Y_{0.95}(\eta^8$-COT)] (**29a**) using a scan rate of 320 Oe/min, and hysteresis experiments using extremely fast sweep rates of up to 700 Oe/s produced a coercive field of H_c = 13 kOe. An attempt to understand the differing SMM properties of **27**−**29** was made by determining the structure of the m_J substates for each Ln^{3+} ion in an idealized $C_{\infty v}$ environment, that is, by discarding the bending that occurs in the molecular structures and treating the ligands as experiencing ring whizzing. Exaggerating the observed molecular symmetry in this way raises questions over the validity of the theoretical argument. The non-SMM behavior of **26** was explained by identifying a ground state with m_J = 0, and for **30** the first excited state has m_J = 0. Complexes **27**−**29** were found to possess bistable ground states and first excited states; however, in the case of **29** the energy gap between $m_J = \pm 15/2$ and $m_J = \pm 13/2$ was calculated as 190 cm^{-1}, which is consistent with the experimental U_{eff} value and therefore points to a thermal relaxation mechanism via the first excited state.

The SMM [Dy(η^8-COT″)(μ:η^8:η^2-COT″)Li(dme)(thf)], where COT″ = 1,4-bis(trimethylsilyl)cyclooctatetraene (**31**), shows multiple relaxation mechanisms, which can be observed by applying dc fields of various strengths.[49] In zero applied field, a thermally activated relaxation with U_{eff} = 12.5 cm^{-1} (τ_0 = 6 × 10^{-6} s) was characterized, and at temperatures below 3.75 K a QTM pathway was also identified. In applied fields greater than 100 Oe, a second thermally activated relaxation process becomes apparent, and at 200 Oe the original thermal relaxation has U_{eff} = 20.9 cm^{-1} with τ_0 = 6 × 10^{-6} s, and the second thermal relaxation has U_{eff} = 29.9 cm^{-1} with τ_0 = 3 × 10^{-7} s. In the optimum field of H_{dc} = 600 Oe, a single relaxation was presumed to be taking place, with U_{eff} = 29.9 cm^{-1} (τ_0 = 3 × 10^{-7} s).

Polyoxometallates (POMs) are robust ligands capable of encapsulating lanthanides in high-symmetry coordination environments, making them well suited to SMM applications. The POM-containing complexes $[Ln(W_5O_{18})_2]^{9-}$ are known with Ln = Tb (**32**), Dy (**33**), Ho (**34**), and Er (**35**), with the Ln^{3+} cation in a near-ideal {LnO_8} square-antiprismatic geometry, with a twist angle of 44.2° between the two square planes of the coordinating oxygens (Figure 10).[50]

The erbium-POM **35** is an SMM: an Arrhenius analysis of the $\chi''(\nu)$ data yielded U_{eff} = 38 cm^{-1} (τ_0 = 1.6 × 10^{-8} s), and the occurrence of a single relaxation mechanism was implied by the corresponding Cole−Cole plot, which was modeled with α = 0.03. Although **34** shows frequency dependence of χ' and χ'', the effects are less pronounced. Interestingly, $[TbPc_2]^-$ (**1**/**1a**) and $[Er(W_5O_{18})_2]^{9-}$ (**35**) are SMMs, but $[Tb(W_5O_{18})_2]^{9-}$ (**32**) and $[ErPc_2]^-$ (**35**) are not, possibly suggesting some sort of "inverse" relationship. This was interpreted using a detailed ligand field analysis of the POM complexes, which revealed that the ground state of **32** has m_J = 0; that is, it is not bistable. In contrast, the ground state of **35** has $m_J = \pm 13/2$ and can display easy-axis magnetization. In terms of molecular structure, the POM complexes are axially compressed and the phthalocyanine complexes are axially relatively elongated: even though the structural differences are slight, they do result in significant changes to the ligand field parameters and the stabilization of larger m_J values in **35**. The tetrametallic dysprosium-POM complex anion $[Dy_4\{As_5W_{40}O_{144}(H_2O)$-(glycine)$\}]^{21-}$ (**36**) can also be regarded as a monometallic SMM because the intramolecular Dy···Dy distances are quite long, at 5.944(3)−10.776(3) Å. Complex **36** has a relatively small anisotropy barrier of 2.7 cm^{-1} (τ_0 = 1.9 × 10^{-5} s).[51]

Double deprotonation of tetramethyldibenzotetraaza[14]-annulene gives the dianionic tetradentate ligand $[tmtaa]^{2-}$, which can be regarded as an analogue of the $[Pc]^{2-}$ ligand, but with a slightly smaller cavity size and only partial delocalization of the π electron density. The important difference between the $[tmtaa]^{2-}$ and $[Pc]^{2-}$ ligands stems from the 2-fold symmetry of the former, which allows investigations of the impact of a descent in molecular symmetry on ac magnetic susceptibility, relative to 4-fold symmetric Ln-SMMs such as **2**. The complexes $[Dy(tmtaa)_2K(DME)_2]$ (**37**), [K(DME)(18-crown-6)$][Dy(tmtaa)_2]$ (**38**) (Figure 11), and their diluted analogues $[Y_{0.95}Dy_{0.05}(tmtaa)_2K(DME)_2]$ (**37a**), [K(DME)(18-crown-6)$][Y_{0.95}Dy_{0.05}(tmtaa)_2]$ (**38a**), each contain eight-coordinate dysprosium in a square-prismatic environment.[52]

The X-band EPR spectra of the powdered tmtaa complexes at 5 K reveal the presence of significant magnetic anisotropy but, crucially, not of the Ising-type, as exemplified by **38** with the parameters $g_\perp$ = 1.25 and $g_\parallel$ = 15.15 ($g_\perp$ = 1.26 and $g_\parallel$ = 15.45 for **38a**). The $\chi''(T)$ ac susceptibility studies of all four tmtaa complexes revealed a frequency dependence at low temperatures in a small field of H_{dc} = 100 Oe, and from the experiments on **37a** and **38a** anisotropy barriers of 20 cm^{-1} (τ_0 = 7.06 × 10^{-8} s) and 24 cm^{-1} (τ_0 = 5.75 × 10^{-8} s), respectively, were extracted, that is, slightly smaller than those determined for the various forms of **2** in zero dc field. A secondary relaxation process, which shortcuts the thermal energy barrier, is also present in molecules of **37a** and **38a** at very low temperatures.

The trigonal prismatic complex $[Dy(H_2BPzMe_2)_3]$ (**39**), where H_2BPzMe_2 = dihydro-bis(dimethylpyrazolyl)borate, shows no frequency-dependent ac susceptibility curves under

dx.doi.org/10.1021/cr400018q | Chem. Rev. XXXX, XXX, XXX−XXX

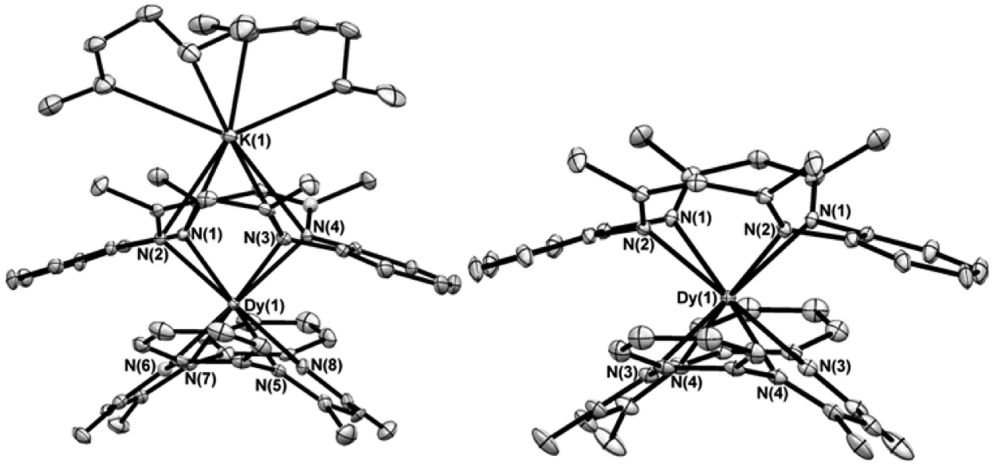

Figure 11. Molecular structures of **37** (left) and **38** (right) from ref 52.

any conditions in its pure form, but does show SMM behavior in zero field when diluted as $[Dy_aY_b(H_2BPzMe_2)_3]$ (a = 1, b = 65, **39a**; a = 1, b = 130, **39b**).[53] The ac susceptibility studies on dilute **39a**/**b** revealed the occurrence of two relaxation processes, the resolution of which improved with increasing dilution. Furthermore, increasing the level of dilution increased the anisotropy barrier and decreased τ_0 at 130:1 dilution in zero applied field; hence the relaxation in **39b** is characterized by U_{eff} = 16 cm^{-1} and $\tau_0 = 4 \times 10^{-7}$ s.

The monometallic complex cation $[Dy(L^2H_3)_2]^+$ (**40**), in which the ligand L^2H_3 (shown below) forms in situ via a Schiff-base condensation between 3-formylsalicylic acid and tris(2-ethylamino)amine, features a dysprosium(III) center in a distorted square-antiprismatic environment.

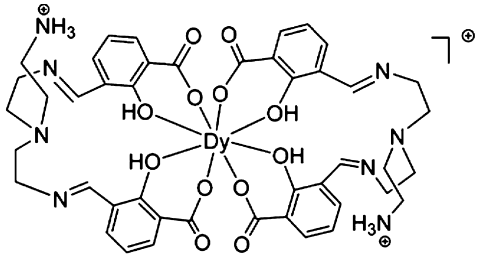

Pure **40** only shows frequency-dependent $\chi''(T)$ peaks in an applied field of 2000 Oe; however, the diluted analogue $[Dy_{0.195}Y_{0.805}(L^2H_3)_2]^+$ (**40a**) shows a similar response in field of only 200 Oe, with U_{eff} = 42 cm^{-1} and $\tau_0 = 4.4 \times 10^{-11}$ s. Ab initio calculations on **40** allowed the g-tensors for the ground Kramers doublet (i.e., the ground m_J sublevel) to be determined as g_x = 0.0238, g_y = 0.0445, and g_z = 18.7688. The computational study identified that intermolecular dipolar interactions in crystals of **40** (and **40a**) are probably too weak to influence the magnetism of individual dysprosium ions, and disorder and uncertainties in the H-atom positions may contribute to uncertainty in the direction of the anisotropy axis on the Dy centers.

In the multidentate Schiff-base/phenolate-ligated complex $[Dy(hmb)(NO_3)_2(dmf)]$ (**41**) (dmf = dimethylformamide, Hhmb = N'-(2-hydroxy-3-methoxybenzylidene)-benzohydrazide, which contains a nine-coordinate Dy(III) ion, the SMM properties are also not observable in zero applied field. However, in the optimum field of H_{dc} = 1800 Oe, slow relaxation of the magnetization is induced, with U_{eff} = 24 cm^{-1} ($\tau_0 = 3.2 \times 10^{-6}$ s).

3.1.2.1. β-Diketonate Monometallic Ln-SMMs. The ac magnetic susceptibility properties of several eight-coordinate, distorted square-antiprismatic β-diketonate (acetylacetonate) complexes of the type $[Ln(\beta\text{-diketonate})_3(L)_n]$ have been studied. Such complexes are readily accessible with a broad range of diketonates, and with uncharged ligands L that can be mono- or bidentate (n = 2 or 1, respectively) (Figures 12 and 13).

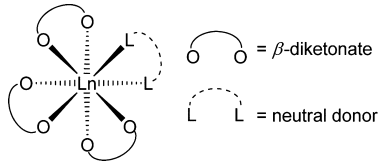

Figure 12. Idealized square-antiprismatic structure of $[Ln(\beta\text{-diketonate})_3(L)_n]$ complexes.

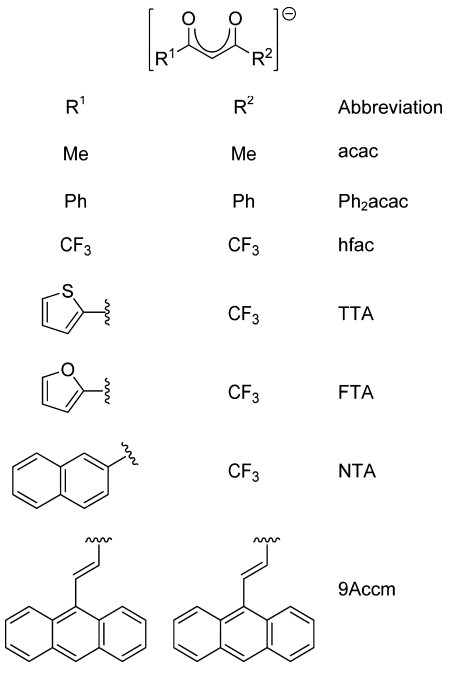

Figure 13. β-Diketonate ligands used in Ln-SMMs.

dx.doi.org/10.1021/cr400018q | *Chem. Rev.* XXXX, XXX, XXX−XXX

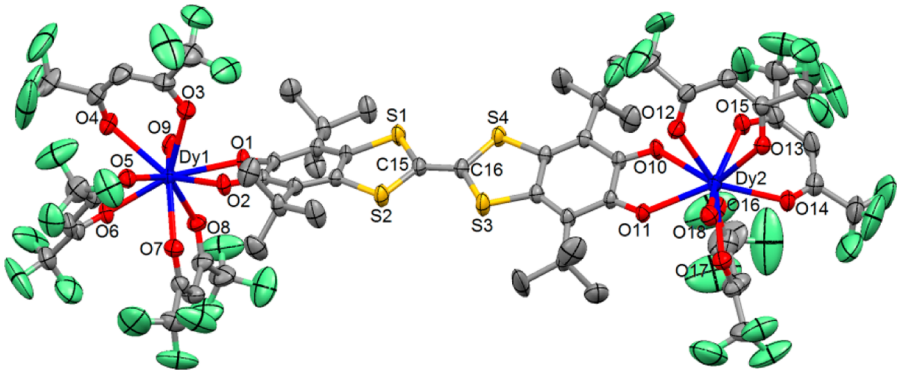

Figure 14. Molecular structure of **50** (from ref 63).

The out-of-phase susceptibility of undiluted polycrystalline $[Dy(acac)_3(H_2O)_2]$ (**42**) (acac = acetyl acetonate) is temperature dependent at ac frequencies greater than ν = 31.6 Hz, leading to U_{eff} = 45.9 cm^{-1} with $\tau_0 = 8.0 \times 10^{-7}$ s.[56] Dilution experiments with Dy:Y ratio of 1:20 (**42a**) apparently decrease the anisotropy barrier slightly to U_{eff} = 44.7 cm^{-1}, although maxima in $\chi''(T)$ can be observed above ac frequencies of ν = 1 Hz. Further dilution to 1:50 (**42b**) increased the anisotropy barrier to U_{eff} = 46.8 cm^{-1}, and the dilution experiments on **42a**/**b** also enabled $M(H)$ hysteresis loops to be recorded at 2 K. Replacing the aquo ligands in **42** with bidentate 1,10′-phenanthroline produces $[Dy(acac)_3(1,10'\text{-phen})]$ (**43**), which shows SMM properties in zero field that are very similar to those of **34**, with U_{eff} = 44.4 cm^{-1}.[57]

Small differences in the molecular structures of $[Dy(TTA)_3(2,2'\text{-bipy})]$ (**44**) and $[Dy(TTA)_3(1,10\text{-phen})]$ (**45**), where TTA = 1-(2-thiophenyl)-3-trifluoromethylacetylacetonate and bipy = bipyridyl, lead to different SMM properties.[58] Undiluted **44** and **45** both display maxima in $\chi''(T)$ at frequencies greater than 300 Hz, but in zero field they have anisotropy barriers of 40 cm^{-1} ($\tau_0 = 3.4 \times 10^{-7}$ s) and 59 cm^{-1} ($\tau_0 = 3.8 \times 10^{-7}$ s), respectively; that is, that of **45** is almost 50% greater than that of **44**. Dilution experiments with the isostructural yttrium complexes (Dy:Y = 0.05:0.95), giving **44a** and **45a**, significantly increased the anisotropy barriers to 67 and 75 cm^{-1} in **44a** and **45a**, respectively, with $M(H)$ hysteresis being measured at 1.9 K in both cases. These observation suggest that nearest-neighbor dipolar interactions in **44** and **45** are significant. The larger U_{eff} values determined for **45** have been interpreted in terms of the greater deviation from ideal square antiprismatic geometry in **44** (ϕ = 39.7°) relative to that in **45** (ϕ = 42.1°). Replacing the bidentate *N*-donor ligand in **44** and **45** with 4,5-pinene-bipyridyl (PBP) gives $[Dy(TTA)_3(4,5\text{-PBP})]$ (**46**), which shows no maxima in the $\chi''(T)$ plot in zero field, but applying a 2 kOe field allowed a barrier of U_{eff} = 28.5 cm^{-1} to be extracted.[59] Ligand field analysis of **42**, **44**, and **45** identified that, within the ^6H electronic ground state of Dy(III), the lowest Kramers doublet has $m_J = \pm 13/2$ and the first excited Kramers doublet has $m_J = \pm 11/2$. The calculated energy gaps between ground and first-excited sublevels in **42**, **44**, and **45** are 27.8, 20.1, and 29.3 cm^{-1}, respectively: these values are thought to be consistent with the U_{eff} values determined from ac susceptibility measurements, and therefore imply thermally assisted relaxation.

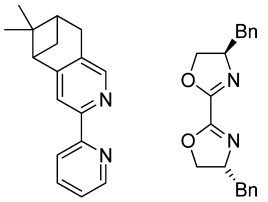

PBP BBO

The C_3-symmetric, square-antiprismatic complex $[Dy(FTA)_3(BBO)]$ (**47**), with FTA = 1-(2-furanyl)-3-trifluoromethylacetylacetonate and BBO = *S*,*S*-bis(4-benzyl-2-oxazoline), is a bifunctional material, displaying ferroelectric properties and SMM behavior in zero-field.[60] The best fit of the ac susceptibility data produced U_{eff} = 37.8 cm^{-1} with $\tau_0 = 8.7 \times 10^{-6}$ s. The chirality in **46** originates from the oxazoline ligand, and although this property produces no improvements in the anisotropy barrier relative to, for example, **42**−**45**, the ferroelectric hysteresis is a direct consequence of the polarity of the C_3 molecular symmetry. The chiral complex $[Dy(Ph_2acac)_3(R\text{-}L^3)]$ (**48**), where R-L^3 = *R*-2,5-bis(4,5-pinene-2-pyridyl)pyrazine, is also an SMM with U_{eff} = 33 cm^{-1} ($\tau_0 = 1.37 \times 10^{-7}$ s); however, the nonpolar space group precludes any ferroelectric properties.[61] The bicapped trigonal prismatic complex $[Dy(NTA)_3(S,S\text{-}Ph_2en)]$ (**49a**), where NTA is 1-(2-naphthyl)-3-trifluoromethyl and *S*,*S*-Ph_2en is 1*S*,2*S*-diphenylethylenediamine, forms in ethanol solvent, and its distorted dodecahedral isomer (**49b**) forms when acetone is used as the solvent.[62] In an applied field of H_{dc} = 2 kOe, maxima are observed in the $\chi''(T)$ plot for **49a**, with U_{eff} = 21.1 cm^{-1}, but not for **49b**, and although neither compound is an SMM in the strictest sense, the impact of the change in the coordination geometry on the dynamic magnetism (at least in an applied field) is significant.

The dimetallic complex $[Dy_2(hfac)_6(H_2O)_2(L^4)]$ (**50**) (hfac = hexafluoroacetylacetonate, L^4 = 4,4′,7,7′-tetra-*tert*-butyl-2,2′-bi-1,3-benzodithiole-5,5′,6,6′-tetrone) contains nine-coordinate dysprosium ions in D_{3h}-symmetric coordination environments, and illustrates why dividing Ln-SMMs by metal content is artificial (Figure 14).[63] While **50** obviously contains two dysprosium ions, their intramolecular separation is almost 17.5 Å, implying that only single ion effects are likely to be important. The intermolecular Dy···Dy separation of approximately 5.96 Å means that **50** could instead be regarded as a pseudodimer; however, no significant intermolecular interactions (via hydrogen bonds) were found. In the related, sterically bulkier complex $[Dy_2(TTA)_6(L^4)]$ (**51**), the eight-coordinate dysprosium ions occupy bicapped trigonal prismatic

dx.doi.org/10.1021/cr400018q | *Chem. Rev.* XXXX, XXX, XXX−XXX

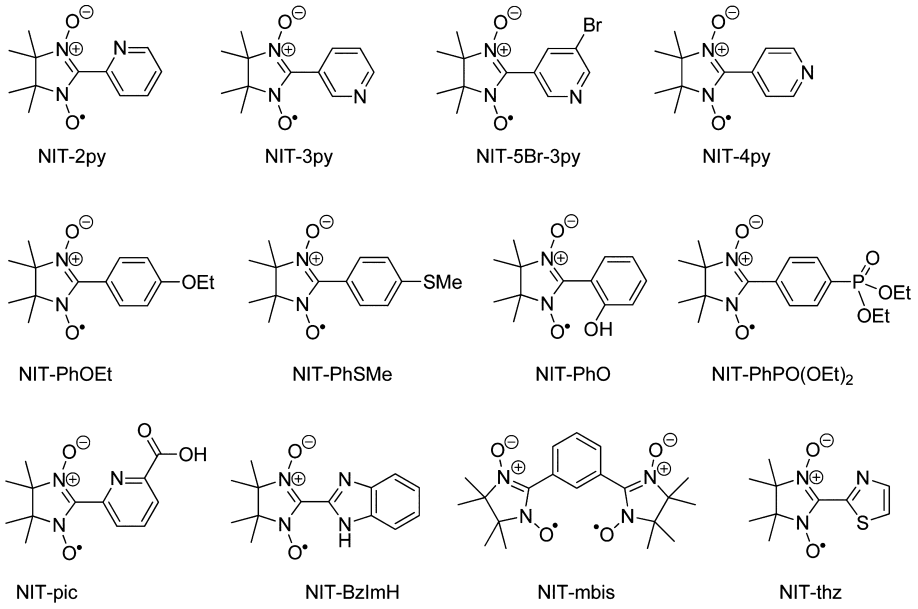

Figure 15. Nitronyl-nitroxide ligands used in Ln-SMMs.

geometries with C_{2v} symmetry, and the intermolecular Dy···Dy separation is much greater, at 11.08 Å. The absence of intra- and intermolecular interactions between the dysprosium centers in **50** and **51** suggests that the symmetry of the local coordination environments can account for why **51** is not an SMM, but **50** is an SMM with a zero-applied-field anisotropy barrier of U_{eff} = 11 cm^{-1} (τ_0 = 2.4 × 10^{-6} s).

The anthracene-substituted, eight-coordinate dysprosium complex [Dy(9Accm)$_2$(NO$_3$)(dmf)$_2$] (**52**) was developed to investigate the properties of an SMM that also has the capability to show fluorescence and to attach to graphite surfaces via $\pi-\pi$ stacking interactions.[64] In an applied field of 1000 Oe, temperature- and frequency-dependent out-of-phase susceptibility was observed in **52** below 10 K, with maxima being observed up to 6 K, and an anisotropy barrier of U_{eff} = 16 cm^{-1} (τ_0 = 1.3 × 10^{-6} s). Complex **52** also shows ligand-based luminescence with a broad emission centered on 577 nm. Furthermore, **52** was revealed by atomic force microscopy to have been deposited on highly oriented pyrolitic graphite surfaces via spin-coating experiments.

The study of lanthanide compounds containing radical nitronyl nitroxide (NIT) ligands (Figure 15) is an established branch of molecular magnetism,[65] but such compounds have only recently been developed for Ln-SMM applications. The complexes [Ln(hfac)$_3$(NIT-R)$_n$] have been structurally characterized with NIT-R = NIT-2py = 2-(2′-pyridyl)-4,4,5,5-tetramethylimidazoline-1-oxyl-3-oxide and Ln = Tb (**53**) or Dy (**54**) (Figure 16),[66] both with n = 1; NIT-R = 2-[4-(methylthio)phenyl]-4,4,5,5-tetramethylimidazoline-1-oxyl-3-oxide, Ln = Tb, and n = 1 (**55**);[67] and NIT-R = 2-(2′-thiazolyl)-4,4,5,5-tetramethylimidazoline-1-oxyl-3-oxide, Ln = Tb (**56**), and n = 2.[68]

Each of **53**−**56** shows a frequency dependence of $\chi''(T)$, but only the data for the eight-coordinate terbium complex **53** show maxima, and hence discernible SMM behavior in zero applied field, with U_{eff} = 11.9 cm^{-1} and τ_0 = 9.56 × 10^{-7} s. SMM behavior in zero dc field was also determined for the distorted dodecahedral terbium complex [Tb(hfac)$_3$(NIT-PhOEt)$_2$] (NIT-PhOEt = 4′-ethoxyphenyl-4,4,5,5-tetramethylimidazoline-1-oxyl-3-oxide) (**57**)[69] and the bicapped trigonal

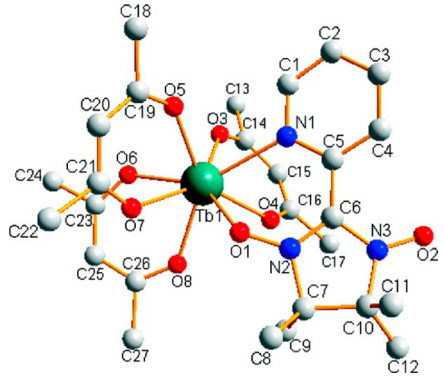

Figure 16. Molecular structure of **53** (from ref 66).

prismatic complex [Dy(tfa)$_3$(NIT-2py)] (**58**),[70] which show U_{eff} = 20.4 cm^{-1} and τ_0 = 2.99 × 10^{-8} s, and U_{eff} = 14.8 cm^{-1} and τ_0 = 1.54 × 10^{-8} s, respectively. Closely related to **57** are the SMMs [Ln(tfa)(NIT-BzImH)], where NIT-BzImH = 2-(2′-benzimidazolyl)-4,4,5,5-tetramethylimidazolyl-1-oxyl-3-oxide (Ln = Tb, **59**; Ln = Dy, **60**).[71] In **59**, the $\chi''(T)$ plots show maxima below 4 K, and the resulting Arrhenius analysis produces U_{eff} = 9.7 cm^{-1} (τ_0 = 4.56 × 10^{-7} s); in **60** no maxima are observed in $\chi''(T)$, but an anisotropy barrier of U_{eff} = 3.2 cm^{-1} (τ_0 = 3.55 × 10^{-7} s) was estimated.

The radical ligand NIT-picolinate coordinates to terbium in a terdentate manner in [Tb(NIT-pic)$_3$] (**61**), resulting in a distorted tricapped trigonal-prismatic geometry.[72] The maxima in the $\chi''(T)$ plot for **61** are well-defined below about 3 K, and the Arrhenius analysis gave U_{eff} = 15.8 cm^{-1} with τ_0 = (5.5 ± 1.1) × 10^{-9} s. Using a Hall probe at temperatures in the range 0.35−3.0 K, $M(H)$ hysteresis loops for **61** were observed, the first time that such an observation had been made on a lanthanide-NIT complex. Below 0.7 K, the coercive field is temperature independent, which suggests that the magnetization reverses via a QTM process. Exchange interactions between terbium and the three radical ligands could in principle alter the structure of the m_J sublevels; however, these interactions are sufficiently weak in **61** that clear SMM

dx.doi.org/10.1021/cr400018q | Chem. Rev. XXXX, XXX, XXX−XXX

Table 3. Dimetallic Lanthanide SMMs[a]

SMM	U_{eff}/cm^{-1} (H_{dc}/Oe)	hysteresis (K)	ref
$[KL_8][Tb_2\{N(SiMe_3)_2\}_4(thf)_2(N_2)]$ (**65**)[b]	227		76b
$[KL_8][Dy_2\{N(SiMe_3)_2\}_4(thf)_2(N_2)]$ (**66**)[b]	123		76a
$[KL_8][Ho_2\{N(SiMe_3)_2\}_4(thf)_2(N_2)]$ (**67**)[b]	73		76b
$[KL_8][Er_2\{N(SiMe_3)_2\}_4(thf)_2(N_2)]$ (**68**)[b]	36 (1000)		76b
$[(\eta^5\text{-Cp})_2Tb(\mu\text{-bpym})]_2[BPh_4]$ Tb (**70**)	44		77
$[(\eta^5\text{-Cp})_2Dy(\mu\text{-bpym})]_2[BPh_4]$ Dy (**71**)	88	6.5	77
[PcTb(μ-Pc)Tb{Pc(OBu)$_8$}] (**72**)			78
[PcY(μ-Pc)Tb{Pc(OBu)$_8$}] (**73**)			78
[PcTb(μ-Pc)Y{Pc(OBu)$_8$}] (**74**)			78
$[Tb_2\{Pc(OBu)_8\}_3]$ (**82**)	230	1.5	80
$[Dy\{Pc(OBu)_8\}_2]_2$ (**83**)$_2$	44	1.8	81
[PcTb(μ-Pc)Tb{(*p*-MeO)PP}] (**84**)			82
[PcTb(μ-Pc)Y{(*p*-MeO)PP}] (**85**)			82
$[Dy_2(ovph)_2Cl_2(MeOH)_3]$ (**87**)	104, 108	1.5[c]	83
$[Dy(Me_5trenCH_2)(\mu\text{-}H)_3Dy(Me_6tren)]^{2+}$ (**88**)	65, 15		84
$[Dy_2(ovph)_2(NO_3)_2(H_2O)_2]$ (**89**)	43		85
$[Dy_2(Hovph)(ovph)(NO_3)_2(H_2O)_4]$ (**90**)	0.9		85
$[Dy_2(HL^6)_4(CO_3)]$ (**92**)	12		86
$[Dy_2(HL^7)_2(NO_3)_2(MeOH)_2]$ (**93**)	29		86
$[Dy(valdien)(NO_3)]_2$ (**97**)	53		87
$[Dy_2(spd)_2(acac)_2(H_2O)]$ (**99**)	25, 56		89
$[Yb_2(spd)_2(acac)_2(H_2O)]$ (**100**)	17 (1600)		90
$[NEt_4]_2[Dy_2(L^8)_4]$ (**101**)	9, 70 (1600)		91
$[NEt_4]_2[Dy_2(L^9)_4]$ (**102**)	49 (1200)		91
$[NEt_4]_2[Dy_2(L^{10})_4]$ (**103**)	14 (1600)		91
$[Dy_2(hmb)(NO_3)_4(dmf)_4]$ (**104**)	29 (1800)		55
$[Dy(hmi)(NO_3)(MeOH)]_2$ (**105**)	39		92
$[\{Dy(hmi)(NO_3)(MeOH)\}_2\cdot MeCN]_\infty$ (**106**)	49		92
$[Dy_2(api)_2]$ (**107**)	18		93
$[Cp_2Dy(\mu\text{-}SSiPh_3)]_2$ (**108**)	133	1.8	95
$[Cp_2Dy(\mu\text{-}Cl)]_2$ (**109a**)	26		96
$[Cp_2Dy(\mu\text{-}Cl)]_\infty$ (**109b**)	68		96
$[Cp_2Dy(thf)(\mu\text{-}Cl)]_2$ (**110**)	34	0.04[c]	96
$[Cp_2Dy(\mu\text{-bta})]_2$ (**111**)	33		97
$[Dy(NaphCO_2)_3(phen)(H_2O)]_2$ (**112**)	20		98
$[Dy(NaphCO_2)_3(phen)]$ (**113**)	4		98
$[\{Dy(OAc)_3(MeOH)\}_2]_\infty$ (**115**)		0.5[c]	99
$[Dy_2(HBpz_3)_4(\mu\text{-ox})]$ (**116**)	29		100
$[Dy_2(3\text{-Htzba})_2(3\text{-tzba})_2(H_2O)_8]$ (**117**)	37		101
$[Dy(hfac)_3(H_2O)_2(pyz)]_2$ (**120**)	77		104
$[Dy_2(Ph_2acac)_6(R\text{-}L^3)]$ (**121**)	62		61
$[Dy(hfac)_3(\mu\text{-pyNO})]_2$ (**122**)	116	1.4	105
$[Dy(hfac)_3\{\mu\text{-(pyNO-ttf)}\}]_2$ (**123**)	60		106
$[Dy(hfac)_3(NIT\text{-}m\text{bis})]_2$ (**124**)$_2$	8		107
$[Tb(hfac)_3\{NITPhPO(OEt)_2\}]_2$ (**125a**)	17, 19 (2000)		108
$[Tb(hfac)_3\{NITPhPO(OEt)_2\}]_2$ (**125b**)	15 (2000)		108
$[Tb(hfac)_3(NIT\text{-3py})]$ (**126**)	13		109
$[Tb(hfac)_3(NIT\text{-5Br-3py})]$ (**127**)	20		110
$[Tb(Ph\text{-tfac})_3(NIT\text{-4py})]$ (**128**)	18		111
$[Dy_2(hfac)_4(NIT\text{-PhO})_2]$ (**130**)	5.3		112

[a] U_{eff} values are extracted from measurements in zero applied dc field, unless followed by a number in parentheses to indicate the strength of the applied field. Hysteresis measurements correspond to polycrystalline samples, except where indicated. Lattice solvent molecules are not listed. [b] $[KL_8] = [K(18\text{-crown-}6)(thf)_2]^+$. [c] Single-crystal micro-SQUID.

behavior is still observed. Other radical ligands, such as tetrafluorotetracyanoquinodimethane ($TCNQF_4$), have also been used in efforts to develop new Ln-SMMs.[73] In the series of complexes $[Ln(TCNQF_4)_2(H_2O)_6]TCNQF_4\cdot(3H_2O)$, with Ln = Tb (**62**), Y:Tb (74:26) (**62a**), and Y:Tb (97:3) (**62b**), SMM behavior was observed with the micro-SQUID technique for **62**; however, complex **62a** displayed SMM and phonon bottleneck effects. The magnetic properties of **62b** were due entirely to the phonon bottleneck, which was assigned to the influence of the $S = 1/2$ $TCNQF_4$ radicals.

The coordination polymer $[Cs\{Dy(Ph_2acac)_4\}]_n$ (**63**) contains dysprosium cations that occupy ideal D_{4d}-symmetric

dx.doi.org/10.1021/cr400018q | Chem. Rev. XXXX, XXX, XXX−XXX

environments through complexation by four $[Ph_2acac]^{2-}$ ligands.[74] Structurally, **63** is a coordination polymer, and the alternating pattern of cesium and dysprosium ions allows the magnetism of **63** to be approximated as a single-ion system. Although frequency-dependent $\chi''(T)$ curves were observed in zero dc field, they do not show maxima. However, micro-SQUID measurements on **63** do show magnetic hysteresis below 0.5 K, and the lack of a QTM step at zero-field implies weak single-chain magnet (SCM) properties.

Studies of ytterbium(III) complexes as candidates for SMM applications are slowly emerging. Ytterbium offers the potential to manipulate easy-plane anisotropy to observe slowly relaxing magnetization, as opposed to the easy-axis anisotropy routinely encountered with terbium(III) and dysprosium(III). To date, only one monometallic ytterbium system has been investigated, the octahedral complex $[Yb(H_3L^5)_2]Cl_3\cdot(5MeOH)\cdot(2H_2O)$ (**64**).[75] Complex **64** does indeed show temperature- and frequency-dependent ac susceptibility in an applied field of 400 Oe, and an anisotropy barrier of $U_{eff} = 3.5$ cm^{-1} and $\tau_0 = 2.0 \times 10^{-5}$ s was cautiously estimated.

3.2. Polymetallic Ln-SMMs

Many polymetallic lanthanide cage complexes with clear SMM properties (and an appreciable number with less clear SMM properties) have been reported in the last several years, the majority of which are based on dysprosium. Indeed, Dy-SMMs are now so common that examples of polymetallic dysprosium compounds that do not show SMM behavior are almost more remarkable than those that do. Examples of Ln-SMMs ranging from dimetallic up to octametallic are known, but with cage complexes containing more than eight lanthanide centers the SMM behavior is usually weak. The following sections illustrate that, in addition to their intriguing magnetic properties, polymetallic Ln-SMMs have also provided a wealth of beautiful structural chemistry. The range of ligand types used to assemble polymetallic SMMs is somewhat limited, with the μ-bridging interactions between lanthanide centers mostly being based on *O*-donors: phenolate, carboxylate, and acetylacetonate ligands have proven to be particularly popular scaffolds for constructing polymetallic SMMs.

3.2.1. Bimetallic SMMs. Single-molecule magnets containing two lanthanide ions form a large subset, with dysprosium-containing versions being particularly common.[15g] The set of $\{Ln_2\}$ SMMs is listed in Table 3 along with pertinent SMM parameters. The range of ligand types used to bridge between the metals in dimetallic SMMs is quite broad, and includes phthalocyanines, phenolates, *N*-donors, halides, thiolates, and carboxylates.

3.2.1.1. Exchange Coupling and Bimetallic SMMs. The radially contracted nature of 4f orbitals tends to result in very weak intramolecular exchange coupling in polymetallic lanthanide compounds. Consequently, in the vast majority of polymetallic Ln-SMMs, the magnetic properties are dominated by single-ion effects. Determination of exchange coupling constants *J* from experimental susceptibility data using simple spin Hamiltonians is usually possible in the case of spin-only gadolinium compounds ($^8S_{7/2}$, $g = 2$), whereas for the other lanthanides the effects of spin−orbit coupling can render this task somewhat formidable. Polymetallic gadolinium compounds have *J*-values typically in the range 0.1−3 cm^{-1}, which is much smaller than any useful energy barrier.

In light of the weak magnetic exchange in most polymetallic lanthanide compounds, the dilanthanide salts $[K(18\text{-crown-}6)(thf)_2][Ln_2\{N(SiMe_3)_2\}_4(thf)_2(\mu{:}\eta^2{:}\eta^2\text{-}N_2)]$ with Ln = Gd (**64**), Tb (**65**), Dy (**66**), Ho (**67**), and Er (**68**) are in a class of their own (Figure 17).[76] Compounds **64**−**68** have remarkable

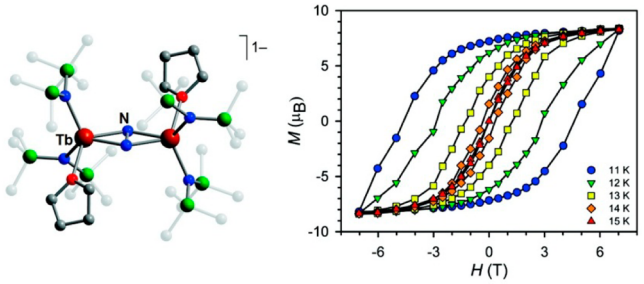

Figure 17. Structure of $[Tb_2\{N(SiMe_3)_2\}_4(thf)_2(\mu{:}\eta^2{:}\eta^2\text{-}N_2)]^-$ and plot of magnetization versus field for **65** using a sweep rate of 0.9 mT s^{-1} (from ref 76b).

electronic structure because of the influence of the radical $[N_2]^{3-}$ ligand ($S = 1/2$), and in the case of **64** a huge intramolecular exchange coupling constant of $J = -27$ cm^{-1} was determined.

The strong exchange coupling in **64** and, by extension, in **65**−**68** occurs as a result of the diffuse spin density on the $[N_2]^{3-}$ ligand, which can penetrate the core-like 4f orbitals of the gadoliniums. The ability of the radical ligand to interact so strongly with the orbital manifold of lanthanides allows one lanthanide ion to serve as a field bias on the other. The effect of this is to shift otherwise-degenerate m_J sublevels to different energies, which significantly reduces the probability of resonant quantum tunneling and lengthens the relaxation time. Thus, the combination of the strong anisotropy of terbium(III) with the strong exchange results in **65** being arguably the most successful SMM to date, due to its $M(H)$ hysteresis occurring at a record T_B of 14 K (using a sweep rate of 0.9 mT s^{-1}). The dysprosium congener **66** shows hysteresis up to $T_B = 8.3$ K, with a sweep rate of 80 mT s^{-1}. The zero-field anisotropy barriers for **65** and **66**, determined from ac susceptibility data, are $U_{eff} = 227$ cm^{-1} ($\tau_0 = 8.2 \times 10^{-9}$ s) and 123 cm^{-1} ($\tau_0 = 8 \times 10^{-9}$ s). Although **67** and **68** do not show $M(H)$ hysteresis, it was possible to measure a zero-field anisotropy barrier of $U_{eff} =$ 73 cm^{-1} for **67**; however, **68** only shows significant SMM behavior in an applied field of 1000 Oe, with $U_{eff} = 36$ cm^{-1}. The much weaker SMM properties of **67** and **68** could be due to weaker anisotropy of holmium(III) and erbium(III), or to weaker exchange as a consequence of the more-contracted nature of the 4f orbitals of these later lanthanides, or to more prominent QTM as a result of hyperfine interactions with ^{165}Ho or ^{167}Er.

The series of radical-bridged complexes $[(\eta^5\text{-}Cp)_2Ln(\mu\text{-}bpym)]_2[BPh_4]$, where Ln = Gd (**69**), Tb (**70**), or Dy (**71**) (Figure 18), were developed using an approach similar to that used for **64**−**68**. In **69**, the diffuse spin density on the bipyrimidyl (bpym) radical-anion ligand promotes strong exchange coupling, with $J = -10$ cm^{-1}.[77] The SMM properties of **70** and **71** should therefore be influenced by an exchange bias as in **65** and **66**, and hence the resulting U_{eff} values are 44 and 88 cm^{-1} in **70** and **71**, respectively. Compound **71** also shows $M(H)$ hysteresis, with distinct steps, below 6.5 K.

3.2.1.2. Multidecker Phthalocyanine SMMs. Triple-decker, dilanthanide tris(phthalocyaninate) complexes with the general formula $[Pc^1Ln(\mu\text{-}Pc^2)Ln(Pc^3)]$ are known in homoleptic and

dx.doi.org/10.1021/cr400018q | Chem. Rev. XXXX, XXX, XXX−XXX

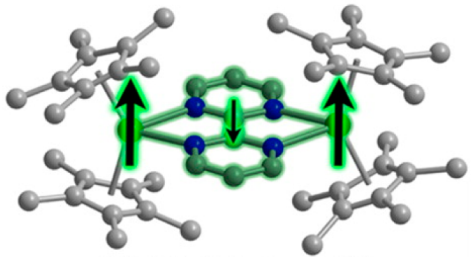

Figure 18. Molecular structure of **69**−**71**, indicating the nature of the exchange coupling (from ref 77).

heteroleptic forms. The metal ions within the triple-decker molecules are separated by approximately 3.6 Å, allowing the effects of intramolecular f−f interactions on dynamic magnetic properties to be investigated. The first such investigation involved the series of complexes [PcTb(μ-Pc)Tb{Pc(OBu)$_8$}] (**72**), [PcY(μ-Pc)Tb{Pc(OBu)$_8$}] (**73**), and [PcTb(μ-Pc)Y{Pc(OBu)$_8$}] (**74**), which were synthesized according to Scheme 3.[78]

Scheme 3

$[TbPc_2] + [Tb(acac)_3] + H_2Pc(OBu)_8 \longrightarrow$ [PcTb(μ-Pc)Tb{Pc(OBu)$_8$}] (**72**)

$[YPc_2] + [Tb(acac)_3] + H_2Pc(OBu)_8 \longrightarrow$ [PcY(μ-Pc)Tb{Pc(OBu)$_8$}] (**73**)

$[TbPc_2] + [Y(acac)_3] + H_2Pc(OBu)_8 \longrightarrow$ [PcTb(μ-Pc)Y{Pc(OBu)$_8$}] (**74**)

Complexes **72**−**74** have to be purified carefully by chromatography to avoid contamination of the desired product with [TbPc$_2$]. The ac susceptibility properties of **72**−**74** were measured in diamagnetic matrices of the all-yttrium triple decker [PcY(μ-Pc)Y{Pc(OBu)$_8$}] (**75**), at dilution levels of 5% (**72a**−**74a**). The out-of-phase susceptibility for **72a** in zero dc field is strongly temperature dependent, with two overlapping maxima being observed at 20 and 27 K. Complexes **73a** and **74a** each feature one maximum in their $\chi''(T)$ plots at lower temperatures, implying that dipolar f−f interactions enhance the SMM properties of the diterbium complex **72a**. Application of H_{dc} = 2000 Oe, with the ac field oscillating at 997 Hz, shifts the $\chi''(T)$ maximum for **74a** to 27 K, suggesting that the terbium ion sandwiched between the two Pc ligands in **72a** gives rise to the 27 K maximum in zero dc field. Similarly, a 2000 Oe dc field increases the temperature of the $\chi''(T)$ maximum for **73a** to 20 K, meaning that the terbium ion in **72a** sandwiched between the bridging Pc ligand and the Pc(OBu)$_8$ ligand is responsible for the 20 K maximum of **72a** in zero dc field.

The significance of intramolecular dipolar f−f interactions over longer distances was demonstrated via the quadruple decker complexes [{(LnPc$_2$)$_2$}$_2$Cd], where Ln = Tb (**76**), Dy (**77**), or Er (**78**).[79] In **76**−**78**, the eight-coordinate cadmium(II) bridges between two {LnPc$_2$} moieties, resulting in Ln···Ln separations of approximately 6.8 Å. The f−f interactions were extracted by subtracting the $\chi_M T(T)$ plots of [(LnPc)$_2$Cd(YPc)$_2$] (Ln = Tb−Er, **79**−**81**) from those of **76**−**78**, and the resulting positive values of $\Delta(\chi_M T)$ for **76** and **77** reveal appreciable, long-range, ferromagnetic f−f interactions, which are particularly prominent below about 10 K. In contrast, **78** shows only weak f−f interactions. For **76** and **77**, the origins of the dipolar ferromagnetic interactions were assigned to the magnetic susceptibility tensors showing significant longitudinal extension. SMM properties were not reported for **76**−**81**.

The crystal and molecular structure of the triple-decker SMM [Tb$_2${Pc(OBu)$_8$}$_3$] (**82**) revealed an intramolecular Tb···Tb distance of 3.52 Å and a shortest intermolecular Tb···Tb distance of 10.98 Å (Figure 19).[80] Relative to the bridging Pc(OBu)$_8$ ligand, the terminal ligands produce a twist angle ϕ of 32°. As with **76**, the Tb···Tb dipolar interactions in the Ising dimer **82** are ferromagnetic, and analysis of the out-of-phase ac susceptibility data in zero dc field gave U_{eff} = 230 cm^{-1} with $\tau_0 = 1.1 \times 10^{-10}$ s. Micro-SQUID magnetization versus field measurements on single crystals of **82** produced hysteresis loops below 1.5 K, and in each case a large step at zero field was observed, suggesting that quantum tunneling occurs. Application of a 3000 Oe dc field to magnetically oriented polycrystalline samples of **82** showed that, in addition to the thermally activated relaxation, a second, temperature-independent relaxation process occurs below 10 K.

In terms of its molecular structure, the double-decker complex [Dy{Pc(OBu)$_8$}$_2$] (**83**) is clearly monometallic; however, the crystal structure reveals that molecules of **83** are arranged as "pseudodimers" along the *b*-axis, with a Dy···Dy separation of 7.56 Å.[81] The value of $\chi_M T$ for **83** in a 1000 Oe applied field, and for the analogous complex diluted into an isostructural yttrium matrix, gradually decreases with decreasing temperature, with a sharper decrease being observed below

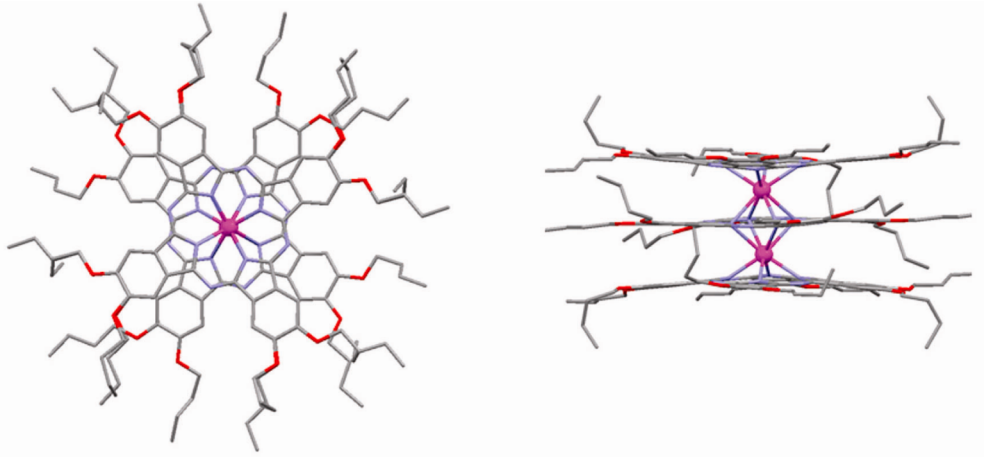

Figure 19. Molecular structure of [Tb$_2${Pc(OBu)$_8$}$_3$] (**82**) (from ref 82a).

dx.doi.org/10.1021/cr400018q | *Chem. Rev.* XXXX, XXX, XXX−XXX

about 15 K. These observations point toward the dysprosium(III) ions in dimers of $(\mathbf{83})_2$ being antiferromagnetically coupled via dipolar interactions. Pure **83** is an SMM with U_{eff} = 44 cm^{-1} and $\tau_0 = 1.3 \times 10^{-5}$ s, and $M(H)$ hysteresis loops were measured on polycrystalline samples below 1.8 K.

In the mixed phthalocyanine-porphyrin triple-decker complex [PcTb(μ-Pc)Tb{(*p*-MeO)PP}] (**84**), where (*p*-MeO)PP is tetra-5,10,15,20-(para-anisolyl)porphyrin, the terbiums are separated by 3.6 Å as in **72**.[82] However, one terbium in **84** occupies an ideal square-antiprismatic coordination site, and the other terbium coordination geometry is square prismatic. The difference in the temperature dependence of $\chi_M T$ for **84** relative to the monometallic analogues [PcTb(μ-Pc)Y{(*p*-MeO)PP}] (**85**) and [PcY(μ-Pc)Tb{(*p*-MeO)PP}] (**86**) revealed that the terbium(III) ions in **84** experience intramolecular ferromagnetic dipolar exchange. Complex **85** shows SMM behavior in zero dc field, but complex **86** does not, and the SMM properties of **84** are much more pronounced than either yttrium-doped analogue. Furthermore, χ'' measured at an ac frequency of 1000 Hz increases in two temperature regions, below 15 K and at 15−30 K, implying that the magnetization relaxation occurs in one terbium at lower temperatures and in the other terbium at higher temperatures. The square-prismatic terbium in **84** also produces a considerably longer relaxation time than that in **86**, the origins of which were determined by a ligand-field analysis. The analysis revealed that the square-antiprismatic terbium hinders the quantum tunneling in **84** as a result of the magnetic dipolar coupling between the two terbium ions.

3.2.1.3. Phenolate-Bridged Ln_2 SMMs. Unsymmetrical didysprosium compounds provide opportunities to study how interactions between Dy(III) ions with different coordination numbers, and hence differing anisotropies, influence dynamic magnetic properties. The phenolate-bridged compound $[Dy_2(ovph)_2Cl_2(MeOH)_3]\cdot MeCN$ (H_2ovph = *ortho*-vanillin picolinylhydrazone) (**87**) contains an eight-coordinate and a seven-coordinate dysprosium, and the dc susceptibility measurements reveal weak intramolecular ferromagnetic coupling (Figure 20).[83]

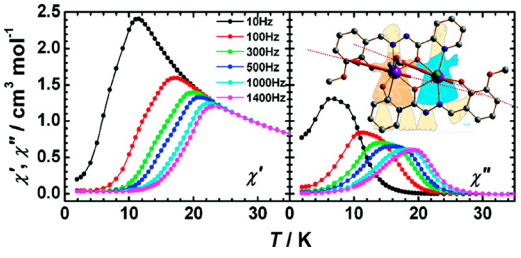

Figure 20. In-phase and out-of-phase susceptibility, molecular structure, and orientations of the anisotropy axes in **87** (from ref 83).

In **87**, the eight-coordinate dysprosium resides in a "hula-hoop" geometry, and the seven-coordinate dysprosium occupies a pentagonal-bipyramidal geometry, although the local symmetry of each ligand field is low. An ab initio computational study of **87** revealed *g*-tensors of g_x = 0.0008, g_y = 0.0018, and g_z = 19.6668 for the eight-coordinate dysprosium, and the seven-coordinate dysprosium has g_x = 0.0027, g_y = 0.0051, and g_z = 19.6880; that is, there is a larger transverse component in the latter case. The ferromagnetic exchange in **87** is dipolar in nature, which stems from the calculated local anisotropy axes and the Dy···Dy axis being aligned almost parallel with each other. A micro-SQUID single-crystal study of **87** showed two-step $M(H)$ hysteresis below 1.5 K, and as the measurement temperature decreased the coercivity increased significantly, implying slow QTM. The out-of-phase susceptibility of **87** revealed the occurrence of two relaxation processes, due to the two distinct dysprosium single-ion environments, and each process has a narrow distribution of relaxation times. The resulting U_{eff} values in zero dc field are 104 and 138 cm^{-1}, with τ_0 values of 2.3×10^{-8} and 7.3×10^{-9} s, respectively. An important observation on **87** is that low-symmetry coordination environments can produce efficient magnetization blocking in dysprosium SMMs.

The only known example of a hydride-bridged SMM, $[Dy(Me_5trenCH_2)(\mu\text{-}H)_3Dy(Me_6tren)][B\{C_6H_3(CF_3)_2\}_4]_2$ (Me_6tren = tris{2-(dimethylamino)ethylamine) (**88**), also contains an eight-coordinate and a seven-coordinate dysprosium(III) center, and features two relaxation processes, with U_{eff} = 65 and 15 cm^{-1}.[84] An ab initio computational study of **88** allowed the higher-energy process to be assigned to the eight-coordinate dysprosium, while fast QTM within the seven-coordinate dysprosium prevents detection of a blocking process.

Single or double deprotonation of H_2ovph can be affected by bases of differing strength, which enables access to a range of didysprosium compounds derived from **87**.[85] Thus, centrosymmetric $[Dy_2(ovph)_2(NO_3)_2(H_2O)_2]\cdot 2H_2O$ (**89**) forms when $Dy(NO_3)_3\cdot 6H_2O$ is reacted with H_2ovph in the presence of triethylamine, whereas the noncentrosymmetric compounds $[Dy_2(Hovph)(ovph)(NO_3)_2(H_2O)_4]\cdot NO_3\cdot 2MeOH\cdot 2H_2O$ (**90**) and $Na[Dy_2(Hovph)_2(\mu\text{-}OH)(OH)(H_2O)_5]\cdot 3Cl\cdot 2H_2O$ (**91**) form when pyridine or sodium azide is used as the base, respectively. In **89**, the eight-coordinate dysprosiums are coupled by weak ferromagnetism, and the dimer shows SMM behavior below about 19 K, with U_{eff} = 48 cm^{-1} and $\tau_0 = 5.3 \times 10^{-7}$ s. In noncentrosymmetric **90**, which contains two nine-coordinate dysprosiums in monocapped square-prismatic environments, the SMM behavior is very weak, with $U_{eff} \approx 0.9$ cm^{-1}. The dysprosiums in noncentrosymmetric **91** are also in monocapped square-prismatic environments; however, this compound is not an SMM. The contrasting responses of **89**−**91** to dynamic magnetic fields were assigned to the influence of the different coordination environments and the different orientations of the easy axes of magnetization. In particular, the dimetallic cores in **89**−**91** are chemically and geometrically distinct, suggesting that different intramolecular magnetic couplings between the Dy(III) ions will also influence the dynamic magnetism.

Using derivatives of the $[ovph]^{2-}$ ligand with differing aryl substituents appears to represent a general route to Dy_2 SMMs with varying magnetic properties. For example, the 1:1 stoichiometric reaction of $Dy(OAc)_3\cdot 4H_2O$ with *N*′-{(2-hydroxy-1-naphthyl)methylene}benzohydrazide (H_2L^6) gives the dimer $[Dy_2(HL^6)_4(CO_3)]\cdot 4H_2O$ (**92**), and $Dy(NO_3)_3\cdot 6H_2O$ reacts with *N*′-{(2-hydroxy-1-naphthyl)-methylene}picolinohydrazide (H_2L^7) in 1:1 stoichiometry to give $[Dy_2(HL^7)_2(NO_3)_2(MeOH)_2]\cdot 4MeCN$ (**93**) (Figure 21).[86] The eight-coordinate dysprosiums in both **92** and **93** reside in $\{N_2O_6\}$ environments; however, the dysprosiums in **92** are antiferromagnetically coupled, whereas those in **93** are ferromagnetically coupled. Both **92** and **93** are SMMs, with the dynamics of the magnetism being temperature dependent above 5 K. The thermally activated relaxation process in **92** has U_{eff} = 12 cm^{-1} ($\tau_0 = 2.04 \times 10^{-5}$ s), but **93** has an anisotropy

dx.doi.org/10.1021/cr400018q | *Chem. Rev.* XXXX, XXX, XXX−XXX

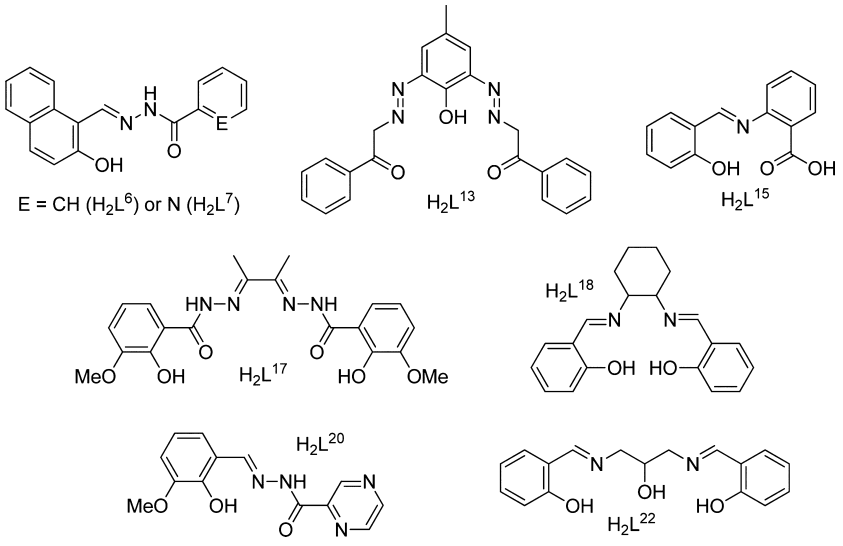

Figure 21. Structures of selected numbered pro-ligands.

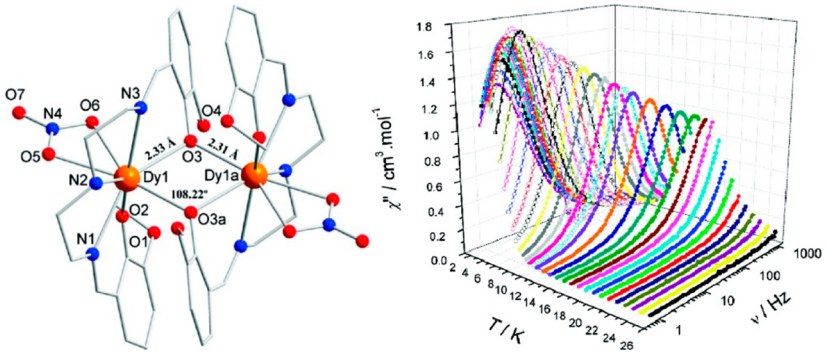

Figure 22. Molecular structure of **97**, and the frequency and temperature dependence of the out-of-phase susceptibility (from ref 87).

barrier of U_{eff} = 29 cm^{-1} (τ_0 = 1.91 × 10^{-6} s), i.e., more than double that of **92**.

The *ortho*-vanilin-derived ligand *N*,*N*″-bis(3-methoxysalicylidene)diethylenetriamine (H_2valdien) can be deprotonated by triethylamine in the presence of lanthanide(III) nitrates to give the centrosymmetric dimers [Ln(valdien)(NO_3)]$_2$, with Ln = Eu (**94**), Gd (**95**), Tb (**96**), Dy (**97**), and Ho (**98**), with **97** being an SMM in zero field.[87] The molecular structure of **97** consists of dysprosium ions complexed by a bidentate nitrate ligand and the three nitrogens and two phenolate oxygens of a valdien ligand, with one of the two phenolate oxygens in each valdien ligand bridging between the two Dy centers (Figure 22).

The asymmetric compound [Dy_2(spd)$_2$(acac)$_2$(H_2O)] (**99**) contains an eight-coordinate dysprosium and a seven-coordinate dysprosium, which arises from the [spd]$^{2-}$ ligand derived from *N*,*N*-bis(salicylidene)-*o*-phenylenediamine (i.e., H_2spd) ligand adopting a terminal bonding mode at the seven-coordinate dysprosium and bridging coordination mode between the two dysprosiums (Figure 23).[89] The eight-coordinate Dy(III) ions are therefore in {N_3O_5} environments, with geometries between the extremes of square antiprismatic and dodecahedral. The $\chi_M T(T)$ data for **97** reveal weak antiferromagnetic coupling, and an ab initio computational study determined an exchange coupling constant of J = −0.21 cm^{-1}. The out-of-phase magnetic susceptibility for **97** is temperature dependent in the range 4−25 K, and the

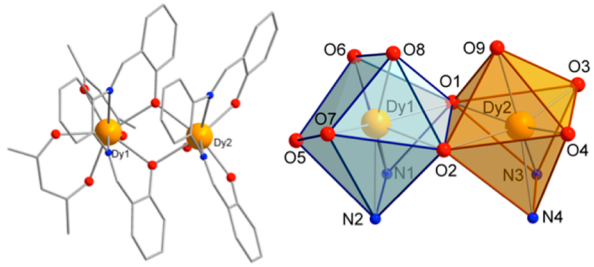

Figure 23. Molecular structure of **99** and polyhedral representations of the Dy coordination environments (from ref 89).

appearance of a single, thermally activated Orbach relaxation was corroborated with a Cole−Cole plot modeled with α < 0.3. The resulting anisotropy barrier was determined to be 53 cm^{-1}, with τ_0 = 6 × 10^{-7} s, and below 4 K, the magnetization in **96** relaxes via QTM. A micro-SQUID single-crystal study of **97** revealed S-shaped, stepped hysteresis below 4 K, using applied fields in the range ±1.5 T. A magnetic dilution study was undertaken by synthesizing **97** in the presence of large excesses of the yttrium analogue, leading to the cocrystallization of **97** and [Dy_aY_b(valdien)(NO_3)]$_2$ (**97a**) and in a diamagnetic matrix.[88] Dilution levels of 1:20, 1:10, and 1:1 Dy:Y were used, with the results demonstrating that the slowly relaxing magnetization in **97** does indeed stem from single-ion effects. The intramolecular exchange interactions in **97** can be regarded as small but significant, because the QTM processes that

dx.doi.org/10.1021/cr400018q | *Chem. Rev.* XXXX, XXX, XXX−XXX

characterize the relaxation at low temperatures are intimately connected with the influence of one Dy(III) ion on its symmetry-related partner. As in the asymmetric compound **87**, the Dy(III) ions in **99** are coupled ferromagnetically, and **99** also shows two relaxation processes in the ac susceptibility. Thus, using an ac frequency of 1500 Hz, a maximum in the plot of $\chi''(T)$ in zero dc field is observed at 6 K, along with a broad shoulder around 8−12 K. One relaxation process in **99** is due to the dysprosium in a square-antiprismatic coordination geometry, and the other is due to the dysprosium in a distorted capped trigonal-prismatic geometry. The U_{eff} values were found to be 25 cm^{-1} ($\tau_0 = 4.2 \times 10^{-7}$ s) and 56 cm^{-1} ($\tau_0 = 8.3 \times 10^{-8}$ s), although it was not possible to assign either process to the corresponding single Dy(III) ion on the basis of susceptibility data alone. The analogous ytterbium complex $[Yb_2(spd)_2(acac)_2(H_2O)]$ (**100**) displays field-induced SMM behavior, with the optimum field of H_{dc} = 1600 Oe producing U_{eff} = 17 cm^{-1} ($\tau_0 = 6.8 \times 10^{-7}$ s) and 56 cm^{-1} ($\tau_0 = 8.3 \times 10^{-8}$ s).[90]

Changing the salen ligand in **99** from *ortho*-disubstituted phenylene to *para*-disubstituted phenylene or 4,4′-biphenyl derivatives results in the formation of the quadruply stranded Dy_2 helicates ΔΔ-/ΛΛ-$[NEt_4]_2[Dy_2(L^8)_4]\cdot(Me_2CO)$ (**101**) and ΔΔ-/ΛΛ-$[NEt_4]_2[Dy_2(L^9)_4]\cdot(H_2O)\cdot(DMF)$ (**102**), where L^8 = *N*,*N*′-bi(3-methoxysalicylidene)benzene-1,4-diamine and L^9 = *N*,*N*′-bi(3-methoxysalicylidene)biphenyl-4,4′-diamine. The same approach using a more flexible methylenediphenylene linker produces the mesocate $[NEt_4]_2[Dy_2(L^{10})_4]\cdot(Et_2O)\cdot(Me_2CO)$ (**103**), where L^{10} = *N*,*N*′-bi(3-methoxysalicylidene)-4,4′-methylenedianiline (Figure 24).[91]

Each dysprosium in **101**−**103** occupies an eight-coordinate, $\{DyN_2O_6\}$ environment, with slight variations in the metal−ligand bond distances, resulting in coordination geometries that

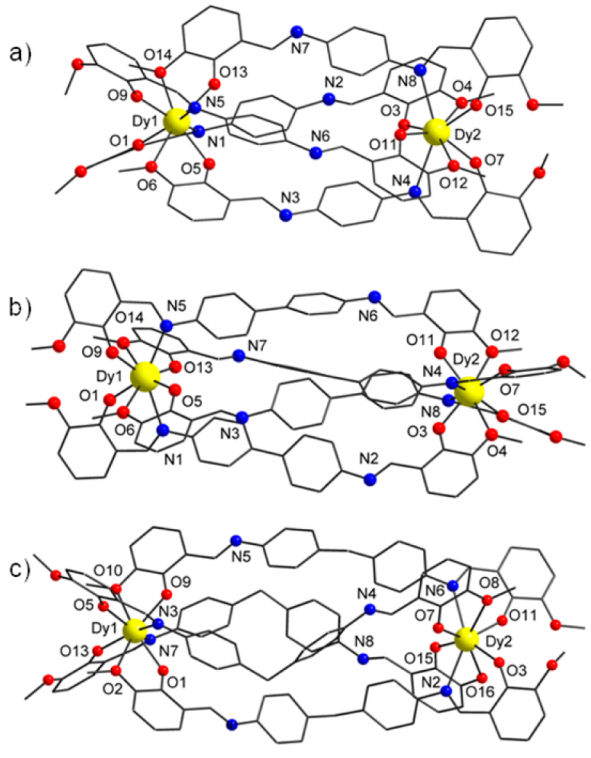

Figure 24. Molecular structures of **101**−**103** (from ref 91).

are intermediate between square-antiprismatic and dodecahedral. The Dy···Dy separations are 10.81, 14.87, and 15.30 Å, in **101**−**103**, respectively. In zero applied dc field, **101**−**103** do not show maxima in their $\chi''(T)$ plots as a result of fast QTM; however, maxima were observed by using optimum applied dc fields of 1600 Oe for **101** and **103**, and 1200 Oe for **102**. In the case of **101**, two relaxation processes were observed, with U_{eff} = 9 and 70 cm^{-1}; **102** and **103** feature one process each, with U_{eff} = 49 and 14 cm^{-1}, respectively. The angles formed between the anisotropy axes on the two Dy(III) ions within molecules of **101**−**103** vary to an extent that may be due, at least partly, to the influence of the different linkers in each case. In **101** and **102**, the axes intersect at similar angles of 55.1° and 52.1°, but a much larger angle of 85.1° was found for **103**. The observations on **101**−**103** can be interpreted as meaning that controlled modification to supramolecular structures may allow targeted increases in the anisotropy barrier, although the properties of single ions should still have the dominant influence over the magnetic properties. The ac susceptibility properties of $[Dy_2(hmb)(NO_3)_4(dmf)_4]\cdot(dmf)$ (**104**) are reminiscent of those of **101**−**103** in that no SMM behavior in zero applied field was observed, but in the optimum applied field of H_{dc} = 1800 Oe it was possible to determine U_{eff} = 29 cm^{-1} ($\tau_0 = 1.6 \times 10^{-6}$ s).

Variations in synthesis conditions produced the SMMs $[Dy(hmi)(NO_3)(MeOH)]_2$ (**105**) (Figure 25) and $[\{Dy(hmi)(NO_3)(MeOH)\}_2\cdot MeCN]_\infty$ (**106**), where hmi = (2-hydroxy-3-methoxy)phenylmethylene (isonicotino)hydrazine.[92]

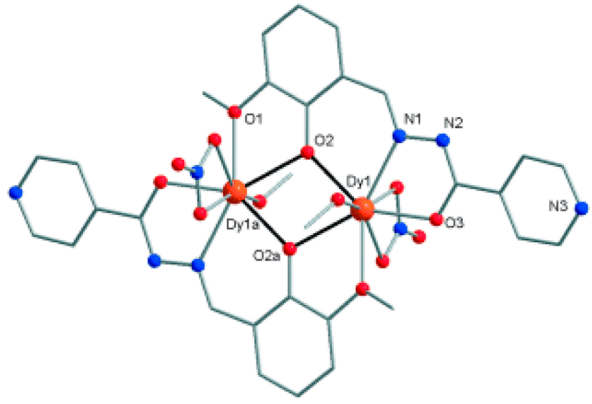

Figure 25. Molecular structure of **105** (from ref 92).

Although **105** and **106** feature structurally very similar dimetallic units, the dimers of **106** assemble into a coordination network by virtue of interdimer interactions between the hmi 4-pyridyl substituent and a dysprosium on a neighboring dimer molecule. The static magnetic properties of **105** and **106** are essentially the same, and both are SMMs. Above 8 K, the relaxation of the magnetization in **105** and **106** follows a thermally activated mechanism, resulting in U_{eff} = 39 cm^{-1} ($\tau_0 = 3 \times 10^{-7}$ s) and U_{eff} = 49 cm^{-1} ($\tau_0 = 7 \times 10^{-8}$ s), respectively.

The recently reported phenolate-bridged centrosymmetric dysprosium dimer $[Dy_2(api)_2]$ (**107**), where H_3api = 2-(2-hydroxyphenyl)-1,3-bis[4-(2-hydroxyphenyl)-3-azabut-3-enyl]-1,3-imidazoline, contains square antiprismatic dysprosium environments.[93] Complex **107** shows SMM properties in zero applied field, with U_{eff} = 18 cm^{-1} ($\tau_0 = 6.79 \times 10^{-6}$ s).

3.2.1.4. Metallocene-Based Dimetallic SMMs. The structural unit $[Cp_2Ln(\mu\text{-}X)]_2$ (X = heteroatom) has been known

dx.doi.org/10.1021/cr400018q | *Chem. Rev.* XXXX, XXX, XXX−XXX

since the mid-1970s, with almost 300 examples deposited in the Cambridge Structural Database.[94] However, SMMs based on lanthanide cyclopentadienides were only reported in 2010, and they include $[Cp_2Dy(\mu\text{-}SSiPh_3)]_2$ (**108**), $[Cp_2Dy(\mu\text{-}Cl)]_2$ (**109a**), $[Cp_2Dy(\mu\text{-}Cl)]_\infty$ (**109b**), $[Cp_2Dy(thf)(\mu\text{-}Cl)]_2$ (**110**), $[Cp_2Dy(\mu\text{-}bta)]_2$ (bta = benzotriazolate) (**111**), and $[Cp_2Ln(\mu\text{-}bpym)]_2[BPh_4]$ (bypm = bipyrimidyl radical anion) (Ln = Tb **70**; Ln = Dy **71**, see above).[95−97] The SMM **108** is notable for being the first to contain a thiolate ligand (Figure 26), and the ac susceptibility studies revealed a large U_{eff} value

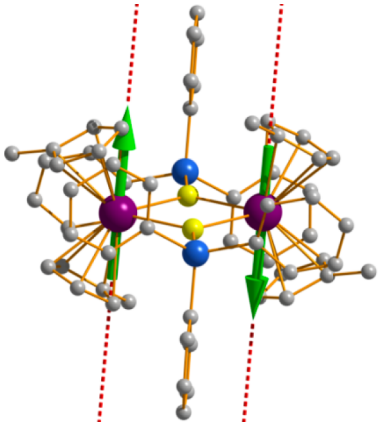

Figure 26. Optimized structure of **108** showing the orientation of the anisotropy axes (dashed red line) and the antiferromagnetic exchange coupling (green arrows), from ref 95.

of 133 cm^{-1}, with $\tau_0 = 2.38 \times 10^{-7}$ s.[95] An ab initio computational study of **108**−**111** revealed that the Dy(III) ions engage in weak antiferromagnetic exchange, and that the anisotropy axes are generally oriented almost perpendicular to the Dy_2X_2 plane. The U_{eff} values in **109**−**111** are much smaller, with U_{eff} = 26, 68, 34, and 33 cm^{-1}, respectively. The differing U_{eff} values in **109a** and **109b**, which cosublime as polymorphs, are intriguing because the only major difference in the structures of their $\{Cp_2Dy(\mu\text{-}Cl)\}$ repeat units is the Cl−Dy−Cl angles of ca. 80° and 90°.[96] In the case of **108**, the magnitude of the anisotropy barrier agrees well with the energy gap of 113 cm^{-1} between the ground state and first-excited Kramers' doublet, as determined by ab initio calculations, which is consistent with the magnetization in **108** relaxing via a thermally activated Orbach process. The calculated *g*-tensors for **108** are g_x = 0.0012, g_y = 0.0019, and g_z = 19.3611, and it is significant that the transverse *g*-values are approximately 20 times smaller than the analogous *g*-values calculated for **110**. Indeed, the magnetization in **110** relaxes via a QTM process below temperatures of about 5 K; however, in **108** the QTM is only observed at temperatures below 2 K, hence the substantial difference in anisotropy barriers.

3.2.1.5. Carboxylate-Bridged and Related Ln_2 SMMs. In an unusual single-crystal-to-single-crystal (SCSC) transformation, the dimeric complex $[Dy(NaphCO_2)_3(phen)(H_2O)]_2$ (**112**) was converted by calcination into the dehydrated analogue $[Dy(NaphCO_2)_3(phen)]$ (**113**) ($NaphCO_2$ = β-naphthoic acid).[98] Both dimers crystallize in the $P\bar{1}$ space group, but with unit cell volumes of 1806.8(3) and 1777.93(7) $Å^3$, respectively. In **112**, the nine-coordinate dysprosium ions occupy capped square-antiprismatic environments with approximate local C_{4h} symmetry, and in **113** the dysprosium ions are eight-coordinate with approximate D_{4d} symmetry (Figure 27). The SCSC transformation also produces a change in the μ-bridging mode of the four $[NaphCO_2]^-$ ligands, which switches from $\mu{:}\eta^1{:}\eta^2$ in **112** to $\mu{:}\eta^1{:}\eta^1$ in **113**, and the intermolecular Dy···Dy separation increases from 9.9 to 10.5 Å. Both **112** and **113** are SMMs; however, **112** produces an anisotropy barrier of U_{eff} = 20 cm^{-1} ($\tau_0 = 5.1 \times 10^{-7}$ s), whereas **113** produces U_{eff} = 4 cm^{-1} ($\tau_0 = 8.9 \times 10^{-7}$ s). The switch in SMM properties from **112** to **113** is the first time that such a change was brought about by an SCSC transformation.

Simple, hydrated dysprosium acetylacetonate (**42**) is an SMM; however, the dysprosium acetate dimer

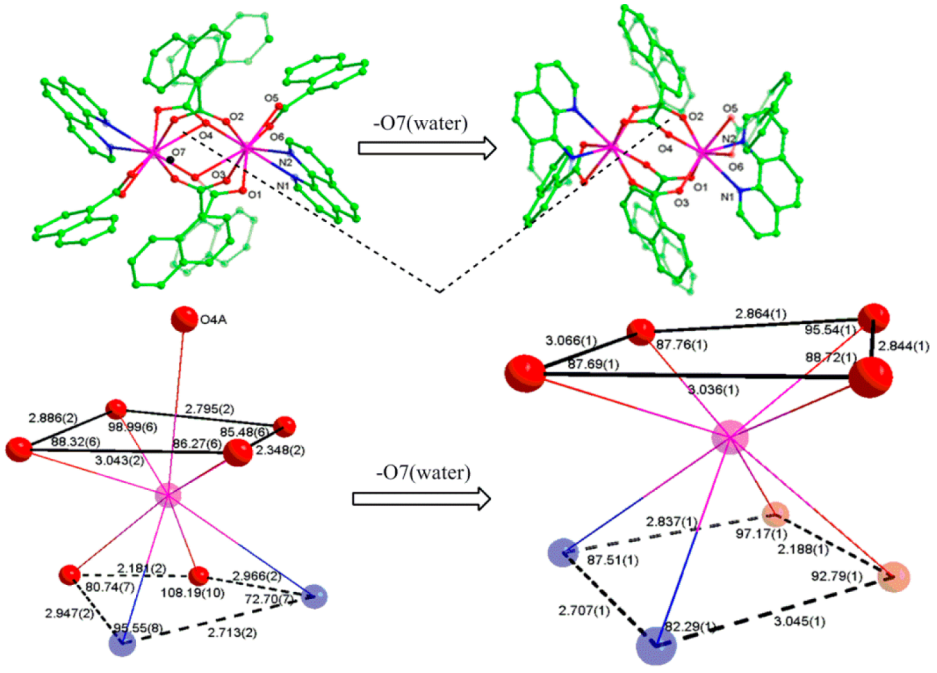

Figure 27. SCSC transformation of **112** (left) and **113** (from ref 98).

dx.doi.org/10.1021/cr400018q | *Chem. Rev.* XXXX, XXX, XXX−XXX

$[Dy_2(OAc)_6(H_2O)_2]\cdot 4H_2O$ (**114**) does not show any SMM properties. When **114** is refluxed in methanol, the result is the coordination polymer of dimers $[\{Dy(OAc)_3(MeOH)\}_2]_\infty$ (**115**), which is a single-chain magnet (SCM).[99] The Dy centers in **115** are nine-coordinate and occupy capped square-antiprismatic environments. Ferromagnetic exchange between nearest-neighbor dysprosium ions is apparent from the dc susceptibility measurements on **115**, and a combination of noncritical scaling theory and ac susceptibility measurements strongly suggested SCM properties. Low-temperature micro-SQUID measurements on **115** (below 0.5 K) also showed stepped hysteresis loops.

In $[Dy_2(HBpz_3)_4(\mu\text{-ox})]$ (**116**), each Dy(III) ion is complexed by two terdentate hydro-tris(pyrazolyl)borate ($HBpz_3$) ligands and a μ-bidentate oxalate (ox) ligand, resulting in distorted square-antiprismatic$\{DyN_6O_2\}$ coordination environments.[100] The dc susceptibility measurements on **116** revealed weak intradimer ferromagnetic exchange, and SMM properties were established from ac susceptibility measurements. Quantum tunneling effects are prominent in the relaxation behavior of **116** below 3 K, and although the relaxation time becomes temperature dependent at higher temperatures, the QTM effects may still influence the dynamics of the magnetism up to 9 K. An anisotropy barrier of U_{eff} = 29 cm^{-1} was obtained from the Arrhenius plot above 7 K.

The centrosymmetric carboxylate-bridged dimer $[Dy_2(3\text{-Htzba})_2(3\text{-tzba})_2(H_2O)_8]\cdot 4H_2O$ (**117**) (Htzba = 3,1*H*-tetrazolylbenzoic acid) consists of eight-coordinate dysprosium ions in a bicapped trigonal prismatic coordination environment.[101] The frequency dependence of the out-of-phase ac susceptibility shows a maximum at a constant frequency of about 20 Hz up to 3 K, but at higher temperatures the peak maximum shifts to higher frequencies, implying a crossover from a QTM relaxation mechanism to a thermally activated process. The resulting Arrhenius analysis on **117** produced U_{eff} = 37 cm^{-1}, with $\tau_0 = 1.3 \times 10^{-9}$ s, and application of a 2000 Oe dc field had little effect on the anisotropy barrier.

The dimetallic carboxylate $[Dy_2(Acc)_4(H_2O)_8]Cl_6$ (**118**) (Acc = cyclohexylcarboxylate) features eight-coordinate, square antiprismatic coordination of the dysprosium ions,[102] and the dimer $[Dy_2L_6(MeOH)_2(H_2O)_2]$ (L = butyrate) (**119**) contains nine-coordinate dysprosium ions.[103] Both **118** and **119** show temperature-dependent ac susceptibility below about 8 K; however, no maxima were observed in the $\chi''(T)$ plots.

3.2.1.6. β-Diketonate Dimetallic Ln-SMMs. When two molecules of $[Dy(hfac)_3(H_2O)_2]$ are linked by a pyrazine ligand, the result is $[Dy(hfac)_3(H_2O)_2(pyz)]_2$ (**120**), which is an SMM with U_{eff} = 77 cm^{-1} ($\tau_0 = 8.4 \times 10^{-10}$ s).[104] Coordination of the pyrazine *N*-donors produces highly distorted tricapped trigonal prismatic environments, and the distortions are thought to be responsible for the enhancement in SMM properties.

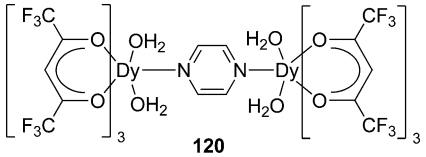

120

Above T = 9 K, a thermally activated mechanism can account for the relaxation of the magnetization in **120**, with a crossover to a QTM regime below 3 K. The dimetallic analogue of chiral **48** is $[Dy_2(Ph_2acac)_6(R\text{-}L^3)]\cdot(2H_2O)$ (**121**), which, in addition to having a larger anisotropy barrier of U_{eff} = 62 cm^{-1} (τ_0 = 5.9 $\times 10^{-8}$ s), also crystallizes in a polar space group and shows ferroelectric properties (Figure 28).[61]

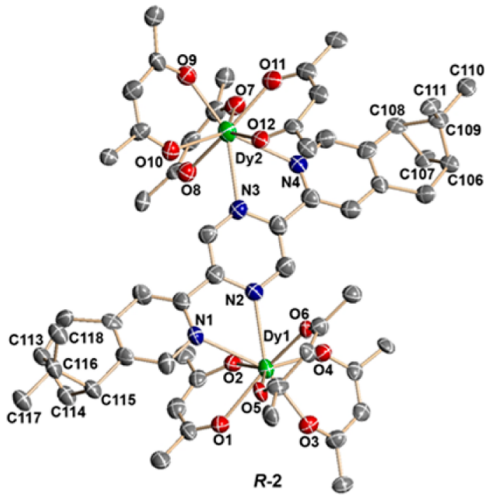

Figure 28. Molecular structure of $[Dy_2(Ph_2acac)_6(R\text{-}L^3)]\cdot(2H_2O)$ (**121**) (from ref 61).

The square-antiprismatic dysprosium ions in the centrosymmetric dimer $[Dy(hfac)_3(\mu\text{-pyNO})]_2$ (**122**) (pyNO = pyridine-*N*-oxide) are coupled through weak antiferromagnetic exchange, and **122** shows SMM behavior in the absence of an applied magnetic field, with an anisotropy barrier of U_{eff} = 116 cm^{-1} ($\tau_0 = 5.62 \times 10^{-11}$ s).[105] Furthermore, $M(H)$ hysteresis loops were observed at 1.4 K. The related dimer $[Dy(hfac)_3\{\mu\text{-(pyNO-ttf)}\}]_2$ (**123**) (pyNO-ttf = pyridyl-*N*-oxide-tetrathiafulvalene) shows properties similar to those observed in **122**, with U_{eff} = 60 cm^{-1} ($\tau_0 = 5.5 \times 10^{-7}$ s).[106] In an applied field, the magnetization relaxes via two nonthermally activated mechanisms, one of which is due to fast QTM that can be suppressed through the application of a static field, and the other may occur as a consequence of the antiferromagnetic exchange.

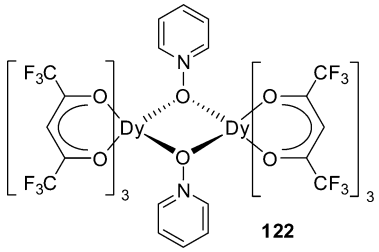

122

Intermolecular arene $\pi-\pi$ stacking interactions result in the dimeric dysprosium biradical complex $[Dy(hfac)_3(NIT\text{-}m\text{bis})]_2$ (NIT-*m*bis =1,3-bis-(1′-oxyl-3′-oxido-4′,4′,5′,5′-tetramethyl-4,5-hydro-1*H*-imidazol-2-yl)benzene, $[\mathbf{124}]_2$.[107] At room temperature, the value of the $\chi_M T$ product is greater than that expected for four S = 1/2 radicals and two uncoupled Dy(III) ions, and although the value of $\chi_M T$ decreases down to 30 K, at lower temperatures it increases due to ferromagnetic interactions. The temperature dependence of $\chi_M T$ at lower temperatures could be due to intra- or interligand ferromagnetic interactions involving the radical NO groups, in addition to interactions with the dysprosium centers. In zero dc field below 2.5 K, $[\mathbf{124}]_2$ shows SMM behavior, with U_{eff} = 8 cm^{-1} and $\tau_0 = 2.3 \times 10^{-8}$ s. Below 1.2 K, the relaxation shows a decreasing dependence on temperature, with a relaxation time

dx.doi.org/10.1021/cr400018q | *Chem. Rev.* XXXX, XXX, XXX−XXX

of τ = 40 ms below 0.8 K. In an applied field of 1 kOe, the Arrhenius analysis produces parameters similar to those obtained in zero field, suggesting that there is negligible QTM in zero field.

The diterbium macrocycle $[Tb(hfac)_3\{NITPhPO(OEt)_2\}]_2$ (**125**) crystallizes as two polymorphs, one in which molecules of **125** are well isolated from each other (**125a**) and one in which close contacts between the radical NO groups occur (**125b**).[108] The dimers **125a** and **125b** have very similar molecular structures (Figure 29), with both featuring eight-coordinate terbium ions in bicapped trigonal prismatic geometries: **125a** crystallizes as **125a**·$2CH_2Cl_2$ in the monoclinic space $P2_1/n$, and **125b** crystallizes without solvent in the triclinic space group $P\bar{1}$. Slight differences in the coordination geometries are thought to be responsible for the differing temperature dependences of $\chi_M T$ for **125a** and **125b** in the range 50−150 K, and at lower temperatures weak intermolecular ferromagnetic exchange may occur in both. Below 9 K, the larger differences in $\chi_M T$ can be accounted for by interdimer dipolar exchange, which should be different based on the contrasting packing motifs. The ac susceptibility studies on pure **125a** and **125b** revealed that both are SMMs, and a dependence of SMM properties on crystal packing was identified. Compound **125a** shows thermally activated SMM behavior in zero applied field with U_{eff} = 17 cm^{-1} ($\tau_0 = 3.36 \times 10^{-9}$ s); however, **125b** shows a very weak frequency dependence of χ'' in zero field. Under an applied field of 2 kOe, both **125a** and **125b** are SMMs, with thermally activated relaxation mechanisms and U_{eff} = 19 cm^{-1} ($\tau_0 = 2.64 \times 10^{-9}$ s) and 15 cm^{-1} ($\tau_0 = 1.76 \times 10^{-9}$ s), respectively, although the slowly relaxing magnetization is observed at higher temperatures in **125a**.

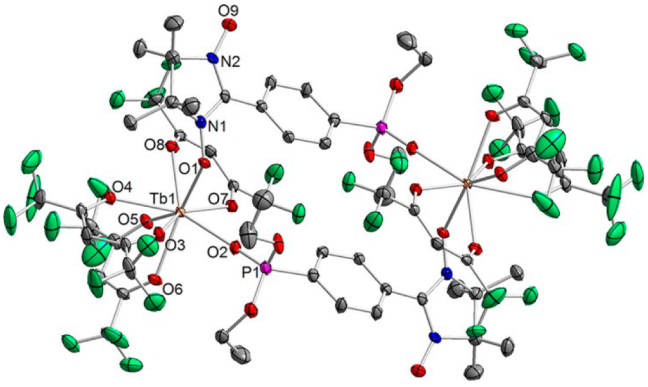

Figure 29. Molecular structure of **125a**, taken from ref 108. Unlabeled atoms are carbon (gray) and fluorine (green).

The nitronyl-nitroxide-bridged centrosymmetric dimers $[Tb(hfac)_3(NIT\text{-}3py)]_2$ (**126**),[109] $[Tb(hfac)_3(NIT\text{-}5Br\text{-}3py)]_2$ (**127**),[110] and $[Tb(Ph\text{-}tfac)_3(NIT\text{-}4py)]_2$ (**128**)[111] contain eight-coordinate terbium ions, and in static magnetic fields each shows evidence of intramolecular ferromagnetic coupling. In zero applied field and a weak oscillating field, **126**−**128** are SMMs with anisotropy barriers of U_{eff} = 13 cm^{-1} ($\tau_0 = 8.8 \times 10^{-8}$ s), 20 cm^{-1} ($\tau_0 = 5.9 \times 10^{-9}$ s), and 18 cm^{-1} ($\tau_0 = 4.1 \times 10^{-8}$ s). Interestingly, the closely related dimer $[Tb(hfac)_3(NIT\text{-}4py)]$ (**129**) does not show a frequency dependence of the ac susceptibility above 2 K, which is thought to be due to the different substitution pattern on the pyridyl ring of **129** relative to that in **126**. The phenolate-bridged dimer $[Dy_2(hfac)_4(NIT\text{-}PhO)_2]$ (**130**) contains two monocapped octahedral dysprosium ions, and although the SMM properties are quite weak, with no maxima in $\chi''(T)$, it was possible to estimate an anisotropy barrier of $U_{eff} \approx 5.3$ cm^{-1} ($\tau_0 \approx 3.0 \times 10^{-6}$ s).[112]

3.3. Trimetallic SMMs

Single-molecule magnets whose properties arise from three lanthanide ions form a relatively small group, and such SMMs are currently only known with dysprosium (Table 4). Despite the limited number of examples, trimetallic Ln-SMMs can be subdivided into two types based on the structural arrangement of the metal ions, that is, triangular or linear.

3.3.1. Dysprosium Triangles and Vortex Spin Chirality. One of the most remarkable types of dysprosium cage to have been studied in the context of molecular nanomagnetism are the triangular complex cations $[Dy_3(\mu_3\text{-}OH)_2(ovn)_3Cl_2(H_2O)_4]^{2+}$ (**131**) and $[Dy_3(\mu_3\text{-}OH)_2(ovn)_3Cl(H_2O)_5]^{3+}$ (**132**) (ovn = *ortho*-vanillin, Figure 6).[113] Depending on the recrystallization conditions, the Dy_3 triangles can form as [**131**][**132**][Cl]$_5$·(19 H_2O) or as [**132**][Cl]$_3$·(4 H_2O)·(2 MeOH)·(0.7 MeCN), with the two crystal structures differing in the nature of the chloride-bridged hydrogen-bonding networks linking the individual triangles (Figure 30).

The structures of **131** and **132** are essentially the same, with the cocrystallization of **131** and **132** from water being refined as 50:50 site disorder of a chloro and aquo ligand. In **131** and **132**, each dysprosium ion is eight coordinate, and occupies a site described as being based on a pentagonal bipyramid, in which one of the notionally pentagonal sites occurs twice, above and below the pentagonal plane. Despite their differing H-bonded

Table 4. Trimetallic Lanthanide SMMs[a]

Ln-SMM	U_{eff}/cm^{-1} (H_{dc}/Oe)	ref
$[Dy_3(\mu_3\text{-}OH)_2(ovn)_3Cl_2(H_2O)_4]^{2+}$ (**131**)	25	113
$[Dy_3(\mu_3\text{-}OH)_2(Hpovh)_3(NO_3)_3(MeOH)_2(H_2O)]$ (**134**)	37, 4.2	118
$[Dy_3(\mu_3\text{-}OH)_2(H_2vovh)_3Cl_2(H_2O)_4]\cdot Cl_4$ (**135**)	15	118
$Dy_3(HL)(H_2L)(NO_3)_4]$ (**136**)	63, 29	119
$[Dy_3(\mu_3\text{-}OMe)_2(HL^{12})_3(SCN)]$ (**137**)	6.2, 3.1	120
$[Dy_3(vanox)_2(Hvanox)_4(EtOH)_2][ClO_4]$ (**138**)	48, 20	122
$[Dy_3(vanox)_2(Hvanox)_4(OH)(H_2O)]$ (**139**)	26	123
$[Dy_3(vanox)_2(Hvanox)_4(NO_3)(MeOH)]$ (**140**)	27	123
$[Dy_3(vanox)_2(Hvanox)_4(Cl_3CCO_2)(MeOH)]$ (**141**)	27.5	123
$[Dy_3(Hsal)_5(sal)_2(phen)_3]$ (**142**)	45	124
$[Dy_3(ppch)_2]$ (**143**)	9.7 (1800)	125

[a]Lattice solvent not listed.

dx.doi.org/10.1021/cr400018q | *Chem. Rev.* XXXX, XXX, XXX−XXX

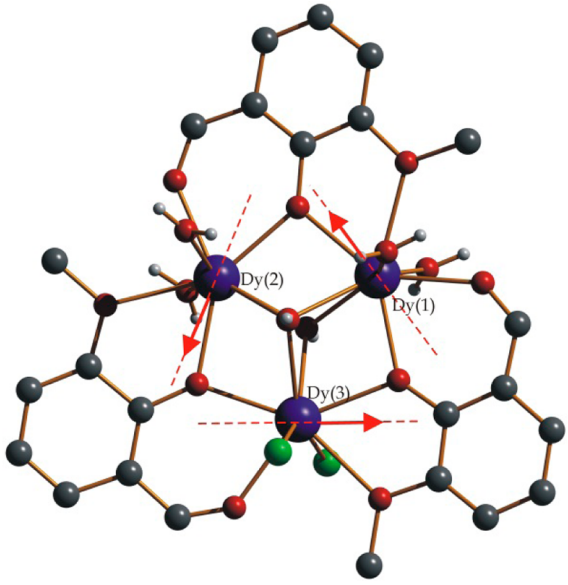

Figure 30. Molecular structure of $[Dy_3(\mu_3\text{-}OH)_2(ovn)_3Cl_2(H_2O)_4]^{2+}$ (**131**), showing the orientation of the anisotropy axes (dashed lines) and ordering of the magnetization in the ground state (from ref 115a).

networks, [**131**][**132**][Cl]$_5$ and [**132**][Cl]$_3$ display identical dc and ac magnetic properties. At 300 K, the $\chi_M T$ product in a dc field of 1 kOe corresponds to the value expected for three uncoupled Dy(III) ions, and a gradual decrease is observed down to about 50 K. A gradual decrease in $\chi_M T$ due to depopulation of the m_J sublevels then occurs, but below 30 K a precipitous drop in $\chi_M T$ is observed, resulting in a diamagnetic ground state at 1.8 K (Figure 31).

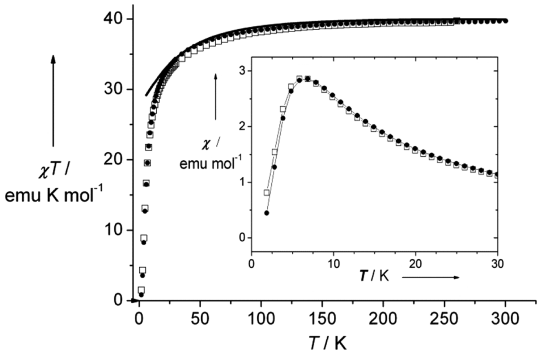

Figure 31. Temperature dependence of χT and χ (inset) for **131**, in an applied field of H_{dc} = 1 kOe (from ref 113).

For a system containing an odd number of unpaired electrons, this observation is unprecedented. Polycrystalline samples of both Dy_3 triangles also show SMM behavior below 20 K, and frequency-dependent maxima were observed in the plot of χ''_M. Below T = 7.15 K, the relaxation time τ deviates from Arrhenius behavior, and at a constant temperature of 7.15 K τ is strongly field-dependent, both of which indicate resonant QTM. Thus, despite the nonmagnetic ground state observed for **131** and **132** in static magnetic fields, in a small dynamic field the triangles are SMMs in the same temperature range, the latter likely being due to population of an excited m_J state.

The nature of the nonmagnetic ground state in the Dy_3 triangles was elucidated by experimental studies of face-indexed single crystals of **131**,[114] and by high-level CASSCF-type ab initio calculations.[115] The two independent studies were mutually consistent, and produced a picture in which the easy axes of magnetization are noncollinear, lying effectively in the plane of the Dy_3 triangle, and not perpendicular to it. The overall spin structure accounts for the nonmagnetic ground state, and has been described as almost perfectly toroidal or, alternatively, as vortex spin-chirality (Figure 30).

An implication of the spin chirality is that the doubly degenerate ground state can be regarded as comprising two forms, based on opposite rotations of their respective vortices. To convert one spin "enantiomer" into the other, consecutive reversal of the spins on the individual Dy sites in **131** is therefore necessary, with the energy barrier to this process representing the barrier to blocking of the magnetization. This is fundamentally new physics shown by the Dy_3 triangles, and it has an important implication as the chiral nature of the spin in such materials could represent an advance toward the development of noncollinear molecular spintronics and qubits. Indeed, it has been suggested that the vortex nature of the spin offers long decoherence times, which may indicate that the triangles possess the ability to carry out logic-gate operations.[116]

The reaction of $DyCl_3\cdot(6H_2O)$ with 0.5 stoichiometric equiv of *ortho*-vanillin and 0.5 equiv of 2-hydroxymethyl-6-methoxyphenol (H_2L^{11}) results in the hexametallic SMM $[Dy_6(\mu_3\text{-}OH)_4(ovn)_2L^{11}{}_2Cl(H_2O)_9]^{5+}$ (**133**), which can be regarded as a coupled version of two Dy_3 triangles based on **131** and **132**.[117] The dimeric structure of **133** stems from the bridging tendency of the benzyloxy groups, to produce a $\{Dy_2O_2\}$ core reminiscent of that observed in **87**. The two triangular Dy_3 units in **133** deviate slightly from an ideal equilateral geometry, with Dy···Dy distances in the range 3.5127(3)−3.5797(3) Å, and the two Dy_3 planes are parallel and noncoplanar with respect to each other (Figure 32).

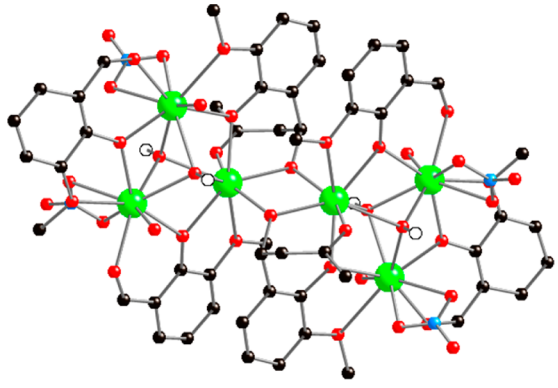

Figure 32. Structure of $[Dy_6(\mu_3\text{-}OH)_4(ovn)_2L^{11}{}_2Cl(H_2O)_9]^{5+}$ (**133**) (from ref 117) (Dy = green; N = blue; O = red).

The dc magnetic susceptibility studies reveal that the properties of **133** are similar to those of **131** and **132**, but with slightly weaker antiferromagnetic character. The temperature dependence of the out-of-phase ac magnetic susceptibility reveals two distinct relaxation processes: a higher-temperature process with a series of maxima centered around 25 K corresponding to 25% of the magnetization; and a more pronounced lower-temperature process with maxima centered around 5 K. Studying the field dependence of the magnetization indicated that the QTM in **133** was much less prominent than in **131** and **132**, and the Arrhenius analysis

dx.doi.org/10.1021/cr400018q | *Chem. Rev.* XXXX, XXX, XXX−XXX

of the higher-temperature ac susceptibility data produced a much larger anisotropy barrier of U_{eff} = 139 cm^{-1} (τ_0 = 1.5 × 10^{-9} s), relative to that determined for the unlinked triangles. Ab initio calculations revealed that the Dy(III) ions in **133** that couple the Dy_3 triangles together (i.e., the dysprosium ions bonded to the μ-alkoxide ligands) possess easy axes disposed at a relatively acute angle of 64.2° with respect to the bisector of the opposite Dy···Dy axis; furthermore, the easy axes of these Dy(III) ions lie out of the Dy_3 planes by 10°. In contrast, the other two Dy(III) ions possess easy axes that are close to perpendicular (82.1° and 82.4°) relative to their respective opposite Dy···Dy axes, and the easy axes show only slight deviations of 3° from the Dy_3 planes. The magnetic properties of a single-crystal of **133** were also studied, which showed that the magnetization has a strong angular dependence. A key result from this study was that the magnetic anisotropy at T = 2.0 K can be described as easy-plane, whereas when the temperature is raised an easy-axis description of the anisotropy is more appropriate, a property that is thought to stem from the linking of two Dy_3 triangles. Therefore, rather than simply being associated with the distinct coordination environment of the phenolate-bridged dysprosium ions, the ac susceptibility is more likely to originate within the different nature of the anisotropy when the excited state becomes thermally populated.

Following the original discovery of the toroidal moment, the phenomenon has also been observed in other Dy_3 triangles. For example, the *ortho*-vanillin pro-ligand can be derivatized to give *N*-(pyridylmethylene)-*ortho*-vanillinhydrazone (H_2povh) and *N*-vanillidene-*ortho*-vanilloylhydrazone (H_3vovh), and reaction of these new ligands with $DyX_3·(6H_2O)$ (X = NO_3 or Cl) gives $[Dy_3(\mu_3\text{-}OH)_2(Hpovh)_3(NO_3)_3(MeOH)_2(H_2O)]·NO_3·(3MeOH)·(2H_2O)$ (**134**) and $[Dy_3(\mu_3\text{-}OH)_2(H_2vovh)_3Cl_2(H_2O)_4]·Cl_4·(2MeOH)·(2MeCN)·(7H_2O)$ (**135**), respectively.[118] The dysprosium ions in **134** and **135** form a near-equilateral triangle, which results in the characteristic diamagnetic ground state at 1.9 K. In **134**, the ac susceptibility data indicate SMM behavior with two relaxation processes, one with U_{eff} = 37 cm^{-1} (τ_0 = 1.4 × 10^{-7} s) and the other with U_{eff} = 4.2 cm^{-1} (τ_0 = 9.5 × 10^{-5} s). SMM **135** produces U_{eff} = 15 cm^{-1} (τ_0 = 1.3 × 10^{-5} s), with the relaxation below 8 K showing the effects of QTM. In $[Dy_3(HL)(H_2L)(NO_3)_4]$ (**136**), where H_4L = tetrakis(2-hydroxyethyl)ethylenediamine, the three dysprosium ions approximately describe an isosceles triangle, with one Dy(III) ion residing in a distorted $\{DyO_8\}$ square-antiprismatic environment, and the other two residing in $\{DyO_7N_2\}$ capped square-antiprismatic environments.[119] Although the triangular arrangement of the Dy(III) ions produces a toroidal arrangement of magnetic moments, the approximate 2-fold symmetry of the isosceles triangle results in a net moment and hence a paramagnetic ground state at 2 K. The temperature and frequency dependence of χ'' reveals the presence of two relaxation processes, at T = 3–9 and 6–22 K, which could be due to the two different dysprosium coordination environments in **136**. The anisotropy barriers are U_{eff} = 29 cm^{-1} (τ_0 = 1.0 × 10^{-6} s) and U_{eff} = 63 cm^{-1} (τ_0 = 5.8 × 10^{-7} s), and micro-SQUID measurements showed $M(H)$ hysteresis below 3.5 K. Another notable feature of **136** is that it crystallizes in the polar space group $Pna2_1$, a property that confers ferroelectricity, thus providing the first example of a lanthanide cage compound to display SMM behavior at low temperatures and a paraelectric to ferroelectric phase transition at a much higher temperature of 470 K.

It is noteworthy that a triangular arrangement of dysprosium ions does not guarantee a low-temperature diamagnetic ground state,[120] as illustrated by the helicate complex $[Dy_3(\mu_3\text{-}OMe)_2(HL^{12})_3(SCN)]·(4MeOH)·(2MeCN)·(2H_2O)$ (**137**) (H_3L^{12} = 2,6-diformyl-4-methylphenol dibenzoylhydrazone), which, in a static dc field of 1 kOe, has $\chi_M T$ = 21.19 cm^3 K mol^{-1} at 2 K. In zero applied field, compound **137** shows two relaxation processes in the ac susceptibility measurements below 8 K, which are characterized by U_{eff} = 3.1 cm^{-1} (τ_0 = 4.4 × 10^{-5} s) and U_{eff} = 6.2 cm^{-1} (τ_0 = 8.9 × 10^{-5} s).[121]

3.3.2. Dy_3 Chains as SMMs. The versatility of *ortho*-vanillin ligand scaffolds in the synthesis of Ln-SMMs was demonstrated in a synthetic procedure where the aldehyde group was oximated, giving *ortho*-vanillin oxime (H_2vanox) (Figure 7).[122] The reaction of $Dy(ClO_4)_3·(6H_2O)$ with H_2vanox resulted in the trimetallic complex $[Dy_3(vanox)_2(Hvanox)_4(EtOH)_2][ClO_4]·(1.5EtOH)·(H_2O)$ (**138**), in which the Dy···Dy···Dy angle is 166.29(1)° (Figure 33).

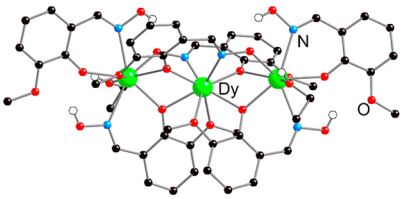

Figure 33. Structure of $[Dy_3(vanox)_2(Hvanox)_4(EtOH)_2]^+$ (**138**) (from ref 122).

In **138**, the central dysprosium ion occupies a $\{DyN_2O_6\}$ environment that is close to ideal dodecahedral, and the terminal dysprosium ions both occupy environments between ideal dodecahedral and square-antiprismatic, also with $\{DyN_2O_6\}$ donor sets. Below 20 K, the dc susceptibility data reveal ferromagnetic interactions between the dysprosiums in **138**, and the ac susceptibility data show more than two maxima, indicating complex relaxation behavior. The Arrhenius analysis allowed two anisotropy barriers to be extracted, with U_{eff} = 20 cm^{-1} (τ_0 = 6.3 × 10^{-5} s) and U_{eff} = 48 cm^{-1} (τ_0 = 5.9 × 10^{-8} s), respectively, and ac measurements in an applied field led to the conclusion that QTM is much less prominent in **138** than in **131** and **132**. Also, in contrast to **131** and **132** are the orientations of the anisotropy easy axes in **138**, which were determined by ab initio calculations to be effectively collinear, a consequence of which is the occurrence of intramolecular ferromagnetic coupling via dipolar interactions.

Variations in the reaction conditions and dysprosium starting materials enabled the synthesis of $[Dy_3(vanox)_2(Hvanox)_4(X)(Y)]·(solvent)$, where X = HO^-, Y = H_2O, solvent = $(MeOH)·(7H_2O)$ (**139**); X = NO_3^-, Y = MeOH, solvent = $(MeOH)·(0.5H_2O)$ (**140**); and X = $[Cl_3CCO_2]^-$, Y = MeOH, solvent = MeOH (**141**).[123] The Dy_3 units in each of **139**–**141** are described as linear, and each complex features eight-coordinate dysprosium ions in $\{DyN_2O_6\}$ environments, except **140**, which features a nine-coordinate dysprosium because of a bidentate nitrate ligand. The anisotropy barriers of **139**–**141** are very similar, with U_{eff} = 26 cm^{-1} (τ_0 = 5.04 × 10^{-7} s), U_{eff} = 27 cm^{-1} (τ_0 = 1.55 × 10^{-6} s), and U_{eff} = 27.5 cm^{-1} (τ_0 = 1.07 × 10^{-7} s), respectively.

Other examples of linear trimetallic SMMs include the carboxylate-bridged complex $[Dy_3(Hsal)_5(sal)_2(phen)_3]$ (H_2sal

dx.doi.org/10.1021/cr400018q | Chem. Rev. XXXX, XXX, XXX–XXX

Table 5. Tetrametallic Lanthanide SMMs[a]

Ln-SMM	U_{eff}/cm^{-1} (H_{dc}/Oe)	ref
$[Dy_4(L^{13})_4(MeOH)_6]$ (**144**)	120, 13.7	126
$[Dy_4(L^{14})_4(HL)_2(Anth)_2(MeOH)_4]$ (**145**)	14	127
$[\{Dy_2(fimc)(\mu\text{-}PhCO_2)_3(\kappa^2\text{-}PhCO_2)_3(MeOH)_2\}_2]$ (**146**)	12	128
$[Er_4(salen)_6]$ (**147**)	9.4 (1000)	129
$[Dy_4(L^{15})_2(HL^{15})_2(\mu\text{-}N_3)_4(\mu_4\text{-}O)]$ (**148**)	63, 35, 188 (1600)	130
$[Dy_4(HL^{16})_4(MeOH)_4]_2$ (**150**)	11 (900)	131
$[Dy_4(Hhpch)_8(\mu_4\text{-}OH)][ClO_4]_3$ (**152**)	21, 11, 4.3, 2.1, 64 (1000)	133
$[Tb_4\{N(SiMe_3)_2\}_4(\mu\text{-}SEt)_8(\mu_4\text{-}SEt)]^-$ (**153**)	4.6	134
$[Dy_4\{N(SiMe_3)_2\}_4(\mu\text{-}SEt)_8(\mu_4\text{-}SEt)]^-$ (**154**)	46	134
$[Dy_4(\mu_3\text{-}OH)_2(bmh)_2(msh)_4Cl_2]$ (**155**)	118, 6.7	135
$[Dy_4(\mu_4\text{-}O)_2(\mu\text{-}OMe)(beh)_2(esh)_4]$ (**156**)	16	136
$[Dy_4(\mu_3\text{-}OH)(\mu\text{-}OH)(2,2\text{-}bpt)_4(NO_3)_4(EtOH)_2]$ (**157**)	56	137
$[Dy_4(\mu_3\text{-}OH)_2(mdeaH)_2(piv)_8]$ (**158**)	4.3	138
$[Dy_4(\mu_3\text{-}OH)_2(ampdH_4)_2(piv)_{10}]$ (**159**)	3.8	139
$[Dy_4(\mu_3\text{-}OH)_2(hmmpH)_2(hmmp)(N_3)_4]\cdot(4MeOH)$ (**161**)	4.9	140
$[Dy_4(\mu_3\text{-}OH)_2(ovn)(piv)_4(NO_3)_2]$ (**162**)	3.5	141
$[Dy_4(\mu_3\text{-}OH)_2(L^{17})_2(acac)_6]$ (**164**)	15 (1400)	143
$[Dy_4(\mu_3\text{-}OH)_4(nic)_6(py)(MeOH)_7][ClO_4]_2$ (**168**)	4	146
$[Dy_4(\mu_3\text{-}OH)_4(TBSOC)(H_2O)_4(MeOH)]$ (**170**)	16	148

[a]Lattice solvent not listed. U_{eff} values are extracted from measurements in zero applied dc field, unless followed by a number in parentheses to indicate the strength of the applied field.

= salicylic acid) (**142**), which contains three chemically different eight-coordinate dysprosium ions.[124] The ac susceptibility data on **142** reveal that χ'' is temperature dependent in two distinct temperature ranges, and when T = 15−35 K the Arrhenius plot produced U_{eff} = 45 cm^{-1} (τ_0 = 1.5 × 10^{-5} s). Below 15 K, an abrupt transition to a temperature-independent regime is observed, indicating relaxation by QTM. Complex **142** is also notable for its luminescence properties upon excitation at 313 nm. Although the complex $[Dy_3(ppch)_2]$ (**143**), where H_2ppch = bis(1-phenylethylidene)pyridine-2,6-bis(carbohydrazonic acid), has a Dy_3 core similar to those of **138**−**142**, SMM properties are only observed in an applied field of H_{dc} = 1.8 kOe, which produces U_{eff} = 9.7 cm^{-1} (τ_0 = 2.28 × 10^{-6} s).[125]

3.4. Tetrametallic SMMs

Increasing the cage nuclearity to four lanthanide ions results in a broad range of structural types (Table 5). With respect to the metal centers, the geometries include one-dimensional linear and zigzag chains; two-dimensional squares and rhomboidal/butterfly arrangements of lanthanide ions; and three-dimensional cubes and tetrahedra. Tetrametallic SMMs, in all but two instances, are based on oxygen-bridging ligands, and dysprosium is once again ubiquitous. This section also illustrates that increasing the structural complexity and the lanthanide content provides no guarantee of enhancements in SMM properties, but despite this apparent trend a considerable amount of fundamental insight into Ln-SMMs has been developed.

3.4.1. Tetrametallic Chain Ln-SMMs. The reaction of (2-hydroxy-3-methoxyphenyl)methylene hydrazide (H_3L^{13}) with $DyCl_3\cdot(6H_2O)$ in methanol/acetonitrile and in the presence of base results in $[Dy_4(L^{13})_4(MeOH)]\cdot(2MeOH)$ (**144**), which contains a Dy_4 chain with Dy−Dy−Dy angles of 149.99(1)° (Figure 34).[126] The two internal dysprosiums in **144** are eight-coordinate and occupy distorted bicapped trigonal prismatic $\{DyNO_7\}$ environments, and the two terminal dysprosiums are nine-coordinate and reside in monocapped square antiprismatic $\{DyNO_8\}$ sites. The dysprosium ions are bridged by formally

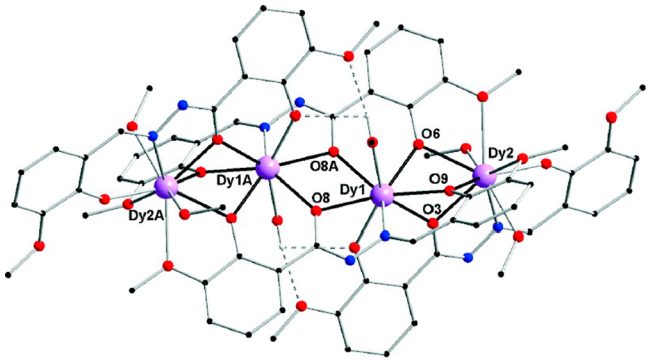

Figure 34. Molecular structure of $[Dy_4(L^{13})_4(MeOH)_6]$ (**144**) (from ref 126).

anionic phenolate or amido oxygen donors. The ac magnetic susceptibility studies on **144** clearly show two relaxation processes, one with $\chi''(T)$ centered around T = 25 K and one below 10 K. Below 6 K, the relaxation time τ develops a weak dependence on temperature, indicating a crossover from a thermally activated Orbach relaxation mechanism to a direct Raman mechanism. The slower of the two processes produced U_{eff} = 120 cm^{-1} (τ_0 = 1.2 × 10^{-7} s), and the faster relaxation process produced U_{eff} = 13.7 cm^{-1} (τ_0 = 7.8 × 10^{-6} s).

The tetrametallic chain $[Dy_4(L^{14})_4(HL^{14})_2(Anth)_2(MeOH)_4]\cdot(5MeOH)$ (**145**), in which H_2L^{14} = *N*-(2-carboxyphenyl)salicylidenimine and H(Anth) is anthranilic acid, contains two square-antiprismatic dysprosium environments and two irregular dysprosium environments, and the Dy−Dy−Dy angle is 109.77°.[127] Across a temperature range of 5.5−9 K, the semicircular Cole−Cole plot for **145** was modeled with a small α parameter, which indicated a single thermally activated relaxation process, and below 3 K the relaxation time is temperature independent. The Arrhenius analysis of the higher temperature $\chi''(\nu)$ data produced an anisotropy barrier of U_{eff} = 14 cm^{-1}. The complex $[Dy_4(fimc)_2(\mu\text{-}PhCO_2)_6(\kappa^2\text{-}PhCO_2)_6(MeOH)_4]$, where L = 2,6-bis((*E*)-((furan-2-

dx.doi.org/10.1021/cr400018q | Chem. Rev. XXXX, XXX, XXX−XXX

ylmethyl)imino)methyl)-4-cresol (fimc) (**146**), consists of a near-linear chain of benzoate-bridged dysprosium ions in bicapped trigonal-prismatic geometries.[128] The two symmetry-related terminal dysprosiums are complexed by a bidentate *N*,*O*-fimc ligand, and two μ-bridging and one terminal bidentate benzoate ligands, and the internal dysprosium ions are bonded to four μ-bridging and one terminal bidentate benzoate ligands, and two methanol ligands. The χ'' data for **146** are temperature dependent below 8 K, and the relaxation time shows a linear varation temperature in the range 4−8 K, which resulted in U_{eff} = 12 cm^{-1} (τ_0 = 6.7 × 10^{-6} s). Below 2.5 K, the relaxation time measured for **146** is temperature independent.

The tetrametallic zigzag chain compound $[Er_4(salen)_6]\cdot(13H_2O)$ (**147**) is notable for being a rare example of an erbium(III) complex to show slowly relaxing magnetization, albeit in an applied field of 1 kOe.[129] The erbium ions are complexed by tetradentate salen ligands, and the two erbium ions at the end of the chain are in distorted-dodecahedral environments, whereas the two central erbium ions are in capped trigonal prismatic environments. The fast QTM that occurs in **147** in zero applied field is thought to be due to magnetic coupling between adjacent erbium centers, to hyperfine interactions with ^{167}Er nuclei (22.95% abundance), and to the absence of strict C_4 rotational symmetry axes passing through the erbium ions. The relaxation time τ reaches a maximum with H_{dc} = 1 kOe; hence the ac susceptibility collected in such an applied field revealed a frequency dependence of χ'', and resulted in an anisotropy barrier of U_{eff} = 9.4 cm^{-1} (τ_0 = 4.1 × 10^{-7} s). The Cole−Cole plots for **147** also implied that only one of the two types of erbium ion is responsible for blocking the reversal of the magnetization in an applied field.

3.4.2. Tetrametallic Square Ln-SMMs. The reaction of $DyCl_3\cdot(6H_2O)$ with the ditopic carbohydrazone ligand H_2L^{15} in the presence of sodium azide results in the formation of the [2 × 2] square grid $[Dy_4(L^{15})_2(HL^{15})_2(\mu\text{-}N_3)_4(\mu_4\text{-}O)]\cdot(14H_2O)$ (**148**) (Figure 35).[130] The dysprosium ions in **148** occupy nine-coordinate $\{DyN_3O_6\}$ environments, and the square geometry of the compound is reflected in the range of cis Dy−(μ_4-O)−Dy angles of 88.9−91.4°. Below 30 K, two overlapping relaxation processes in zero applied field were identified in the ac magnetic susceptibility studies on **148**, and a deconvolution of the $\chi''(T)$ peaks allowed anisotropy barriers of U_{eff} = 35 cm^{-1} (τ_0 = 3.0 × 10^{-9} s) and U_{eff} = 63 cm^{-1} (τ_0 = 4.5 × 10^{-7} s) to be determined. Application of the optimum dc field of 1.6 kOe to **148** produced a single set of $\chi''(T)$ peaks and a substantial increase in the anisotropy barrier to U_{eff} = 188 cm^{-1} (τ_0 = 4.0 × 10^{-10} s). The terbium square $[Tb_4(L^{15})_2(HL^{15})_2(\mu\text{-}N_3)_4(\mu_4\text{-}O)]\cdot(14H_2O)$ (**149**) is isostructural to **148**; however, it shows no SMM properties in the absence or presence of an applied dc field. The square complex $[Dy_4(HL^{16})_4(MeOH)_4]_2\cdot 7CH_2Cl_2\cdot MeOH$ (**150**) has a [2 × 2] grid structure similar to that of **148**; however, there is no μ_4-bridging ligand in the center, resulting in coordination numbers of eight with dodecahedral geometries for each dysprosium.[131] Complex **150** shows a very weak out-of-phase component to the magnetic susceptibility in zero dc field, but in an applied field of 900 Oe it was possible to induce SMM behavior, with U_{eff} being estimated as 11 cm^{-1} (τ_0 = 1.3 × 10^{-6} s).

The hydroxide-centered thiacalixarene-ligated dysprosium square $[Dy_4(\mu_4\text{-}OH)(PTC4A)_2Cl_3(MeOH)_2(H_2O)_3]\cdot 4.7MeOH\cdot 2H_2O$ (H_4PTC4A = *p*-phenylthiacalix[4]arene) (**151**) contains four nine-coordinate dysprosium ions, and although χ'' shows a temperature dependence below 6 K, no maxima were observed, and it was not possible to determine an anisotropy barrier.[132]

The hydroxide-centered dysprosium square $[Dy_4(Hhpch)_8(\mu_4\text{-}OH)][ClO_4]_3\cdot(2MeCN)\cdot(MeOH)\cdot(4H_2O)$, where H_2hpch = 2-hydroxybenzaldehyde(pyridine-4-carbonyl (**152**), contains nine-coordinate dysprosium ions in distorted monocapped square-antiprismatic environments and shows multiple relaxation processes below 20 K.[133] In zero applied field, the relaxation in **152** can be subdivided into a slow and a fast process below 4 K, and a slow and a fast process that can be fitted to the Arrhenius law between 12 and 16 K. The lower-temperature processes produced U_{eff} = 4.3 cm^{-1} (slow, τ_0 = 1.96 × 10^{-3} s) and U_{eff} = 2.3 cm^{-1} (fast, τ_0 = 1.82 × 10^{-4} s); and the higher-temperature processes produced U_{eff} = 21 cm^{-1} (slow, τ_0 = 3.0 × 10^{-5} s) and U_{eff} = 11 cm^{-1} (τ_0 = 3.7 × 10^{-5} s). In an interesting parallel to the field-enhanced SMM properties of **148**, application of H_{dc} = 1 kOe to **152** results in only one relaxation process at higher temperatures, and a 3-fold increase in the anisotropy barrier to U_{eff} = 64 cm^{-1} (τ_0 = 2.0 × 10^{-7} s).

In light of the differing dynamic magnetic properties of isostructural **148** and **149**, the observation of SMM properties in the thiolate-bridged squares $[Li(thf)_4][Ln_4\{N(SiMe_3)_2\}_4(\mu\text{-}SEt)_8(\mu_4\text{-}SEt)]$, where Ln = Tb is $[Li(thf)_4]$[**153**] and Ln = Dy is $[Li(thf)_4]$[**154**], is intriguing (Figure 36).[134] The lanthanide centers in **153** and **154** each reside in distorted six-coordinate $\{LnNS_5\}$ environments, and are rare examples of SMMs in which the metal ions are bridged by soft donors. Analysis of the $\chi''(\nu)$ data for **153** in zero applied field yielded a small anisotropy barrier of U_{eff} = 4.6 cm^{-1} (τ_0 = 1.5 × 10^{-5} s); however, under the same conditions the Arrhenius analysis on **154** produced U_{eff} = 46 cm^{-1} (τ_0 = 4.30 × 10^{-6} s). The much smaller anisotropy barrier in **153** was assigned to the appreciable deviations from strict axial symmetry of the terbium environments, which is a non-Kramers' ion, whereas the same geometric deviations for the Kramers' ion Dy(III) are thought to have much less of an impact on the dynamics of the magnetization.

3.4.3. Butterfly- or Diamond-Shaped Ln$_4$ SMMs. The diamond-shaped cage $[Dy_4(\mu_3\text{-}OH)_2(bmh)_2(msh)_4Cl_2]$ (**155**), in which H_2bmh = bis(2-hydroxy-3-methoxybenzylidene)

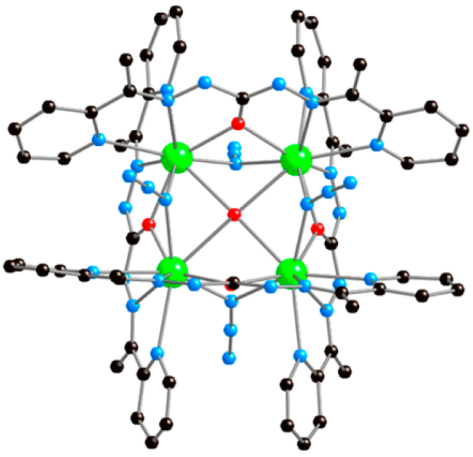

Figure 35. Molecular structure of $[Dy_4(L^{15})_2(HL^{15})_2(\mu\text{-}N_3)_4(\mu_4\text{-}O)]$ (**148**) viewed along the crystallographic *b*-axis (Dy = green; N = blue; O = red) (from ref 130).

dx.doi.org/10.1021/cr400018q | *Chem. Rev.* XXXX, XXX, XXX−XXX

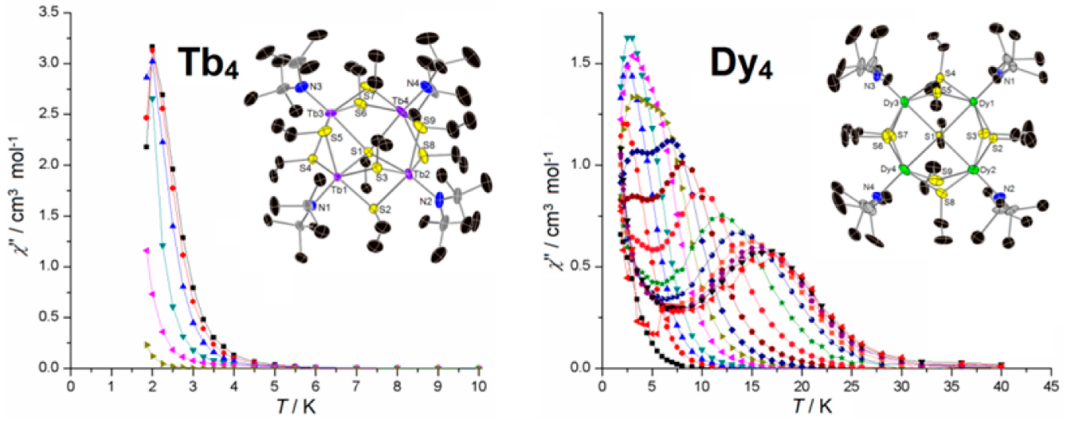

Figure 36. Molecular structures and out-of-phase susceptibility versus temperature for **153** and **154** (from ref 134).

hydrazone and Hmsh = 3-methoxysalicylaldehyde hydrazone, forms from the reaction of $DyCl_3 \cdot (6H_2O)$ with *ortho*-vanillin in DMF/CH_2Cl_2 and triethylamine, followed by the addition of $N_2H_4 \cdot H_2O$. The structure of **155** consists of four coplanar dysprosium ions that each occupy eight-coordinate distorted square antiprismatic environments, with two symmetry related dysprosium ions having a $\{DyN_2O_5Cl\}$ donor set, and the other two having a $\{DyN_2O_6\}$ donor set (Figure 37).[135]

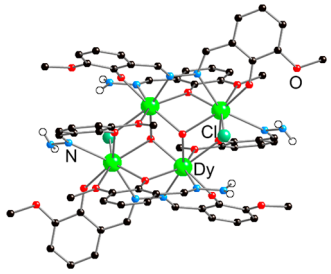

Figure 37. Molecular structure of **155** (from ref 135).

The out-of-phase magnetic susceptibility in zero applied field for **155** is temperature dependent below 35 K with ac frequencies in the range ν = 10−1500 Hz. At the highest frequency used, maxima in $\chi''(T)$ occur at 9 and 30 K, indicating that two relaxation mechanisms operate in **155**. From an Arrhenius analysis of the relaxation times, anisotropy barriers of U_{eff} = 6.7 cm^{-1} ($\tau_0 = 3.2 \times 10^{-5}$ s) and U_{eff} = 118 cm^{-1} ($\tau_0 = 4 \times 10^{-7}$ s) were determined for the low- and high-temperature relaxation processes, respectively. A single-crystal micro-SQUID study of **155** also revealed $M(H)$ hysteresis below 7 K. Ab initio calculations showed that the magnetic moments on the two types of dysprosium are strongly axial, with $g_{\|}$ = 19.5 for the $\{DyN_2O_5Cl\}$ dysprosium centers and $g_{\|}$ = 19.2 for the $\{DyN_2O_6\}$ dysprosium centers, and with $g_{\perp}$ being negligible in both cases. The occurrence of two magnetically distinct dysprosium(III) ions is thus consistent with the observation of two different relaxation processes in **155**.

Changing the *ortho*-vanillin pro-ligand to 3-ethoxysalicylaldehyde, and changing the reaction solvent to methanol, results in a different tetrametallic cage complex, $[Dy_4(\mu_4\text{-}O)_2(\mu\text{-}OMe)\text{-}(beh)_2(esh)_4] \cdot (MeOH)$ (**156**), where H_2beh = bis(2-hydroxy-3-ethoxybenzylidene) hydrazone and Hesh = 3-methoxysalicylaldehyde hydrazone.[136] The Dy(III) ions in **156** create a tetrahedral core around a μ_4-oxo ligand, with each metal center being eight-coordinate. Furthermore, the $[beh]^{2-}$ ligands formed in situ create a conformational lock that results in molecules of **156** being chiral. Below 15 K, the plot of $\chi''(T)$ is frequency dependent, and the Arrhenius analysis produced U_{eff} = 16 cm^{-1} ($\tau_0 = 8.2 \times 10^{-8}$ s). The single-crystal micro-SQUID study of **156** showed $M(H)$ hysteresis at sub-Kelvin temperatures, and the ab initio computational study showed that the magnetic moments of the individual Dy(III) ions are indeed axial, but somewhat less so than those in **155** (g_z = 18.1889−19.4623).

The power of carefully executed ab initio calculations was again illustrated in a study of the centrosymmetric diamondoid cage complex $[Dy_4(\mu_3\text{-}OH)(\mu\text{-}OH)(2,2\text{-}bpt)_4(NO_3)_4\text{-}(EtOH)_2]$ (**157**), where 2,2-Hbpt = 3,5-bis(2-pyridyl)-1,2,4-triazole. In **157**, the four Dy(III) ions are coplanar, and each occupies a distorted square-antiprismatic $\{DyN_4O_4\}$ environment (Figure 38).[137] The calculations revealed that the ground

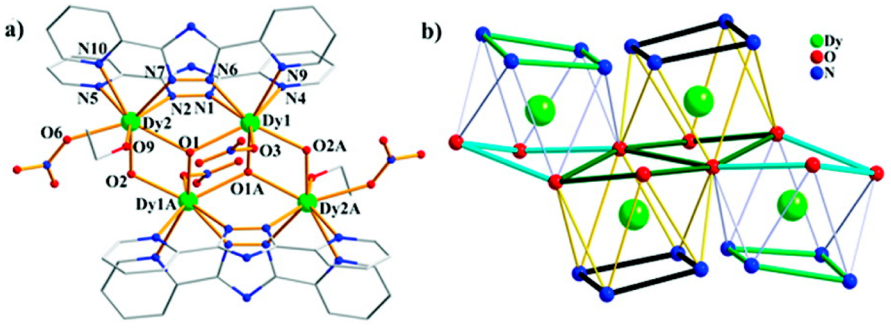

Figure 38. Molecular structure of **157** (from ref 137).

dx.doi.org/10.1021/cr400018q | *Chem. Rev.* XXXX, XXX, XXX−XXX

state of **157** is nonmagnetic and that a toroidal arrangement of the four magnetic moments occurs; furthermore, the first excited exchange doublet was calculated to possess the largest moment. SMM behavior was also identified, with the blocking of the magnetization occurring in the first excited state and not in the nonmagnetic ground state. An anisotropy barrier of U_{eff} = 56 cm^{-1} ($\tau_0 = 5.75 \times 10^{-6}$ s) was determined for the thermally activated relaxation process in **157** in the approximate temperature range 12−20 K, with the relaxation at lower temperatures being accounted for by a QTM process.

Several other Dy_4 cages based on butterfly like arrays of dysprosium ions have also been reported to be either weak SMMs in zero applied field, or to be field-induced SMMs. In $[Dy_4(\mu_3\text{-}OH)_2(mdeaH)_2(piv)_8]$ (H_2mdea = *N*-methyldiethanolamine, piv = pivalate) (**158**), the wing-tip dysprosium ions occupy distorted dodecahedral $\{DyNO_7\}$ environments, and the body dysprosium ions occupy irregular $\{DyO_8\}$ environments.[138] Analysis of the ac susceptibility data on **158** produced U_{eff} = 4.3 cm^{-1} ($\tau_0 = 2.4 \times 10^{-5}$ s) with H_{dc} = 0. The centrosymmetric butterfly $[Dy_4(\mu_3\text{-}OH)_2(ampdH_4)_2(piv)_{10}]$ ($ampdH_4$ = 3-amino-3-methylpentane-1,5-diol) (**159**) also contains eight-coordinate dysprosium ions, each in $\{DyO_8\}$ environments, but with the wing-tip dysprosium ions in square-antiprismatic environments and the body dysprosium ions in bicapped trigonal prismatic sites.[139] The zero-field anisotropy barrier in **159** was determined to be U_{eff} = 3.8 cm^{-1} ($\tau_0 = 1.1 \times 10^{-5}$ s). The isostructural complexes $[Dy_4(\mu_3\text{-}OH)_2(hmmpH)_2(hmmp)Cl_4]\cdot(3MeCN)\cdot(MeOH)$ (**160**) and $[Dy_4(\mu_3\text{-}OH)_2(hmmpH)_2(hmmp)(N_3)_4]\cdot(4MeOH)$ (**161**), where $hmmpH_2$ = 2-[(2-hydroxyethylimino)methyl]-6-methoxyphenol, both contain dysprosium ions in distorted square-antiprismatic environments.[140] Compounds **159** and **161** show a dependence of the dynamic magnetic properties on the chloride or azide ligands, whereby the graphs of $\chi''(T)$ for **160** show no maxima and those for **161** show maxima below 3 K at ac frequencies of ν = 100−1500 Hz, producing U_{eff} = 4.9 cm^{-1} ($\tau_0 = 3.8 \times 10^{-5}$ s). The different ac susceptibility behaviors of **160** and **161** in zero applied field are thought to be due to slight variations in molecular structure and to the different ligand fields generated by the chloride and azide anions. The *ortho*-vanillin-bridged butterfly shaped complex $[Dy_4(\mu_3\text{-}OH)_2(ovn)(piv)_4(NO_3)_2]\cdot(3CH_2Cl_2)\cdot(1.5H_2O)$ (**162**) contains tricapped trigonal prismatic dysprosium ions in the wing-tip positions and distorted square-antiprismatic dysprosium ions in the body positions.[141] SMM behavior was observed in **162** below about 8 K, and a best-fit according to the Arrhenius law gave a small anisotropy barrier of U_{eff} = 3.5 cm^{-1} ($\tau_0 = 3 \times 10^{-5}$ s).

Frequency-dependent behavior of $\chi''(T)$ was observed for the butterfly shaped cages $[Dy_4(\mu_3\text{-}OH)_2(php)_2(OAc)_6(H_2O)_2]\cdot(4MeOH)\cdot(2H_2O)$ (**163**)[142] and $[Dy_4(\mu_3\text{-}OH)_2(L^{17})_2(acac)_6]\cdot(2H_2L^{17})\cdot(2MeCN)$ (**164**),[143] where H_2php = 2,6-(picolinoylhydrazone)pyridine and H_2L^{17} = bis-(salicylidene)-1,2-cyclohexanediamine; however, no peak maxima were present for either compound. In the case of **164**, applying an optimum static field of H_{dc} = 1400 Oe did reveal $\chi''(T)$ maxima, and produced an anisotropy barrier of U_{eff} = 15 cm^{-1} ($\tau_0 = 3.66 \times 10^{-6}$ s).

3.4.4. Cube-like Ln_4 SMMs. It has been reported that tetrametallic dysprosium compounds containing $[Dy_4(\mu_3\text{-}OH)_4]^{8+}$ heterocubane cores are likely to be SMMs only if the Dy−O−Dy angles are greater than 99°, when "favorable magnetic interactions" can be enabled by the bridging hydroxide ligands.[146] Whereas some evidence does exist to support this hypothesis, it must be considered in light of the fact that very few examples of cubane-like Dy_4 SMMs are known, and that the known examples typically have very small anisotropy barriers.

Varying the dysprosium precursor and the solvent of the 1:1:1 stoichiometric reaction of the Schiff-base ligand 2-[{(2-hydroxy-3-methoxyphenyl)methylidene}amino] benzoic acid (H_2L^{18}) with potassium hydroxide and either $DyCl_3\cdot(6H_2O)$ or $Dy(NO_3)_3\cdot(6H_2O)$ produced the cubane-containing $[Dy_4(\mu_3\text{-}OH)_4(\mu\text{-}OH)_2(HL^{18})_4(C_6H_4NH_2CO_2)_2(H_2O)_4]$ (**165**) or the bis-cubane octametallic complex $[\{Dy_4(\mu_3\text{-}OH)_4\}_2(OH)_2(HL^{18})_{10}(C_6H_4NH_2CO_2)_2(NO_3)_2(H_2O)_4]$ (**166**).[144] The dysprosium centers in **165** and **166** reside in chemically and geometrically similar $\{DyO_8\}$ environments; however, whereas **165** shows no SMM properties, **166** does show some frequency-dependent $\chi''(T)$ behavior, although no maxima were observed and a U_{eff} value could not be obtained. The intracube Dy−O−Dy angles in **166** are in the range 102.5(4)−109.3(4)°; in contrast, the analogous angles in **165** are on average more acute, and these subtle differences in molecular structure could be responsible for the differing dynamic magnetic properties of the two compounds. In the bis-cubane cage complex $[Dy_4(\mu_3\text{-}OH)_2(\mu_3\text{-}O)_2(cpt)_6(MeOH)_6(H_2O)]$ (**167**), where Hcpt = 4-(4-carboxyphenyl)-1,2,4-triazole, the two cubane units are linked by two $[cpt]^-$ ligands; however, the dysprosium ions are separated by a sufficiently large distance to render intercubane interactions very weak.[145] The Dy(III) centers are all eight-coordinate, and even though the Dy−O−Dy interactions are 103.7(4)−108.9(5)° (i.e., much greater than 99°), the response of **167** to alternating current magnetic fields is too weak to allow an anisotropy barrier to be determined, although a micro-SQUID study at T = 40 mK did show small hysteresis loops. The cubane-containing $[Dy_4(\mu_3\text{-}OH)_4(nic)_6(py)(MeOH)_7][ClO_4]_2\cdot(py)\cdot(4MeOH)$ (**168**) (nic = iso-nicotinate) shows a variation in $\chi''(T)$ similar to **167** across a range of frequencies; that is, weak SMM behavior is apparent but no maxima were observed.[146] The carbonate-bridged tetrametallic species $[Dy_4(3\text{-}bpp)\text{-}(CO_3)_6(H_2O)_3]\cdot(dmso)\cdot(18H_2O)$ (**169**), where bpp = 2,6-di(pyrazol-3-yl)pyridine, contains a tetrahedral array of dysprosium ions, with three eight-coordinate dysprosiums and one nine-coordinate dysprosium. The SMM properties of **169** are also quite weak; however, an anisotropy barrier of 4 cm^{-1}, with $\tau_0 \approx 10^{-6}$ s, was estimated.[147]

The calixarene-supported SMM $[Dy_4(\mu_3\text{-}OH)_4(TBSOC)\text{-}(H_2O)_4(MeOH)]\cdot(4H_2O)$ (H_4TBSOC = *p-tert*-butylsulfonylcalix[4]arene) (**170**) contains a distorted cubane core in which the calixarene ligands bridge the metal centers via its phenolate oxygens donors (Figure 39).[148] The Dy(III) ions are eight-coordinate in $\{DyO_8\}$ environments, and the Dy−O−Dy angles are in the range 106.1(4)−107.9(3)°. The $\chi''(T)$ plots are frequency dependent below about 7 K and at ac frequencies in the range 50−1488 Hz. The anisotropy barrier extracted from the Arrhenius analysis of **170** is U_{eff} = 16 cm^{-1} ($\tau_0 = 1.1 \times 10^{-8}$ s).

3.5. Pentametallic and Hexametallic SMMs

Single-molecule magnets containing five or six lanthanide ions are uncommon, and all but one example contain dysprosium. The μ-bridging ligands in Ln-SMMs with five or more lanthanides are invariably *O*-donors, with alkoxides, phenolates, hydroxide, and carboxylates being widely used (Table 6). The

dx.doi.org/10.1021/cr400018q | *Chem. Rev.* XXXX, XXX, XXX−XXX

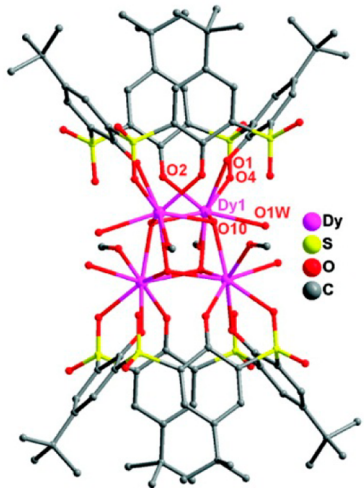

Figure 39. Molecular structure of **170** (from ref 148).

range of structural types becomes much more varied than those seen in SMMs with fewer than five lanthanide ions, and controlling the symmetry of the ligand field at individual lanthanide ions is commensurately more challenging.

3.5.1. Pentametallic Ln-SMMs. At the time of writing, the iso-propoxide-bridged dysprosium pyramid $[Dy_5(\mu_5\text{-}O)(\mu_3\text{-}O^iPr)_4(\mu\text{-}O^iPr)_4(O^iPr)_5]$ (**171**), which consists of six-coordinate dysprosium ions, holds the record for the highest anisotropy barrier in a polymetallic SMM in zero applied field (Figure 40).[149] The pyramid **171** crystallizes as two polymorphs that display the same magnetic properties. The SMM properties of **171** become apparent below about 50 K from ac susceptibility measurements, with a frequency-dependent maximum in $\chi''(T)$ plots being observed at 40 K (Figure 40). The variation of ln τ with T^{-1} is linear above 35 K, and the resulting Arrhenius analysis produced an anisotropy barrier of $U_{eff} = 367 \pm 7.5$ cm^{-1} ($\tau_0 = 4.7 \times 10^{-10}$ s). A second thermally activated relaxation process in **171** below 12 K is also evident, with an estimated $U_{eff} = 32.4 \pm 0.5$ cm^{-1} ($\tau_0 = 3.8 \times 10^{-6}$ s), although this process also overlaps with QTM at very low temperatures. A number of important principles were combined in the design of **171**: first, the predominance of single-ion effects was taken into account; second, by analogy to the family of phthalocyanine SMMs, the (approximate) local 4-fold symmetry of the dysprosium coordination environments was considered important to enhance the single-ion anisotropy; third, triangular Dy_3 structural motifs, which can produce unusual effects such as those observed in **131**, are prevalent within **171**. Whether or not the combination of these properties are indeed responsible for the very large anisotropy barrier in **171**, which contains Kramers' ions, is not yet clear. However it is noteworthy that neither the isostructural terbium (non-Kramers' ion) nor erbium (Kramers' ion) analogues of **171** show any SMM properties. In contrast, the holmium version $[Ho_5(\mu_5\text{-}O)(\mu_3\text{-}O^iPr)_4(\mu\text{-}O^iPr)_4(O^iPr)_5]$ (**172**) shows frequency-dependent $\chi''(T)$ curves in zero field but with no maxima; however, in an applied field of $H_{dc} = 3.5$ kOe, an anisotropy barrier of $U_{eff} = 278 \pm 3.5$ cm^{-1} ($\tau_0 = 1.5 \times 10^{-9}$ s) was determined, suggesting very efficient QTM in zero applied field.[150] Indeed, only narrow $M(H)$ hysteresis was found in **171** and **172** due to fast QTM at temperatures below 4 K, which is most likely due to hyperfine interactions.

Although the pyramidal structure of $[Dy_5(\mu_4\text{-}OH)(\mu_3\text{-}OH)_4(Ph_2acac)_{10}]$ (**173**) is similar to that of **171**, important differences could account for the less-pronounced SMM properties, such as the lack of a μ_5-oxo ligand; the fact that the Dy(III) ions in **173** are eight-coordinate; and the lack of 4-fold symmetry in all but the apical dysprosium coordination sites.[151] Below 8 K, the out-of-phase susceptibility of **173** is temperature and frequency dependent, and the relaxation behavior follows the Arrhenius law in the range 1.8−3.6 K, which results in an estimated anisotropy barrier of $U_{eff} = 23$ cm^{-1} ($\tau_0 = 4.5 \times 10^{-9}$ s).

The trigonal bipyramidal cage complex $[Dy_5(\mu_3\text{-}OH)_6(acc)_6(H_2O)_{10}][Cl]_9{\cdot}24H_2O$ (acc = 1-aminocyclohexane carboxylic acid) (**174**) contains five crystallographically unique Dy(III) ions, with the three equatorial dysprosiums in square-antiprismatic environments and the two apical dysprosiums in bicapped trigonal prismatic environments.[152] Compound **174** shows no SMM properties in the $\chi''(T)$ data; however, it was seemingly possible to determine an anisotropy barrier using a Debye model and the $\chi''(\nu)$ data, which produced $U_{eff} \approx 1.3$ cm^{-1} ($\tau_0 \approx 1.01 \times 10^{-6}$ s).

3.5.2. Hexametallic Ln-SMMs. The structure of the recently reported hexametallic cage $[Dy_6(L^{19})(\mu_4\text{-}O)$-

Table 6. Penta- and Hexametallic Lanthanide SMMs[a]

Ln-SMM	U_{eff}/cm^{-1} (H_{dc}/Oe)	hysteresis (K)	ref
$[Dy_5(\mu_5\text{-}O)(\mu_3\text{-}O^iPr)_4(\mu\text{-}O^iPr)_4(O^iPr)_5]$ (**171**)	367, 32.4		149
$[Ho_5(\mu_5\text{-}O)(\mu_3\text{-}O^iPr)_4(\mu\text{-}O^iPr)_4(O^iPr)_5]$ (**172**)	278 (3500)		150
$[Dy_5(\mu_4\text{-}OH)(\mu_3\text{-}OH)_4(Ph_2acac)_{10}]$ (**173**)	23		151
$[Dy_5(\mu_3\text{-}OH)_6(acc)_6(H_2O)_{10}][Cl]_9$ (**174**)	1.3		152
$[Dy_6(\mu_3\text{-}OH)_4(ovn)_2(L^{11})_2Cl(H_2O)_9]^{5+}$ (**133**)	139		117
$[Dy_6(L^{19})(\mu_4\text{-}O)(NO_3)_4(MeOH)]$ (**175**)	23.6, 28.3	0.03	153
$[Dy_6(\mu_3\text{-}CO_3)_2(ovph)_4(Hovph)_2Cl_4(H_2O)_2]$ (**176**)	53		154
$[Dy_6(\mu_3\text{-}CO_3)_2(OAc)_3(L^{20})_5(HL^{20})(MeOH)]$ (**177**)	39		155
$[Dy_6(\mu_3\text{-}OH)_3(\mu_3\text{-}CO_3)(\mu\text{-}OMe)(HL^{21})_6(MeOH)_4(H_2O)_2]$ (**178**)	26, 3.9		156
$[Dy_6(L^{22})_4(\mu_3\text{-}OH)_4(MeOH)_2(NO_3)_2]$ (**179**)	2.2		157
$[Dy_6(teaH)(teaH_2)(CO_3)(NO_3)(chp)(H_2O)][NO_3]$ (**180**)	2.6		158
$[Tb_6(teaH)(teaH_2)(CO_3)(NO_3)(chp)(H_2O)][NO_3]$ (**181**)	3.3		158
$[Dy_6(\mu_3\text{-}OH)(ovh)_4(avn)_2(NO_3)_4(H_2O)_4][NO_3]_2$ (**183**)	6.7	1.1	160
$[Dy_6(C4A)(\mu_4\text{-}O)(NO_3)_2(HCO_2)(MeO)(dmf)(MeOH)]$ (**184**)	5.3		161

[a]Lattice solvent not listed. U_{eff} values are extracted from measurements in zero applied dc field, unless followed by a number in parentheses to indicate the strength of the applied field.

dx.doi.org/10.1021/cr400018q | Chem. Rev. XXXX, XXX, XXX−XXX

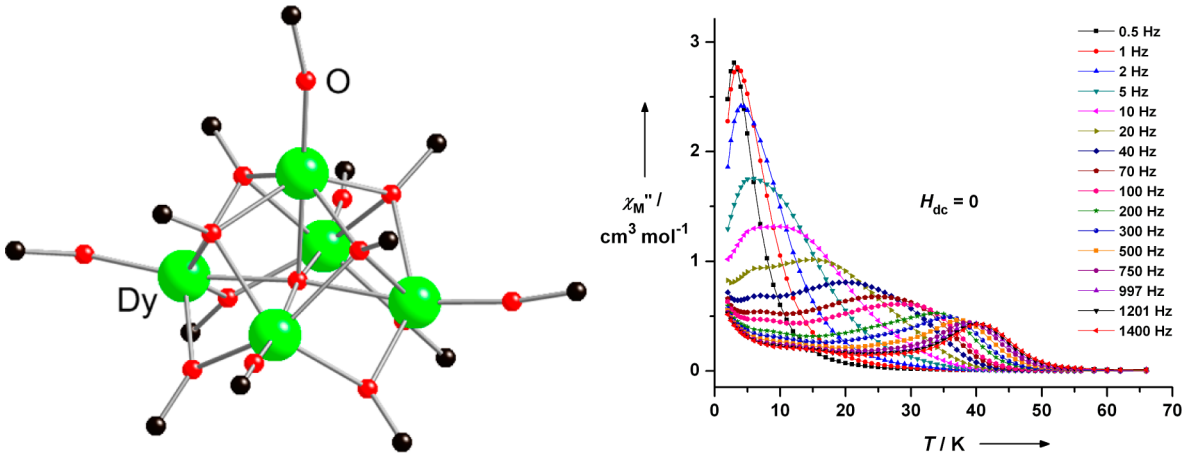

Figure 40. Molecular structure (with the methyl groups and hydrogen atoms omitted) and the $\chi''(T)$ plot of $[Dy_5(\mu_5\text{-}O)(O^iPr)_{13}]$ (**171**) (from ref 149).

$(NO_3)_4(MeOH)]\cdot MeOH$ (**175**) can be regarded as consisting of two edge-sharing triangles, in which five dysprosium ions occupy eight-coordinate square-antiprismatic environments and the sixth is nine-coordinate monocapped square antiprismatic (Figure 41).[153]

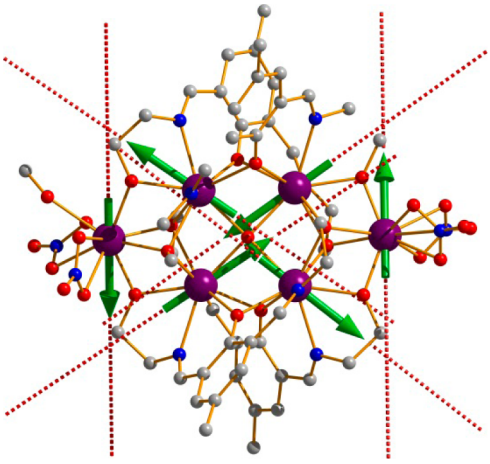

Figure 41. Molecular structure of **175**, showing the orientation of the anisotropy axes (dashed lines) and ordering of the magnetization in the ground state (Dy = purple; O = red; N = blue) (from ref 153).

In contrast to **133**, the anisotropy axes on the dysprosium ions within each triangle of **175**, which were determined by ab initio calculations, lie within their respective triangular planes. Thus, the overall arrangement of the six axes is almost perfectly toroidal, in a manner reminiscent of the prototype triangle **131**. The magnetic interactions between the dysprosium ions in **175** were also investigated by calculations, which found that not only were the intratriangle interactions of a magnitude similar to those found in **131**, crucially the intertriangle interactions are also strong, which is likely to stabilize the overall toroidal moment around the Dy_6 cage. Complex **175** is also an SMM, showing two relaxation processes in the ac susceptibility data, with U_{eff} = 23.6 cm^{-1} ($\tau_0 = 5.8 \times 10^{-8}$ s) and 28.3 cm^{-1} ($\tau_0 = 1.2 \times 10^{-7}$ s).

Ligands derived from the pro-ligand (*E*)-*N*′-(2-hydroxybenzylidene)picolinohydrazide, such as H_2ovph, H_2L^{20}, and H_2L^{21}, in the presence of carbon dioxide appear to be well suited to the formation of Dy_6 cage complexes. The complexes $[Dy_6(\mu_3\text{-}CO_3)_2(ovph)_4(Hovph)_2Cl_4(H_2O)_2]\cdot(3MeOH)\cdot(H_2O)\cdot(MeCN)$ (**176**)[154] (Figure 42) and $[Dy_6(\mu_3\text{-}CO_3)_2(OAc)_3(L^{20})5(HL^{20})(MeOH)]\cdot(5MeOH)\cdot(4H_2O)\cdot(EtOH)$ (**177**)[155] each consist of trigonal prismatic arrays of Dy(III) ions in which the triangular faces are centered on the carbon atom of a carbonate ligand, and the midpoint of each triangle edge is bridged by a carbonate oxygen atom. Additional μ-bridging interactions occur via the alkoxide oxygens, and in both **176** and **177**, the dysprosium ions occupy distorted dodecahedral geometries, with four $\{DyN_2O_5Cl\}$ and two $\{DyN_2O_6\}$ environments in **176** and six $\{DyN_2O_6\}$ environments in **177**. Complex **176** is an SMM in zero applied field, with $\chi''(T)$ being frequency dependent below 25 K and the anisotropy barrier being 53 cm^{-1} ($\tau_0 = 1.2 \times 10^{-6}$ s). In **177**, the anisotropy barrier was estimated as 39 cm^{-1} ($\tau_0 = 6.6 \times 10^{-6}$ s), and $M(H)$ hysteresis was observed below 5.0 K using a sweep rate of 70 mT s^{-1}.

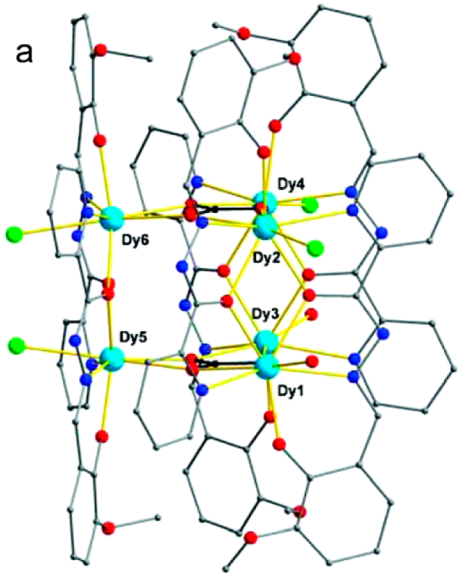

Figure 42. Molecular structure of **176** (from ref 154).

Using reaction conditions similar to those in the synthesis of **176**, but removing the *ortho*-methoxy substituent from the H_2ovph pro-ligand, enables access to a different hexametallic

dx.doi.org/10.1021/cr400018q | *Chem. Rev.* XXXX, XXX, XXX−XXX

complex, $[Dy_6(\mu_3\text{-}OH)_3(\mu_3\text{-}CO_3)(\mu\text{-}OMe)(HL^{21})_6(MeOH)_4(H_2O)_2]\cdot(3MeOH)\cdot(2H_2O)$ (**178**) (Figure 43).[156] The

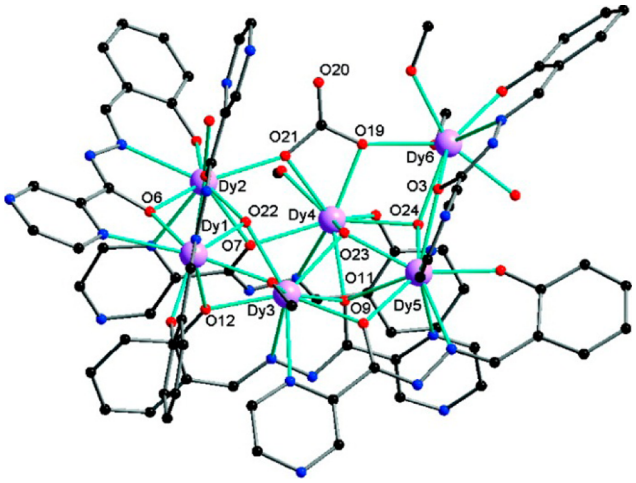

Figure 43. Molecular structure of **178** (from ref 167).

structure of **178** is based on an irregular array of the eight-coordinate dysprosium ions, with the μ-carbonate ligands presumably being derived from atmospheric carbon dioxide. Analysis of the ac susceptibility data and the relaxation times identified two thermal relaxation process in **178**, characterized by 26 cm^{-1} ($\tau_0 = 3.8 \times 10^{-6}$ s) and 3.9 cm^{-1} ($\tau_0 = 4.2 \times 10^{-5}$ s). The ladder-like structure of $[Dy_6(L^{22})_4(\mu_3\text{-}OH)_4(MeOH)_2(NO_3)_2]\cdot6MeCN$ (**179**) is based on phenolate and alkoxide bridges in addition to terminal coordination of the imino nitrogen atoms and bidentate nitrate anions.[157] Complex **179** is a very weak SMM, with the anisotropy barrier being determined from the $\chi''(\nu)$ data as $U_{eff} = 2.2$ cm^{-1} ($\tau_0 = 2.8 \times 10^{-5}$ s).

The hexametallic complex $[Dy_6(teaH)(teaH_2)(CO_3)(NO_3)(chp)(H_2O)][NO_3]\cdot(4.5MeOH)\cdot(1.5H_2O)$ (**180**) ($teaH_3$ = triethanol-amine, chpH = 6-chloro-2-hydroxypyridine) also contains a carbonate ligand formed as a result of fixation of atmospheric CO_2.[158] The six dysprosium ions are arranged into a trapezoid of four coplanar dysprosium ions (all eight-coordinate), with the other two dysprosiums above and below the plane (both nine coordinate). Below 6 K, the out-of-phase ac susceptibility is temperature- and frequency-dependent, although no maxima were observed in the $\chi''(T)$ graphs; however, an anisotropy barrier of $U_{eff} \approx 2.6$ cm^{-1} ($\tau_0 = 7.89 \times 10^{-6}$ s) was estimated. The terbium analogue of **180** (**181**) was similarly estimated to have $U_{eff} = 3.3$ cm^{-1} ($\tau_0 = 1.43 \times 10^{-6}$ s). In the related, teaH-ligated macrocycle $[Dy_6(teaH)_6(NO_3)_6]\cdot(8MeOH)$ (**182**), the six eight-coordinate dysprosium ions are symmetry-related via an S_6 axis passing through the center of, and perpendicular to, the macrocycle. Although no SMM properties were found in **182**, a high-level ab initio computational study did reveal the presence of a toroidal magnetic moment and a nonmagnetic ground state, which originates in the high symmetry of the hexametallic wheel.[159]

The linking of two Dy_3 triangles, in a manner similar to that used for **133** (see above), via a base-catalyzed aldol condensation between acetone and *ortho*-vanillin in the presence of $Dy(NO_3)_3\cdot(5H_2O)$, gives $[Dy_6(\mu_3\text{-}OH)(ovh)_4(avn)_2(NO_3)_4(H_2O)_4][NO_3]_2\cdot(H_2O)\cdot(3Me_2CO)$ (**183**), in which the $[avn]^{2-}$ ligand is the product of the in situ aldol reaction.[160] The two triangles in **183** are linked by μ-alkoxide ligands, and within each triangle all of the Dy(III) centers are eight coordinate. The SMM properties of **183** were apparent in the plots of $\chi''(T)$ below 18 K; however, the anisotropy barrier was quite small at $U_{eff} = 6.7$ cm^{-1} ($\tau_0 = 2 \times 10^{-6}$ s). A micro-SQUID study of **183** produced two-step $M(H)$ hysteresis loops below $T = 1.1$ K at a sweep rate of 0.14 T s^{-1}, which is thought to be a consequence of toroidal magnetic moments within each triangle, in a manner similar to that seen in **133**.

To date, the only hexametallic SMM with an octahedral Ln_6 core is the calixarene-encapsulated cage $[Dy_6(C4A)(\mu_4\text{-}O)(NO_3)_2(HCO_2)(MeO)(dmf)(MeOH)]$ (**184**), in which the six dysprosium ions occupy $\{DyO_8\}$ environments. The out-of-phase susceptibility in **184** is temperature and frequency dependent below 9 K, and **184** has an anisotropy barrier of $U_{eff} = 5.3$ cm^{-1} ($\tau_0 = 1.1 \times 10^{-6}$ s).[161]

3.6. Heptametallic and Higher-Nuclearity SMMs

Two trends begin to emerge for polymetallic lanthanide cages containing seven or more metal ions. First, the number of such polymetallic compounds to be investigated in this context declines rapidly as the cage nuclearity increases. Second, the number of genuine SMMs with well-defined slowly relaxing magnetization decreases equally rapidly, and of those SMMs with, say, unambiguous anisotropy barriers, very few produce barriers of large magnitude (Table 7). Precisely why SMM behavior is seemingly not prominent in higher-nuclearity cages has not been determined beyond arguments that invoke fast and efficient QTM at low temperatures, which seems obvious based on literature precedent. Even in SMMs with "simple" molecular structures, the effects of *J*-type exchange coupling, intra- and intermolecular dipolar interactions, and the often surprising orientations of the easy axes of magnetization (where it has been possible to determine them) can compromise SMM properties. It seems not unlikely that such complications will only be magnified in systems with elaborate molecular architectures, with up to 30 lanthanide ions.

To date, the only heptametallic Ln-SMM with a substantial anisotropy barrier is the disc-like complex

Table 7. Higher-Nuclearity Lanthanide SMMs[a]

Ln-SMM	U_{eff}/cm^{-1} (H_{dc}/Oe)	ref
$[Dy_7(OH)_6(thmeH_2)_5(thmeH)(tpa)_6(MeCN)_2][NO_3]_2$ (**185**)	97	162
$[Dy_8(\mu_4\text{-}CO_3)_4(L^{20})_8(H_2O)_8]$ (**186**)	52	164
$[Dy_8(OH)_8(phendox)_6(H_2O)_8]Cl_2$ (**188**)	3	166
$[Dy_{11}(OH)_{11}(phendox)_6(phenda)_3(OAc)_3][OH]$ (**191**)	1.2	166
$[2Cl\subset Dy_{12}(OH)_{16}(phenda)_8(H_2O)_8]$ [Dy(phenda)] (**192**)	4.7	169
$[2Cl\subset Dy_{12}(OH)_{16}(phenda)_8(H_2O)_8][OH]_2$ (**193**)	2.3	169

[a]Lattice solvent not listed.

dx.doi.org/10.1021/cr400018q | *Chem. Rev.* XXXX, XXX, XXX–XXX

$[Dy_7(OH)_6(thmeH_2)_5(thmeH)(tpa)_6(MeCN)_2][NO_3]_2$ (**185**) ($thmeH_3$ = tris(hydroxymethyl)ethane, tpaH = triphenylacetic acid). The structure of the $\{Dy_7\}$ disc (Figure 44) consists of a central dysprosium ion in a hexagonal $\{Dy_6\}$ wheel.[162] Six μ_3-OH ligands bridge between the central dysprosium the peripheral dysprosium ions, and the peripheral dysprosium ions are each bridged by 2.121 $[thmeH]^{2-}$ and $[thmeH_2]^-$ ligands, and by a 2.11 $[tpa]^-$ ligand (using the Harris notation to describe ligand binding modes[163]). The coordination environment of the central dysprosium ion is completed by two acetonitrile ligands, one above and one below the plane of the disc. Complex **185** shows frequency-dependent out-of-phase susceptibility below 28 K, and at higher ac frequencies multiple relaxation pathways are apparent, which are most likely due to the two different types of dysprosium coordination environment. Applying the Arrhenius analysis to the ac susceptibility data for **185** above 10.5 K produces U_{eff} = 97 cm^{-1} ($\tau_0 = 7.2 \times 10^{-9}$ s), and below 10 K the relaxation gradually switches from a thermally activated mechanism to a QTM regime.

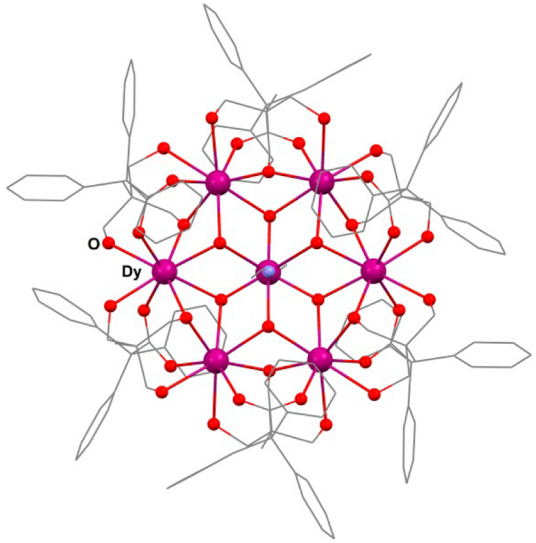

Figure 44. Molecular structure of **185** (from ref 162).

Using reaction conditions similar to those that enabled the synthesis of the Dy_6 SMM **177**, but with $DyCl_3\cdot(6H_2O)$ as the Dy(III) source, results in the octametallic cage complex $[Dy_8(\mu_4\text{-}CO_3)_4(L^{20})_8(H_2O)_8]\cdot(10MeOH)\cdot(2H_2O)$ (**186**).[164] The molecular structure of **186** is based on a square-antiprismatic $[Dy_8(\mu_3\text{-}CO_3)_4]^{16+}$ core in which the dysprosium ions are all connected by four 4.221 carbonate ligands. Eight L^{20} ligands coordinate in a 2.1211 mode, and each dysprosium is also complexed by one aquo ligand. The overall dysprosium coordination geometries are either dodecahedral $\{DyN_2O_6\}$ or monocapped square-antiprismatic $\{DyN_2O_7\}$ (Figure 45).

The Arrhenius plot for **186** is linear above 8 K, which results in an anisotropy barrier of U_{eff} = 52 cm^{-1} ($\tau_0 = 2.1 \times 10^{-6}$ s). Using a conventional SQUID magnetometer, a butterfly shaped hysteresis loop was also observed for **186** at 1.9 K.

The structure of the heptametallic cage complex $[Dy_7(\mu_3\text{-}OH)_5(MeOsalox)_2(MeOsaloxH)_4(PhCO_2)_7(OH)(H_2O)1.5\text{-}(MeOH)_{0.5}]\cdot2.5MeOH\cdot5.25H_2O$ (**187**) is reported to be based on a "jigsaw puzzle" arrangement of the dysprosium ions, with five edge-sharing Dy_3 triangles.[165] Regardless of the elaborate molecular structure, only a very weak temperature dependence of χ'' was observed, and an anisotropy barrier could not be determined. The structure of $[Dy_8(OH)_8(phendox)_6(H_2O)_8]\text{-}Cl_2\cdot(OH)_2\cdot18H_2O\cdot18MeOH$ (**188**) contains two $\{Dy_4(\mu_3\text{-}OH)_4\}$ tetrahedra bridged by the oxime oxygen atoms of the phendox ligands.[166] Despite the apparent similarities in the cube-based structure of **188** and those of **165**−**170** (section 3.4.4), compound **188** shows very weak SMM properties, and an anisotropy barrier could not be determined from an Arrhenius analysis. An alternative method based on modeling of a Debye function did, however, produce U_{eff} = 3 cm^{-1} ($\tau_0 = 1.3 \times 10^{-6}$ s).

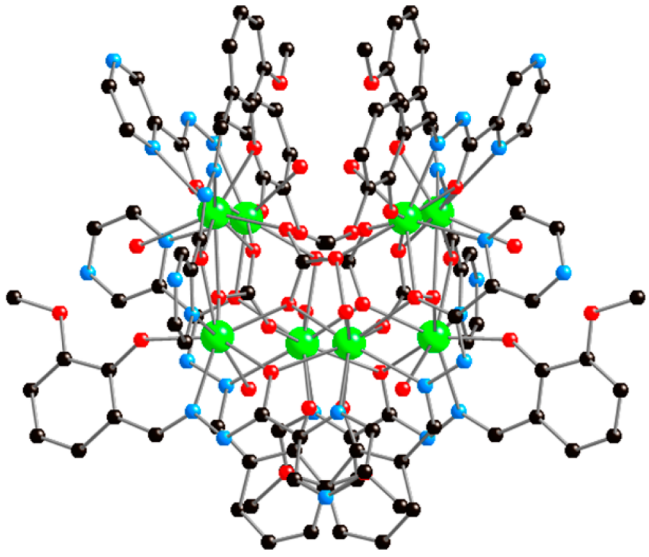

Figure 45. Molecular structure of **186** (Dy = green; N = blue; O = red) (from ref 164).

The nonametallic cage $[Dy_9(OH)_{10}(hmp)_8(NO_3)_8(DMF)_8]\text{-}(OH)\cdot1.6H_2O\cdot0.6DCM$ (**189**) was synthesized from the reaction of $Dy(NO_3)_3\cdot xH_2O$, 2-(hydroxymethyl)pyridine (hmpH), and triethylamine.[167] The structure of **189** features two apical-vertex-sharing square-based pyramids, with two μ_4-OH centered Dy_4 square bases connected to the apical dysprosium ion via eight μ_3-OH ligands. Eight $[hmp]^-$ ligands bind in a 2.21 mode on the edges of the Dy_4 squares. Despite the interesting structure of **189**, $\chi''(T)$ shows only a weak temperature dependence below 3 K; hence an anisotropy barrier could not be determined.

The decametallic cage $[Dy_{10}(\mu_3\text{-}OH)_4(O_2CMe)_{20}(H_2L^{30})_2(H_3L^{30})_2\{NH_2C(CH_2OH)_3\}_2]$ (**190**) contains a Dy_{10} core that can be described as consisting of two Dy_5 bow-tie units, which are connected by two acetate ligands in a 2.11 bonding mode.[168] Two further acetates bind in a 2.11 mode, eight in a 2.21 mode, six in a 1.10 mode, and two in a 1.11 mode. Two H_2L^{35} ligands bind in a 3.12112 mode, and two H_3L^{35} ligands bind in a 2.12111 mode. Despite the unusual molecular structure, **190** shows a weak temperature dependence of χ'' below 7 K, and an anisotropy barrier could not be determined.

The Dy_{11} core of $[Dy_{11}(OH)_{11}(phendox)_6(phenda)_3\text{-}(OAc)_3][OH]\cdot40H_2O\cdot7MeOH$ (**191**) ($phendaH_2$ = 1,10-phenanthroline-2,9-dicarboxylic acid) can be described as comprising two cubane-like $\{Dy_4(\mu_3\text{-}OH)_4\}$ motifs positioned above and below the center of a Dy_3 equilateral triangle.[166] Complex **191** contains four μ_3-OH ligands, three 3.111111

dx.doi.org/10.1021/cr400018q | Chem. Rev. XXXX, XXX, XXX−XXX

$[phenda]^{2-}$ ligands, six 4.211111 $[phendox]^{2-}$ ligands, and three chelating acetate ligands. The out-of-phase susceptibility in **191** is weakly temperature dependent below 5 K, and although an Arrhenius analysis was not possible, an anisotropy barrier of $U_{eff} \approx 1.2$ cm^{-1} ($\tau_0 \approx 7.5 \times 10^{-6}$ s) could apparently be determined from the variation of $\ln(\chi''/\chi')$ with T^{-1}.

The cage complexes $[2Cl\subset Dy_{12}(OH)_{16}(phenda)_8(H_2O)_8]\cdot[X]_2\cdot(solvent)$, where $[X]_2\cdot(solvent) = [Dy(phenda)]\cdot(16dmso)\cdot(10MeOH)\cdot(45H_2O)$ (**192**) or $[OH]_2\cdot(15MeOH)\cdot(40H_2O)$ (**193**), have very similar Dy_{12} core structures that can be regarded as four vertex-sharing $[Dy_4(\mu_3\text{-}OH)_4]$ cubanes (Figure 46).[169]

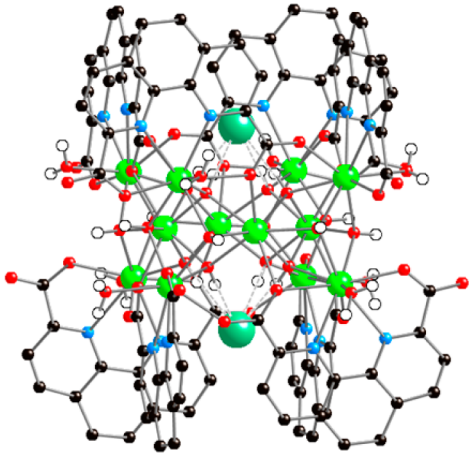

Figure 46. Molecular structure of **192** (Dy = green; N = blue; O = red; Cl = turquoise) (from ref 169).

Eight $[phenda]^{2-}$ ligands bind in a 3.12111 mode, and the coordination sphere of each dysprosium ion is completed by one water molecule. The structures of **192** and **193** are quite unusual; however, their SMM properties are weak. Below 5 K, both **192** and **193** show slight variations in χ'' with temperature but with no maxima, and analysis of the ac susceptibility data enabled anisotropy barriers of $U_{eff} = 4.7$ cm^{-1} ($\tau_0 = 7.51 \times 10^{-7}$ s) and 2.3 cm^{-1} ($\tau_0 = 1.37 \times 10^{-5}$ s) to be determined for **192** and **193**, respectively. The $[valdien]^{2-}$ ligand developed in studies of the dimetallic SMM **80** has also been used to synthesize, through trivial variations in the dysprosium precursor material, the dodecametallic complexes $[Dy_{12}(valdien)_6(OH)_4(O)_2(CO_3)_6]\cdot[Dy_{12}(valdien)_6(OH)_4O_4(CO_3)_6](ClO_4)_4\cdot xH_2O$, or [**194**][**195**] $(ClO_4)_4\cdot xH_2O$, which cocrystallize as independent molecules in the same unit cell. The structure of **194** and the wheel-like structure of **195** are unusual, but despite the molecular structures the magnetic properties have no remarkable features, with χ'' being weakly temperature-dependent below 4 K.[170]

The highest nuclearity lanthanide cage to be investigated within the context of single-molecule magnetism is $[Dy_{30}I(\mu_3\text{-}OH)_{24}(\mu_3\text{-}O)_6(NO_3)_9(nic)_{41}(OH)_3(H_2O)_{38}]$ (**196**). Complex **196** contains six $\{Dy_4(\mu_3\text{-}OH)_4\}$ tetrahedra linked to six dysprosium ions via nine 3.221 nitrate ions. A total of 41 $[nic]^-$ ligands, 38 aquo ligands, six μ_3-oxo ligands, and three hydroxide ligands link the dysprosium ions together.[171] Complex **196** shows some temperature and frequency dependence of out-of-phase susceptibility below 6 K, but with no maxima.

4. CONCLUSIONS

The field of lanthanide single-molecule magnets has grown very rapidly in the past decade. While a wide range of synthetic chemistry has been explored to create new SMMs, quite a lot still remains to be explored with regards to developing and understanding the properties of these materials. Indeed, the field is probably only just entering its adolescence, and its continued rapid development should provide an even more fundamental knowledge and potential for future applications of Ln-SMMs.

Two points seem worth making as the field progresses. First, for 3d-SMMs, it was clear from the mid-1990s what properties were required to establish an SMM. The main criteria were magnetic hysteresis, which often required very low temperature single-crystal measurements, and/or frequency-dependent peaks in the out-of-phase susceptibility that would allow an anisotropy barrier, or energy barrier to magnetization reversal, to be calculated. Unfortunately, these guiding principles have not been stringently applied to 4f-element SMMs. Too often, Ln-SMMs have been claimed with little justification beyond a feeble rise in the out-of-phase susceptibility at the lowest temperatures attainable with a conventional SQUID magnetometer. For completeness, in this Review we have included all claims of Ln-SMM behavior, but it would be beneficial if the area returned to a stricter definition of an SMM: if there are no maxima in the $\chi''(T)$ data, acquired across a range of ac frequencies, or if there is no clear $M(H)$ hysteresis, then the compound should not be claimed as an SMM. The beautiful structural chemistry is still worth reporting, but inaccurate claims concerning the physics of the system are distracting and could impede the development of the field.

The use of small applied external fields to establish SMM behavior is also debatable, but is often justified to develop an understanding of quantum tunneling processes. Quantum tunneling of magnetization can be extremely efficient in 4f-SMMs, and use of a small external field to switch off this relaxation path can allow the thermal energy barrier to be measured. This is particularly relevant to SMMs based on quadrupolar spin-active lanthanide nuclei with high natural abundance, for example, ^{159}Tb and ^{165}Ho. However, it should always be clearly stated that anisotropy barriers derived in this way have indeed been derived using an applied external field; hence they are not absolutely comparable to energy barriers derived in zero applied field.

The second point concerns theoretical understanding of the energy barriers in Ln-SMMs. There is healthy debate about the best route to follow. Beautiful computational work from the Chibotaru group,[172] and more recently from Sessoli and co-workers,[45] has shown that high-level ab initio calculations using CASSCF approaches are extremely valuable. These calculations are computationally demanding, and they are not trivial to perform accurately; however, it is conceivable that they could be readily performed inaccurately in the wrong hands. Such calculations also require much greater informed intervention from the expert theorist. In contrast, conventional DFT calculations are easier to perform, but they offer little insight in the dynamic magnetic properties of the f-elements. Whether use of ab initio calculations will ever become general, or whether they will always involve high-quality theorists, is an open question. The field of 3d-SMMs became hugely reliant on a very small number of groups able to perform micro-SQUID measurements to low temperature; it would be unfortunate if

dx.doi.org/10.1021/cr400018q | Chem. Rev. XXXX, XXX, XXX−XXX

the area of Ln-SMMs became similarly reliant on a very small number of theorists. Other groups have proposed a crystal field approach, or more precisely a ligand field approach, where the directionality and charge density of ligand donor atoms are accounted for, as well as the geometry produced by the traditional "point negative charges" of crystal field theory. This approach looks much less computationally demanding, but probably has some restrictions, for example, the influence of noncovalent intermolecular interactions. However, given its comparative simplicity, and its ability to produce results that can be understood in a simple pictorial way by synthetic chemists, it seems that this ligand field approach should be developed further and its complementarity with CASSCF calculations explored.

An important contribution to the theoretical understanding of Ln-SMMs comes from single-crystal magnetic measurements, which are vital in determining the principle axis of anisotropy in Ln-SMMs. The usefulness of low-temperature emission and absorption spectroscopy to measure the splittings within the lowest energy *J*-multiplets is an important recent development, which remains to be fully explored. Preliminary results suggest this approach could also be very fruitful. We have not discussed at length the use of monometallic Ln-SMMs, particularly the $[Pc_2Tb]$ complexes, in prototype devices. This is remarkable work, with reports of molecular spin valves and spin transistors arising from controlled deposition of Ln-SMMs on substrates such as carbon nanotubes. This area is already opening astonishing new physics, for example, the measurement of a single nuclear spin. Technological applications of this work are not implausible.

In summary, a huge number of Ln-SMMs have been reported in a little less than a decade. The synthetic chemistry methods have been firmly established since Werner's era, so this aspect is, clearly, much more advanced than the low-temperature physical characterization and the theoretical understanding. As the advances in measurement techniques and theoretical models continue, we hope and expect that genuine rational design of SMMs will become commonplace.

AUTHOR INFORMATION

Corresponding Author

*E-mail: richard.layfield@manchester.ac.uk.

Notes

The authors declare no competing financial interest.

Biographies

Daniel N. Woodruff graduated with a first-class Master of Chemistry degree from The University of Manchester in 2009, where he carried out undergraduate research in s-block organometallic chemistry in the Layfield group. He was a Ph.D. student in Manchester from 2009 to 2012, where he worked on a project supervised by Prof. Richard Winpenny and Dr. Richard Layfield, dealing with the applications of organometallic synthesis in molecular magnetism. He is currently a postdoctoral researcher supervised by Prof. Rodolphe Clérac and Dr. Pierre Dechambenoit in the Molecular Magnetic Materials group, in the Centre de Recherche Paul Pascal, Bordeaux, France.

Richard E. P. Winpenny obtained both his degrees from Imperial College, London; his Ph.D. studies with Prof. David Goodgame involved synthesis of coordination polymers. After a period at Texas A&M University, working as a postdoctoral fellow with Prof. John Fackler, Jr., he moved to a lectureship at the University of Edinburgh. In 2000, after 10 years in the frozen wastes of Northern Britain, he was appointed to the Chair of Inorganic Chemistry at the University of Manchester. He holds a Royal Society Wolfson Merit Award for his work in molecular magnetism and won the Royal Society of Chemistry Tilden Prize in 2011. He is currently the Director of the Photon Science Institute in Manchester.

Richard A. Layfield graduated from the University of Leeds, and subsequently obtained his Ph.D. at the University of Cambridge, working under the supervision of Prof. Dominic S. Wright on metal cyclopentadienide chemistry. After spells as a Junior Research Fellow and fixed-term Lecturer in Cambridge, he was appointed to a Lectureship in Inorganic Chemistry at The University of Manchester in 2007. His research interests encompass a range of topics in organometallic chemistry, with emphasis on applications in molecular magnetism and also small-molecule activation reactivity. He has been awarded the Royal Society of Chemistry Meldola Medal (2006), and a Fellowship for Experienced Researchers by the Alexander von Humboldt Foundation (2010–2012).

dx.doi.org/10.1021/cr400018q | *Chem. Rev.* XXXX, XXX, XXX–XXX

ACKNOWLEDGMENTS

The authors thank Nicholas F. Chilton for preparing the cover art work.

REFERENCES

(1) (a) Sessoli, R.; Hui, L.; Schake, A. R.; Wang, S.; Vincent, J. B.; Folting, K.; Gatteschi, D.; Christou, G. *J. Am. Chem. Soc.* **1993**, *115*, 1804. (b) Sessoli, R.; Gatteschi, D.; Caneschi, A.; Novak, M. A. *Nature* **1993**, *365*, 141.

(2) Gatteschi, D.; Sessoli, R.; Villain, J. *Molecular Nanomagnets*; Oxford University Press: Oxford, 2006.

(3) Eliseeva, S. V.; Bünzli, J. C. G. *New J. Chem.* **2011**, *35*, 1165.

(4) (a) Leuenberger, M. N.; Loss, D. *Nature* **2001**, *410*, 789. (b) Ardavan, A.; Rival, O.; Morton, J. J. L.; Blundell, S. J.; Tyryshkin, A. M.; Timco, G. A.; Winpenny, R. E. P. *Phys. Rev. Lett.* **2007**, *98*, 057201.

(5) (a) Mannini, M.; Pineider, F.; Danieli, C.; Totti, F.; Sorace, L.; Sainctavit, P.; Arrio, M. A.; Otero, E.; Joly, L.; Cezar, J. C.; Cornia, A.; Sessoli, R. *Nature* **2010**, *468*, 417. (b) Urdampilleta, M.; Nguyen, N. V.; Cleuziou, J. P.; Klyatskaya, S.; Ruben, M.; Wernsdorfer, W. *Int. J. Mol. Sci.* **2011**, *12*, 6656.

(6) Yoshihara, D.; Karasawa, S.; Koga, N. *J. Am. Chem. Soc.* **2008**, *130*, 10460.

(7) Zadrozny, J. M.; Atanasov, M.; Bryan, A. M.; Lin, C. Y.; Rekken, B. D.; Power, P. P.; Neese, F.; Long, J. R. *Chem. Sci.* **2013**, *4*, 125.

(8) Aromí, G.; Brechin, E. K. *Struct. Bonding (Berlin)* **2006**, *122*, 1.

(9) Milios, C. J.; Vinslava, A.; Wernsdorfer, W.; Moggach, S.; Parsons, S.; Perlepes, S. P.; Christou, G.; Brechin, E. K. *J. Am. Chem. Soc.* **2007**, *129*, 2754.

(10) Ako, A. K.; Hewitt, I. J.; Mereacre, V.; Clérac, R.; Wernsdorfer, W.; Anson, C. E.; Powell, A. K. *Angew. Chem., Int. Ed.* **2006**, *45*, 4926.

(11) Bencini, A.; Gatteschi, D. *Electron Paramagnetic Resonance of Exchange-Coupled Systems*; Springer-Verlag: Berlin, 1990.

(12) (a) Waldmann, O. *Inorg. Chem.* **2007**, *46*, 10035. (b) Ruiz, E.; Cirera, J.; Cano, J.; Alvarez, S.; Loose, C.; Kortus, J. *Chem. Commun.* **2008**, 52.

(13) Neese, F.; Pantazis, D. *Faraday Discuss.* **2011**, *148*, 229.

(14) Nakano, M.; Oshio, H. *Chem. Soc. Rev.* **2011**, *40*, 3239.

(15) (a) Rinehart, J. D.; Long, J. R. *Chem. Sci.* **2011**, *2*, 2078. (b) Sorace, L.; Benelli, C.; Gatteschi, D. *Chem. Soc. Rev.* **2011**, *40*, 3092. (c) Guo, Y. N.; Xu, G. F.; Guo, Y.; Tang, J. *Dalton Trans.* **2011**, *40*, 9953. (d) Sessoli, R.; Powell, A. K. *Coord. Chem. Rev.* **2009**, *253*, 2328. (e) Wang, B. W.; Jiang, S. D.; Wang, X. T.; Gao, S. *Sci. China, Ser. B: Chem.* **2009**, *52*, 1739. (f) Brooker, S.; Kitchen, J. A. *Dalton Trans.* **2009**, 7331. (g) Habib, F.; Murugesu, M. *Chem. Soc. Rev.* **2013**, DOI: 10.1039/C2CS35361J.

(16) See, for example: (a) Mishra, A.; Wernsdorfer, W.; Abboud, K. A.; Christou, G. *J. Am. Chem. Soc.* **2004**, *126*, 15648. (b) Papatriantafyllopoulou, C.; Wernsdorfer, W.; Abboud, K. A.; Christou, G. *Inorg. Chem.* **2011**, *50*, 421. (c) Karotsis, G.; Kennedy, S.; Teat, S. J.; Beavers, C. M.; Fowler, D. A.; Morales, J. J.; Evangelisti, M.; Dalgarno, S. J.; Brechin, E. K. *J. Am. Chem. Soc.* **2010**, *131*, 12983.

(17) (a) Mougel, V.; Chatelain, L.; Pecaut, J.; Caciuffo, R.; Colineau, E.; Griveau, J. C.; Mazzanti, M. *Nat. Chem.* **2012**, *4*, 1011. (b) Antunes, M. A.; Pereira, L. C. J.; Santos, I. C.; Mazzanti, M.; Marcalo, J.; Almeida, M. *Inorg. Chem.* **2011**, *50*, 9915. (c) Mills, D. R.; Moro, F.; McMaster, J.; van Slageren, J.; Lewis, W.; Blake, A. J.; Liddle, S. T. *Nat. Chem.* **2011**, *3*, 454. (d) Rinehart, J. D.; Meihaus, K. R.; Long, J. R. *J. Am. Chem. Soc.* **2010**, *132*, 7572. (e) Magnani, N.; Apostolidis, C.; Morgernstern, A.; Colineau, E.; Griveau, J. C.; Bolvin, H.; Walter, O.; Caciuffo, R. *Angew. Chem., Int. Ed.* **2011**, *50*, 1696. (f) Rinehart, J. D.; Long, J. R. *J. Am. Chem. Soc.* **2010**, *131*, 12558. (g) Magnani, N.; Colineau, E.; Eloirdi, R.; Griveau, J. C.; Caciuffo, R.; Cornet, S. M.; May, I.; Sharrad, C. A.; Collison, D.; Winpenny, R. E. P. *Phys. Rev. Lett.* **2010**, *104*, 197202.

(18) (a) Wybourne, B. G. *Spectroscopic Properties of Rare Earths*; John Wiley and Sons: New York, 1965. (b) Abragam, A.; Bleaney, B. *Electron Paramagnetic Resonance of Transition Ions*; Oxford University Press: New York, 2012.

(19) Sievers, J. *Z. Phys. B: Condens. Matter Quanta* **1982**, *45*, 289.

(20) Morrish, A. H. *The Physical Principles of Magnetism*; Wiley: New York, 1966.

(21) Ishikawa, N.; Sugita, M.; Ishikawa, T.; Koshihara, S.; Kaizu, Y. *J. Am. Chem. Soc.* **2003**, *125*, 8694.

(22) (a) Ishikawa, N. *Struct. Bonding (Berlin)* **2010**, *135*, 211−228. (b) Ishikawa, N. *Polyhedron* **2007**, *26*, 2147.

(23) Candini, A.; Klyatskaya, S.; Ruben, M.; Wernsdorfer, W.; Affronte, M. *Nano Lett.* **2011**, *11*, 2634.

(24) Gonidec, M.; Biagi, R.; Corradini, V.; Moro, F.; De Renzi, V.; del Pennino, U.; Summa, D.; Muccioli, L.; Zannoni, C.; Amabilino, D.; Veciana, J. *J. Am. Chem. Soc.* **2011**, *133*, 6603.

(25) Klyatskaya, S.; Galán Mascarós, J. R.; Bogani, L.; Hennrich, F.; Kappes, M.; Wernsdorfer, W.; Ruben, M. *J. Am. Chem. Soc.* **2011**, *133*, 15143.

(26) Stepanow, S.; Honolka, J.; Gambardella, P.; Vitali, L.; Abdurakhmanova, N.; Tseng, T. Z.; Rauschenbach, S.; Tait, S. L.; Sessi, V.; Klyatskaya, S.; Ruben, M.; Kern, K. *J. Am. Chem. Soc.* **2010**, *132*, 11900.

(27) Katoh, K.; Komeda, T.; Yamashita, M. *Dalton Trans.* **2011**, *40*, 4708.

(28) (a) Cornia, A.; Mannini, M.; Sainctavit, P.; Sessoli, R. *Dalton Trans.* **2011**, *40*, 3076. (b) Katoh, K.; Isshiki, H.; Komeda, T.; Yamashita, M. *Coord. Chem. Rev.* **2011**, *255*, 2124.

(29) Vincent, R.; Klyatskaya, S.; Ruben, M.; Wernsdorfer, W.; Balestro, F. *Nature* **2012**, *488*, 357.

(30) Urdampilleta, M.; Klyatskaya, S.; Ruben, M.; Wernsdorfer, W. *Nat. Mater.* **2011**, *10*, 502.

(31) (a) Ishikawa, N.; Sugita, M.; Okubo, T.; Tanaka, N.; Iino, T.; Kaizu, Y. *Inorg. Chem.* **2003**, *42*, 2440. (b) Ishikawa, N. *J. Phys. Chem. A* **2003**, *107*, 5831. (c) Ishikawa, N.; Sugita, M.; Ishikawa, T.; Koshihara, S.; Kaizu, Y. *J. Phys. Chem. B* **2004**, *108*, 11265.

(32) Ishikawa, N.; Sugita, M.; Wernsdorfer, W. *Angew. Chem., Int. Ed.* **2005**, *44*, 2931.

(33) Ishikawa, N.; Sugita, M.; Wernsdorfer, W. *J. Am. Chem. Soc.* **2005**, *124*, 3650.

(34) Branzoli, F.; Carretta, P.; Filibian, M.; Zoppellaro, G.; Graf, M. J.; Galan-Mascaros, J. R.; Fuhr, O.; Brink, S.; Ruben, M. *J. Am. Chem. Soc.* **2009**, *131*, 4387.

(35) Waters, M.; Moro, F.; Krivokapic, I.; McMaster, J.; van Slageren, J. *Dalton Trans.* **2012**, *41*, 1128.

(36) Gonidec, M.; Amabilino, D.; Veciana, J. *Dalton Trans.* **2012**, *41*, 13632.

(37) Takamatsu, S.; Ishikawa, N. *Polyhedron* **2007**, *26*, 1859.

(38) Ishikawa, N.; Sugita, M.; Tanaka, N.; Ishikawa, T.; Koshihara, S.; Kaizu, Y. *Inorg. Chem.* **2004**, *43*, 5498.

(39) Takamatsu, S.; Ishikawa, T.; Koshihara, S.; Ishikawa, N. *Inorg. Chem.* **2007**, *46*, 7250.

(40) Ishikawa, N.; Mizuno, Y.; Takamatsu, S.; Ishikawa, T.; Koshihara, S. *Inorg. Chem.* **2008**, *47*, 10217.

(41) Gonidec, M.; Davies, E. S.; McMaster, J.; Amabilino, D. B.; Veciana, J. *J. Am. Chem. Soc.* **2010**, *132*, 1756.

(42) Gonidec, M.; Luis, F.; Vilchez, A.; Esquena, J.; Amabilino, D. B.; Veciana, J. *Angew. Chem., Int. Ed.* **2010**, *49*, 1623.

(43) Wang, H.; Wang, K.; Tao, J.; Jiang, J. *Chem. Commun.* **2012**, *24*, 2973.

(44) Car, P. E.; Perfetti, M.; Mannini, M.; Favre, A.; Caneschi, A.; Sessoli, R. *Chem. Commun.* **2011**, *47*, 3751.

(45) (a) Cucinotta, G.; Perfetti, M.; Luzon, J.; Etienne, M.; Car, P. E.; Caneschi, A.; Calvez, G.; Bernot, K.; Sessoli, R. *Angew. Chem., Int. Ed.* **2012**, *51*, 1606. (b) Boulon, M. E.; Cucinotta, G.; Luzon, J.; Degl'Innocenti, C.; Perfetti, M.; Bernot, K.; Calvez, G.; Caneschi, A.; Sessoli, R. *Angew. Chem., Int. Ed.* **2013**, *52*, 350.

(46) Watanabe, A.; Yamashita, A.; Nakano, M.; Yamamura, T.; Kajiwara, T. *Chem.-Eur. J.* **2011**, *17*, 7428.

(47) (a) Jiang, S.; Wang, B.; Sun, H.; Wang, Z.; Gao, S. *J. Am. Chem. Soc.* **2011**, *133*, 4730. (b) Jiang, S.; Liu, S.; Zhou, L.; Wang, B.; Wang, Z.; Gao, S. *Inorg. Chem.* **2012**, *51*, 3079.
(48) (a) Schumann, H.; Köhn, R.; Reier, F. W.; Dietrich, A.; Pickardt, J. *Organometallics* **1989**, *8*, 1388. (b) Evans, W. J.; Johnston, M. A.; Clark, R. D.; Ziller, J. W. *J. Chem. Soc., Dalton Trans.* **2000**, 1609.
(49) (a) Jeletic, M.; Lin, P.; Le Roy, J. J.; Korobkov, I.; Gorelsky, S. I.; Murugesu, M. *J. Am. Chem. Soc.* **2011**, *133*, 19286. See also: (b) Le Roy, J. J.; Jeletic, M.; Gorelsky, S. I.; Korobkov, I.; Ungur, L.; Chibotaru, L. F.; Murugesu, M. *J. Am. Chem. Soc.* **2013**, *135*, 3502.
(50) (a) AlDamen, M. A.; Clemente-Juan, J. M.; Coronado, E.; Martí-Gastaldo, C.; Gaita-Ariño, A. *J. Am. Chem. Soc.* **2008**, *130*, 8874. (b) AlDamen, M. A.; Cardona-Serra, S.; Clemente-Juan, J. M.; Coronado, E.; Gaita-Ariño, A.; Martí-Gastaldo, C.; Luis, F.; Montero, O. *Inorg. Chem.* **2009**, *48*, 3467. (c) Luis, F.; Martínez-Perez, M. J.; Montero, O.; Coronado, E.; Cardona-Serra, S.; Martí-Gastaldo, C.; Clemente-Juan, J. M.; Sesé, J.; Drung, D.; Schurig, T. *Phys. Rev. B* **2010**, *82*, 060403−1.
(51) Ritchie, C.; Speldrich, M.; Gable, R. W.; Sorace, L.; Kögerler, P.; Boskovic, C. *Inorg. Chem.* **2011**, *50*, 7004.
(52) Williams, U. J.; Mahoney, B. D.; DeGregorio, P. T.; Carroll, P. J.; Nakamaru-Ogiso, E.; Kikkawac, J. M.; Schelter, E. J. *Chem. Commun.* **2012**, *48*, 5593.
(53) Meihaus, K.; Rinehart, J. D.; Long, J. R. *Inorg. Chem.* **2011**, *50*, 8484.
(54) Bhunia, A.; Gamer, M. T.; Ungur, L.; Chibotaru, L. F.; Powell, A. K.; Lan, Y.; Roesky, P. W.; Menges, F.; Riehn, C.; Niedner-Schattenberg, G. *Inorg. Chem.* **2012**, *51*, 9589.
(55) Lin, P. H.; Korobkov, I.; Burchell, T. J.; Murugesu, M. *Dalton Trans.* **2012**, *41*, 13649.
(56) Jiang, S.; Wang, B.; Su, G.; Wang, Z.; Gao, S. *Angew. Chem., Int. Ed.* **2010**, *49*, 7448.
(57) Chen, G.; Gao, C.; Tian, J.; Tang, J.; Gu, W.; Liu, X.; Yan, S.; Liao, D.; Cheng, P. *Dalton Trans.* **2011**, *40*, 5579.
(58) Bi, Y.; Guo, Y.; Zhao, L.; Guo, Y.; Lin, S.; Jiang, S.; Tang, J.; Wang, B.; Gao, S. *Chem.-Eur. J.* **2011**, *17*, 12476.
(59) Wang, Y.; Li, X.; Wang, T.; Song, Y.; You, X. *Inorg. Chem.* **2010**, *49*, 969.
(60) Li, D.; Wang, T.; Li, C.; Liu, D.; Li, Y.; You, X. *Chem. Commun.* **2010**, *46*, 2929.
(61) Li, X. L.; Chen, C. L.; Gao, Y. L.; Liu, C. M.; Feng, X. L.; Gui, Y. H.; Fang, S. M. *Chem.-Eur. J.* **2012**, *18*, 14632.
(62) Li, D.; Zhang, X.; Wang, T.; Ma, B.; Li, C.; Li, Y.; You, X. *Chem. Commun.* **2011**, *47*, 6867.
(63) Pointillart, F.; Klementieva, S.; Kuropatov, V.; Le Gal, Y.; Golhen, S.; Cador, O.; Cherkasov, V.; Ouahab, L. *Chem. Commun.* **2012**, *48*, 714.
(64) Menelaou, M.; Ouharrou, F.; Rodríguez, L.; Roubeau, O.; Teat, S. J.; Aliaga-Alcalde, N. *Chem.-Eur. J.* **2012**, *18*, 11545.
(65) (a) Bogani, L. *J. Appl. Phys.* **2011**, *109*, 07B115−1. (b) Bernot, K.; Luzon, J.; Bogani, L.; Etienne, M.; Sangreggorio, C.; Shanmugam, M.; Caneschi, A.; Sessoli, R.; Gatteschi, D. *J. Am. Chem. Soc.* **2009**, *131*, 5573.
(66) Wang, X.; Li, L.; Liao, D. *Inorg. Chem.* **2010**, *49*, 4735.
(67) Wang, X.; Bao, X.; Xu, P.; Li, L. *Eur. J. Inorg. Chem.* **2011**, 3586.
(68) Wang, X.; Tian, H.; Ma, Y.; Yang, P.; Li, L.; Liao, D. *Inorg. Chem. Commun.* **2011**, *14*, 1728.
(69) Zhou, N.; Ma, Y.; Wang, C.; Xu, G. F.; Tang, J.; Xu, J.; Yan, S.; Cheng, P.; Li, L.; Liao, D. *Dalton Trans.* **2009**, *38*, 8489.
(70) Mei, X.; Ma, Y.; Li, L.; Liao, D. *Dalton Trans.* **2012**, *41*, 505.
(71) Hu, P.; Zhu, M.; Mei, X.; Tian, H.; Ma, Y.; Li, L.; Liao, D. *Dalton Trans.* **2012**, *41*, 14651.
(72) Coronado, E.; Gimenez-Saiz, C.; Recuenco, A.; Tarazon, A.; Romero, F. M.; Camon, A.; Luis, F. *Inorg. Chem.* **2011**, *50*, 7370.
(73) Lopez, N.; Prosvirin, A. V.; Zhao, H.; Wernsdorfer, W.; Dunbar, K. R. *Chem.-Eur. J.* **2009**, *15*, 11390.
(74) Thielemann, D. T.; Klinger, M.; Wolf, T. J. A.; Lan, Y.; Wernsdorfer, W.; Busse, M.; Roesky, P. W.; Unterreiner, A. N.; Powell, A. K.; Junk, P. C.; Deacon, G. B. *Inorg. Chem.* **2011**, *50*, 11990.
(75) Liu, J. L.; Yuan, K.; Leng, J. D.; Ungur, L.; Wernsdorfer, W.; Guo, F. S.; Chibotaru, L. F.; Tong, M. L. *Inorg. Chem.* **2012**, *51*, 8538.
(76) (a) Rinehart, J. D.; Fang, M.; Evans, W. J.; Long, J. R. *Nat. Chem.* **2011**, *3*, 538. (b) Rinehart, J. D.; Fang, M.; Evans, W. J.; Long, J. R. *J. Am. Chem. Soc.* **2011**, *133*, 14236.
(77) Demir, S.; Zadrozny, J. M.; Nippe, M.; Long, J. R. *J. Am. Chem. Soc.* **2012**, *134*, 18546.
(78) Ishikawa, N.; Otsuka, S.; Kaizu, Y. *Angew. Chem., Int. Ed.* **2005**, *44*, 731.
(79) Fukuda, T.; Kuroda, W.; Ishikawa, N. *Chem. Commun.* **2011**, *47*, 11686.
(80) (a) Katoh, K.; Kajiwara, T.; Nakano, M.; Nakazawa, Y.; Wernsdorfer, W.; Ishikawa, N.; Breedlove, B. K.; Yamashita, M. *Chem.-Eur. J.* **2011**, *17*, 117. (b) Katoh, K.; Horii, Y.; Yasuda, N.; Wernsdorfer, W.; Toriumi, K.; Breedlove, B. K.; Yamashita, M. *Dalton Trans.* **2012**, *41*, 13582.
(81) Katoh, K.; Umetsu, K.; Breedlove, B. K.; Yamashita, M. *Sci. China Chem.* **2012**, *55*, 918.
(82) Sakaue, S.; Fuyuhiro, A.; Fukuda, T.; Ishikawa, N. *Chem. Commun.* **2012**, *48*, 5337.
(83) Guo, Y.; Xu, G.; Wernsdorfer, W.; Ungur, L.; Guo, Y.; Tang, J.; Zhang, H.; Chibotaru, L. F.; Powell, A. K. *J. Am. Chem. Soc.* **2011**, *133*, 11948.
(84) Venugopal, A.; Tuna, F.; Spaniol, T. P.; Ungur, L.; Chibotaru, L. F.; Okuda, J.; Layfield, R. A. *Chem. Commun.* **2013**, *49*, 901.
(85) Guo, Y.; Chen, X.; Xue, S.; Tang, J. *Inorg. Chem.* **2011**, *50*, 9705.
(86) Zou, L.; Zhao, L.; Chen, P.; Guo, Y.; Guo, Y.; Lib, Y.; Tang, J. *Dalton Trans.* **2012**, *41*, 2966.
(87) Long, J.; Habib, F.; Lin, P. H.; Korobkov, I.; Enright, G.; Ungur, L.; Wernsdorfer, W.; Chibotaru, L. F.; Murugesu, M. *J. Am. Chem. Soc.* **2011**, *133*, 5319.
(88) Habib, F.; Lin, P. H.; Long, J.; Korobkov, I.; Wernsdorfer, W.; Murugesu, M. *J. Am. Chem. Soc.* **2011**, *133*, 8830.
(89) Lin, P. H.; Sun, W. B.; Yu, M. F.; Li, G. M.; Yan, P. F.; Murugesu, M. *Chem. Commun.* **2011**, *47*, 10993.
(90) Lin, P. H.; Sun, W. B.; Yan, P. F.; Ungur, L.; Chibotaru, L. F.; Murugesu, M. *Dalton Trans.* **2012**, *41*, 12349.
(91) Habib, F.; Long, J.; Lin, P. H.; Korobkov, I.; Ungur, L.; Wernsdorfer, W.; Chibotaru, L. F.; Murugesu, M. *Chem. Sci.* **2012**, *3*, 2158.
(92) Lin, P. H.; Burchell, T. J.; Clérac, R.; Murugesu, M. *Angew. Chem., Int. Ed.* **2008**, *47*, 8848.
(93) Nematirad, M.; Gee, W. J.; Langley, S. K.; Chilton, N. F.; Moubaraki, B.; Murray, K. S.; Batten, S. R. *Dalton Trans.* **2012**, *41*, 13711.
(94) (a) Allen, F. H. *Acta Crystallogr.* **2002**, *B58*, 380. (b) ConQuest, Version 1.14.
(95) Tuna, F.; Smith, C. A.; Bodensteiner, M.; Ungur, L.; Chibotaru, L. F.; McInnes, E. J. L.; Winpenny, R. E. P.; Collison, D.; Layfield, R. A. *Angew. Chem., Int. Ed.* **2012**, *51*, 6976.
(96) Sulway, S. A.; Layfield, R. A.; Tuna, F.; Wernsdorfer, W.; Winpenny, R. E. P. *Chem. Commun.* **2012**, *48*, 1508.
(97) Layfield, R. A.; McDouall, J. J. W.; Sulway, S. A.; Tuna, F.; Collison, D.; Winpenny, R. E. P. *Chem.-Eur. J.* **2010**, *16*, 4442.
(98) Song, Y. M.; Luo, F.; Luo, M. B.; Liao, Z. W.; Sun, G. M.; Tian, X. Z.; Zhu, Y.; Yuan, Z. J.; Liu, S. J.; Xu, W. Y.; Feng, X. F. *Chem. Commun.* **2012**, *48*, 1006.
(99) Zheng, Y. Z.; Lan, Y.; Wernsdorfer, W.; Anson, C. E.; Powell, A. K. *Chem.-Eur. J.* **2009**, *15*, 12566.
(100) Xu, G.; Wang, Q.; Gamez, P.; Ma, Y.; Clérac, R.; Tang, J.; Yan, S.; Cheng, P.; Liao, D. *Chem. Commun.* **2010**, *46*, 1506.
(101) Liang, L.; Peng, G.; Li, G.; Lan, Y.; Powell, A. K.; Deng, H. *Dalton Trans.* **2012**, *41*, 5816.
(102) Peng, J.; Ren, Y.; Kong, X.; Long, L.; Huang, R.; Zheng, L. *CrystEngComm* **2011**, *13*, 2084.
(103) Joarder, B.; Chaudhari, A. K.; Rogez, G.; Ghosh, S. K. *Dalton Trans.* **2012**, *41*, 7695.
(104) Ma, Y.; Xu, G. F.; Yang, X.; Li, L. C.; Tang, J.; Yan, S. P.; Cheng, P.; Liao, D. Z. *Chem. Commun.* **2010**, *46*, 8264.

(105) Yi, X.; Bernot, K.; Pointillart, F.; Poneti, G.; Calvez, G.; Daiguebonne, C.; Guillou, O.; Sessoli, R. *Chem.-Eur. J.* **2012**, *18*, 11379.
(106) Pointillart, F.; Le Gal, Y.; Golhen, S.; Cador, O.; Ouahab, L. *Chem.-Eur. J.* **2011**, *17*, 10397.
(107) Bernot, K.; Pointillart, F.; Rosa, P.; Etienne, M.; Sessoli, R.; Gatteschi, D. *Chem. Commun.* **2010**, *46*, 6458.
(108) Pointillart, F.; Bernot, K.; Poneti, G.; Sessoli, R. *Inorg. Chem.* **2012**, *51*, 12218.
(109) Tian, H.; Liu, R.; Wang, X.; Yang, P.; Li, Z.; Li, L.; Liao, D. *Eur. J. Inorg. Chem.* **2009**, 4498.
(110) Xu, J. X.; Ma, Y.; Liao, D. Z.; Xu, G. F.; Tang, J.; Wang, C.; Zhou, N.; Yan, S. P.; Cheng, P.; Li, L. C. *Inorg. Chem.* **2009**, *48*, 8890.
(111) Mei, X. L.; Liu, R. N.; Wang, C.; Yang, P. P.; Li, L. C.; Liao, D. Z. *Dalton Trans.* **2012**, *41*, 2904.
(112) Liu, R.; Zhang, C.; Li, L.; Liao, D.; Sutter, J. P. *Dalton Trans.* **2012**, *41*, 12139.
(113) Tang, J.; Hewitt, I.; Madhu, N. T.; Chastanet, G.; Wernsdorfer, W.; Anson, C. E.; Benelli, C.; Sessoli, R.; Powell, A. K. *Angew. Chem., Int. Ed.* **2006**, *45*, 1729.
(114) (a) Luzon, J.; Bernot, K.; Hewitt, I. J.; Anson, C. E.; Powell, A. K.; Sessoli, R. *Phys. Rev. Lett.* **2008**, *100*, 247205. (b) Salman, Z.; Giblin, S. R.; Lan, Y.; Powell, A. K.; Scheuermann, R.; Tingle, R.; Sessoli, R. *Phys. Rev. B* **2010**, *82*, 174427.
(115) (a) Chibotaru, L. F.; Ungur, L.; Soncini, A. *Angew. Chem., Int. Ed.* **2008**, *47*, 4126. (b) Van den Heuvel, W.; Chibotaru, L. F. *Phys. Rev. B* **2010**, *82*, 174436. (c) Plokhov, D. I.; Zvezdin, A. K.; Popov, A. I. *Phys. Rev. B* **2011**, *83*, 184415.
(116) (a) Soncini, A.; Chibotaru, L. F. *Phys. Rev. B* **2010**, *81*, 132403. (b) Georgeot, B.; Mila, F. *Phys. Rev. Lett.* **2010**, *104*, 200502.
(117) Hewitt, I. J.; Tang, J.; Madhu, N. T.; Anson, C. E.; Lan, Y.; Luzon, J.; Etienne, M.; Sessoli, R.; Powell, A. K. *Angew. Chem., Int. Ed.* **2010**, *49*, 6352.
(118) Xue, S.; Chen, X. H.; Zhao, L.; Guo, Y. N.; Tang, J. *Inorg. Chem.* **2012**, *51*, 13264.
(119) Wang, Y. X.; Shi, W.; Li, H.; Song, Y.; Fang, L.; Lan, Y.; Powell, A. K.; Wernsdorfer, W.; Ungur, L.; Chibotaru, L. F.; Shen, M.; Cheng, P. *Chem. Sci.* **2012**, *3*, 3366.
(120) Lin, S. Y.; Guo, Y. N.; Guo, Y.; Zhao, L.; Zhang, P.; Ke, H.; Tang, J. *Chem. Commun.* **2012**, *48*, 6924.
(121) Lin, S. Y.; Zhao, L.; Guo, Y. N.; Zhang, P.; Guo, Y.; Tang, J. *Inorg. Chem.* **2012**, *51*, 10522.
(122) Hewitt, I. J.; Lan, Y.; Anson, C. E.; Luzon, J.; Sessoli, R.; Powell, A. K. *Chem. Commun.* **2009**, 6765.
(123) Guo, F. S.; Liu, J. L.; Leng, J. D.; Meng, Z. S.; Lin, Z. J.; Tong, M. L.; Gao, S.; Ungur, L.; Chibotaru, L. F. *Chem.-Eur. J.* **2011**, *17*, 2458.
(124) Liu, C. S.; Du, M.; Sañudo, C. E.; Echeverria, J.; Hu, M.; Zhang, Q.; Zhou, L. M.; Fang, S. M. *Dalton Trans.* **2011**, *40*, 9366.
(125) Anwar, M. U.; Tandon, S. S.; Dawe, L. N.; Habib, F.; Murugesu, M.; Thompson, L. K. *Inorg. Chem.* **2012**, *51*, 1028.
(126) Guo, Y. N.; Xu, G. F.; Gamez, P.; Zhao, L.; Lin, S. Y.; Deng, R.; Tang, J.; Zhang, H. J. *J. Am. Chem. Soc.* **2010**, *132*, 8538.
(127) Ke, H.; Xu, G. F.; Guo, Y. N.; Gamez, P.; Beavers, C. M.; Teat, S. J.; Tang, J. *Chem. Commun.* **2010**, 6057.
(128) Lin, S. Y.; Zhao, L.; Ke, H.; Guo, Y. N.; Tang, J.; Guo, Y.; Dou, J. *Dalton Trans.* **2012**, *41*, 3248.
(129) Koo, B. H.; Lim, K. S.; Ryu, D. W.; Lee, W. R.; Koh, E. K.; Hong, C. S. *Chem. Commun.* **2012**, *48*, 2519.
(130) Anwar, M. U.; Thompson, L. K.; Dawe, L. N.; Habib, F.; Murugesu, M. *Chem. Commun.* **2012**, *48*, 4576.
(131) Xue, S.; Zhao, L.; Guo, Y. N.; Tang, J. *Dalton Trans.* **2012**, *41*, 351.
(132) Bi, Y.; Wang, X. T.; Liao, W.; Wang, X.; Deng, R.; Zhang, H.; Gao, S. *Inorg. Chem.* **2009**, *48*, 11743.
(133) Xue, S.; Zhao, L.; Guo, Y. N.; Chen, X. H.; Tang, J. *Chem. Commun.* **2012**, *48*, 7031.
(134) Woodruff, D. N.; Tuna, F.; Bodensteiner, M.; Winpenny, R. E. P.; Layfield, R. A. *Organometallics* **2013**, *32*, 1224.
(135) Lin, P. H.; Burchell, T. J.; Ungur, L.; Chibotaru, L. F.; Wernsdorfer, W.; Murugesu, M. *Angew. Chem., Int. Ed.* **2009**, *48*, 9489.
(136) Lin, P. H.; Korobkov, I.; Wernsdorfer, W.; Ungur, L.; Chibotaru, L. F.; Murugesu, M. *Eur. J. Inorg. Chem.* **2011**, 1535.
(137) Guo, P. H.; Liu, J. L.; Zhang, Z. M.; Ungur, L.; Chibotaru, L. F.; Leng, J. D.; Guo, F. S.; Tong, M. L. *Inorg. Chem.* **2012**, *51*, 1233.
(138) Abbas, G.; Lan, Y.; Kostakis, G. E.; Wernsdorfer, W.; Anson, C. E.; Powell, A. K. *Inorg. Chem.* **2010**, *49*, 8067.
(139) Abbas, G.; Kostakis, G. E.; Lan, Y.; Powell, A. K. *Polyhedron* **2012**, *41*, 1.
(140) Zheng, Y. Z.; Lan, Y.; Anson, C. E.; Powell, A. K. *Inorg. Chem.* **2008**, *47*, 10813.
(141) Langley, S. K.; Chilton, N. F.; Gass, I. A.; Moubaraki, B.; Murray, K. S. *Dalton Trans.* **2011**, *40*, 12656.
(142) Xue, S.; Zhao, L.; Guo, Y. N.; Deng, R.; Guo, Y.; Tang, J. *Dalton Trans.* **2011**, *40*, 8347.
(143) Yan, P. F.; Lin, P. H.; Habib, F.; Aharen, T.; Murugesu, M.; Deng, Z. P.; Li, G. M.; Sun, W. B. *Inorg. Chem.* **2011**, *50*, 7059.
(144) Ke, H.; Gamez, P.; Zhao, L.; Xu, G. F.; Xue, S.; Tang, J. *Inorg. Chem.* **2010**, *49*, 7549.
(145) Savard, D.; Lin, P. H.; Burchell, T. J.; Korobkov, I.; Wernsdorfer, W.; Clérac, R.; Murugesu, M. *Inorg. Chem.* **2009**, *48*, 11748.
(146) Gao, Y.; Xu, G. F.; Zhao, L.; Tang, J.; Liu, Z. *Inorg. Chem.* **2009**, *48*, 11495.
(147) Gass, I. A.; Moubaraki, B.; Langley, S. K.; Batten, S. R.; Murray, K. S. *Chem. Commun.* **2012**, *48*, 2089.
(148) Liu, C. M.; Zhang, D. Q.; Hao, X.; Zhu, D. B. *Cryst. Growth Des.* **2012**, *12*, 2948.
(149) Blagg, R. J.; Muryn, C. A.; McInnes, E. J. L.; Tuna, F.; Winpenny, R. E. P. *Angew. Chem., Int. Ed.* **2011**, *50*, 6530.
(150) Blagg, R. J.; Tuna, F.; McInnes, E. J. L.; Winpenny, R. E. P. *Chem. Commun.* **2011**, *47*, 10587.
(151) Gamer, M. T.; Lan, Y.; Roesky, P. W.; Powell, A. K.; Clérac, R. *Inorg. Chem.* **2008**, *47*, 6581.
(152) Peng, J. B.; Kong, X. J.; Ren, Y. P.; Long, L. S.; Huang, R. B.; Zheng, L. S. *Inorg. Chem.* **2012**, *51*, 2186.
(153) Lin, S. Y.; Wernsdorfer, W.; Ungur, L.; Powell, A. K.; Guo, Y, N.; Tang, J.; Zhao, L.; Chibotaru, L. F.; Zhang, H. J. *Angew. Chem., Int. Ed.* **2012**, *51*, 12767.
(154) Guo, Y. N.; Chen, X. H.; Xue, S.; Tang, J. *Inorg. Chem.* **2012**, *51*, 4035.
(155) Tian, H.; Wang, M.; Zhao, L.; Guo, Y. N.; Guo, Y.; Tang, J.; Liu, Z. *Chem.-Eur. J.* **2012**, *18*, 442.
(156) Tian, H.; Guo, Y. N.; Zhao, L.; Tang, J.; Liu, Z. *Inorg. Chem.* **2011**, *50*, 8688.
(157) Ke, H.; Zhao, L.; Guo, Y.; Tang, J. *Eur. J. Inorg. Chem.* **2011**, 4153.
(158) Langley, S. K.; Moubaraki, B.; Murray, K. S. *Inorg. Chem.* **2012**, *51*, 3947.
(159) (a) Langley, S. K.; Moubaraki, B.; Forsyth, C. M.; Gass, I. A.; Murray, K. S. *Dalton Trans.* **2010**, *39*, 1705. (b) Ungur, L.; Langley, S. K.; Hooper, T. N.; Moubaraki, B.; Brechin, E. K.; Murray, K. S.; Chibotaru, L. F. *J. Am. Chem. Soc.* **2012**, *134*, 18554.
(160) Hussain, B.; Savard, D.; Burchell, T. J.; Wernsdorfer, W.; Murugesu, M. *Chem. Commun.* **2009**, *45*, 1100.
(161) Bi, Y. F.; Xu, G. C.; Liao, W. P.; Du, S. C.; Deng, R. P.; Wang, B. W. *Sci. China Chem.* **2012**, *55*, 967.
(162) Sharples, J. W.; Zheng, Y.; Tuna, F.; McInnes, E. J. L.; Collison, D. *Chem. Commun.* **2011**, *47*, 7650.
(163) Coxall, R. A.; Harris, S. G.; Henderson, D. K.; Parsons, S.; Tasker, P. A.; Winpenny, R. E. P. *Dalton Trans.* **2000**, 2349.
(164) Tian, H.; Zhao, L.; Guo, Y. N.; Guo, Y.; Tang, J.; Liu, Z. *Chem. Commun.* **2012**, *48*, 708.
(165) Guo, F. S.; Guo, P. H.; Meng, Z. S.; Tong, M. L. *Polyhedron* **2011**, *30*, 3079.
(166) Miao, Y. L.; Liu, J. L.; Li, J. Y.; Leng, J. D.; Ou, Y. C.; Tong, M. L. *Dalton Trans.* **2011**, *40*, 10229.

(167) Alexandropoulos, D. I.; Mukherjee, S.; Papatriantafyllopoulou, C.; Raptopoulou, C. P.; Psycharis, V.; Bekiari, V.; Christou, G.; Stamatatos, T. C. *Inorg. Chem.* **2011**, *50*, 11276.
(168) Ke, H.; Xu, G. F.; Zhao, L.; Tang, J.; Zhang, X. Y.; Zhang, H. J. *Chem.-Eur. J.* **2009**, *15*, 10335.
(169) Miao, Y. L.; Liu, J. L.; Leng, J. D.; Lina, Z. J.; Tong, M. L. *Cryst. Eng. Comm.* **2011**, *13*, 3345.
(170) Zhao, L.; Xue, S.; Tang, J. *Inorg. Chem.* **2012**, *51*, 5994.
(171) Gu, X.; Clérac, R.; Houri, A.; Xue, D. *Inorg. Chim. Acta* **2008**, *361*, 3873.
(172) Ungur, L.; Chibotaru, L. F. *Phys. Chem. Chem. Phys.* **2011**, *13*, 20086.
(173) Ganivet, C. R.; Ballesteros, B.; de la Torre, G.; Clemente-Juan, J. M.; Coronado, E.; Torres, T. *Chem. Eur. J.* **2013**, *19*, 1457.

NOTE ADDED IN PROOF

Very recently, a new record for the highest anisotropy barrier in an SMM has been reported, viz. a heteroleptic terbium bis-phthalocyanine complex was determined to have U_{eff} = 652 cm^{-1}.[173]